ISAS - INTERNATIONAL SCHOOL
FOR ADVANCED STUDIES

Absorption Line Spectral Indices in Stars and Stellar Systems

Thesis presented to the
International School for Advanced Studies, Trieste Italy

-Astrophysics Sector-

in partial fulfilment of the requirements for the degree of

Doctor Philosophiæ

Candidate: Miguel Chávez Dagostino

Supervisors: Prof. Aldo Treves
Prof. Maria Lucia Malagnini

Academic year 1994/1995

SISSA - SCUOLA
INTERNAZIONALE
SUPERIORE
DI STUDI AVANZATI
TRIESTE
Strada Costiera 11

TRIESTE

To my wife
and my little son

To my parents

ABSTRACT

This dissertation is mainly concerned with the study of absorption line spectral indices in cool stars and old stellar systems. From a detailed analysis of the solar intensity spectrum, we derive an atomic and molecular line list with revised line parameters. This line list is then used to compute an extensive grid of stellar synthetic spectra at high resolution in the temperature range T_{eff}=4000–8000 K, surface gravity interval log g=1.0–5.0, and metallicities from [M/H]=-1.0 to +0.5. The computations are done using the most updated version of Kurucz's model atmospheres and numerical codes. The final grid contains a total of 693 synthetic spectra, which can be interpolated at intermediate points in the three dimensional parameter space.

We illustrate the behavior, in terms of the atmospheric parameters, of five spectral indices, Mg_2, Mg_1, Mg_b, Fe5270 and Fe5335, computed from the whole grid of synthetic spectra. As for the spectra, index values for atmospheric parameters within the limits of the grid can be obtained by interpolation and used as input for population synthesis. The drawbacks of using fitting functions instead, are illustrated for the most widely used index, i.e. Mg_2.

Through a correlation and regression analysis, we derive a polynomial fitting function that best correlates the Mg_2 index with the atmospheric parameters. Our results indicate that fitting functions may introduce significant errors when used to compute indices from them.

We present the analysis of intermediate resolution spectra of a selected sample of stars catalogued as super metal-rich (SMR) in the literature. By comparison with suitable theoretical spectra we have selected those stars which, according to our results, are "really" metal rich. We found that of the 78 stars here presented, 55 have metallicities [Fe/H]$\geq$0.1.

The grid of synthetic spectra is applied in the context of population synthesis by using a sub-set of isochrones computed by the Padova group. A preliminary analysis of the variations of integrated spectral indices as function of age and metallicity in single stellar populations and elliptical galaxies is given.

ACKNOWLEDGEMENTS

First, I would like to thank my external supervisor Prof. Maria Lucia Malagnini for suggesting the topic of this thesis. Her close guidance, patience and enthusiasm made this thesis to be a much more thorough piece of work than I would otherwise have done. I am sure that this work is the starting point of a fruitful collaboration. I express my gratitude to Prof. Dennis Sciama for giving me the opportunity of working at SISSA and for his continuous encouragement, particularly during difficult times. I wish to thank my supervisor Prof. Aldo Treves for his well-judged pressure on me to finish bits of work, and for his skills in guiding graduate students. Stimulating discussions with Dr. Carlo Morossi helped a lot to understand many points in the thesis. His advice and help is acknowledged. I will always have in mind the working philosophy *"Ottimo ed abbondante"*.

I also thank Prof. Giorgio Sedmak, for giving me the opportunity of using the facilities of the Trieste Astronomical Observatory.

Thanks to Prof. Alberto Buzzoni for his advice on the part related to the SMR stars. Once again, I foresee a fruitful collaboration.

I am indebted with Dr. Robert Kurucz for his hospitality during my visit to the Harvard-Smithsonian Center for Astrophysics, and for his advice in the use of his models and codes.

The Padova stellar evolution group, in particular Prof. Alessandro Bressan, is acknowledged for making available the stellar isochrones and for giving me the basic inputs on population synthesis.

I am very thankful to Drs. Jorge Ojeda and Alfonso Serrano, former and present directors of the Instituto Nacional de Astrofísica, Optica y Electrónica (INAOE) for the financial support I have received since my arrival to Trieste.

Thanks a lot to my friends of SISSA, most of whom have already left Trieste. In particular, Drs. Licai Deng, Hugo Morales, Nobby Takeuchi, Paul Haines, and more recently Leonardo De Maria, and of course my friends of the student secretariat.

I appreciate the tons of e-mails received from my ex-class mates in México. Dr. Juan Manuel Alcalá, Docs Omar López Cruz, Oscar Martínez and Raúl Mújica, thank you for your friendship.

My deepest gratitude goes to my parents, who always kept an eye on his son on the other side of the ocean, and to my wife Cristina and my son μ-miguelito for being an infinite source of strength, specially when I most needed it.

This work has made use of the SIMBAD data base which is operated by the CDS at Strasbourg.

Contents

1 Introduction 1
- 1.1 On Stellar Populations . . . 1
  - 1.1.1 The stellar content of elliptical galaxies . . . 2
- 1.2 Recent results and open problems . . . 3
  - 1.2.1 The ultraviolet excess in elliptical galaxies . . . 3
  - 1.2.2 The age and chemical composition of old stellar systems . 6
- 1.3 Goals and description of this dissertation . . . 7

2 Building up a Theoretical Spectral Library 9
- 2.1 Spectrum synthesis: an overview . . . 10
  - 2.1.1 Recent improvements . . . 13
- 2.2 The atomic and molecular Data . . . 13
- 2.3 The solar model . . . 17
- 2.4 Observed and computed solar central intensity spectrum . . . 20
  - 2.4.1 Adjusting the line parameters . . . 20
- 2.5 The new grid of synthetic spectra . . . 21

3 Iron and Magnesium Indices: The Calibration 25
- 3.1 Spectral index definitions . . . 27
- 3.2 Spectral indices for the Sun . . . 29
  - 3.2.1 Dependence of solar indices on microturbulence . . . 30
  - 3.2.2 Dependence of solar indices on instrumental profile . . . 32
- 3.3 Comparison with previous theoretical grids . . . 32
- 3.4 Indices and atmospheric parameters . . . 35
- 3.5 Comparison with empirical data . . . 42

4 Observed and Synthetic Spectra of Super Metal-Rich Stars 47
- 4.1 The super metal-rich phenomenon . . . 47
- 4.2 Observations and reductions . . . 48
- 4.3 Iron and magnesium indices in SMR stars . . . 50
- 4.4 Observed versus computed spectra . . . 66
  - 4.4.1 Selecting the set of atmospheric parameters . . . 72

5 Integrated Spectra of Single Stellar Populations 77
- 5.1 From stellar to integrated properties . . . 78
- 5.2 Spectral indices versus age . . . 80

5.2.1 Contributions to the integrated Mg_2 index 83
5.3 A step ahead: Elliptical galaxies 90

6 Discussion and Conclusions **93**
6.1 Summary of the main results of this work 93

Appendix A: Computer Programs for Spectrum Synthesis **95**

Appendix B: Spectral Indices in Tabular Form **97**

Bibliography **113**

List of Tables

2.1 Atomic and molecular species included in the computations 16
2.2 Molecular species in the auxiliary line list 17

3.1 Index definitions 29
3.2 Spectral indices for the Sun 30

4.1 Additional index definitions 54
4.2 Observed SMR stars and spectral indices 55
4.3 Spectral indices from theoretical Spectra 58
4.4 Standard deviations from the residual spectra 70
4.5 Fiducial set of SMR stars 76

5.1 Integrated spectral indices for SSP of different ages and metallicities 84

List of Figures

2.1 Schematic representation of the process of computing a synthetic spectrum 12

2.2 a) Differences in the temperature structure of the model atmospheres in the newest model version and K92. b) Synthetic spectra computed from the same model atmospheres and the line list of Gulati (1991), but different numerical codes. The model fluxes have been computed for the following set of atmospheric parameters: T_{eff} = 4000 K, log g = 1.5 and [M/H] = 0.0, and have been convolved with a Gaussian profile of FWHM=9 Å. 14

2.3 Temperature variation in the solar atmosphere as considered by the K93 theoretical model (solid line) and a semi-empirical one (Maltby et al. 1986, dotted line). Note in the semi-empirical model the rise in temperature above τ_{ross}=2×10^{-4} (log τ_{ross} = -3.6). 18

2.4 Effects of changing the mass-depth variable to eliminate the emission in the strong Mg feature at 5170 Å. 19

2.5 a)- Magnesium feature in the interval 5171–5174 Å. b)- Iron and Chromium features in the region 5327–5331 Å. In both panels the thick solid line corresponds to the observed spectrum and the thin solid and dotted lines indicate the theoretical solar intensity spectra computed with and without adjusting line parameters, respectively. 22

2.6 Histograms of the differences between the computed spectrum and the observed solar central intensity spectrum, before and after performing the modifications to the line parameters. 23

3.1 Definition of a spectral index. The three bands defining the Mg_2 index are shown inside the dotted boxes; the straight solid line represents the pseudocontinuum. An index is measured by comparing the flux in the pseudocontinuum (A) and the average flux in the central bandpass (B). 28

3.2 Differences between the computed and observed solar spectra. Both spectra were normalized to the continuum. Fluxes are given at a wavelength step of 0.83Å. Note that the largest positive residuals appear in the region where the index Fe5015 is defined. 31

3.3 Spectral indices from the solar spectrum as a function of microturbulent velocity, ξ. 33

3.4 Trend of the indices in terms of the FWHM of the gaussian profile used to convolve the solar (filled dots) and 4000/1.5/0.0 (empty dots) models. Note that Mg_1 and Mg_2 vary very little while iron indices change drastically. 34
3.5 Differences between Mg_2 indices computed reported by GMM93 and our grid for different metallicities and gravities as functions of $\theta_{\rm eff}$. The values [M/H] and log g are given in parenthesis in each panel. 36
3.6 Mg_2 indices for different metallicities and gravities as a function of $\theta_{\rm eff}$ =5040/$T_{\rm eff}$. The trend of the index with $\theta_{\rm eff}$, at fixed gravity, is quite similar when varying metallicity, while a clear difference is present at low temperature between giant and dwarf models. Indeed, for dwarfs a plateau is reached, while it is not for giants. In the panel referring to log g = 4.5 dex, the value computed for the solar model (5777/4.43770/0.00) is also plotted (starred symbol). 37
3.7 Same as figure 3.6 for Mg_1. This index increases monotonically till the lowest temperatures considered. Worthey (1992) found that there is a turnover at 4000 K, for both giant and dwarf stars. . . . 38
3.8 Same as figure 3.6 for Mg_b. Note that the maximum of the index strength is displaced towards lower temperatures with decreasing gravity. At the temperature where the maximum is reached differences due to metallicity are enhanced. 39
3.9 Same as figure 3.6 for Fe5270. As in the case of Mg_2, the trend of this index with respect to $\theta_{\rm eff}$, at fixed gravity, respond in a similar way to metallicity changes. It is also clear that a plateau is reached at the lowest temperatures for log g = 4.5. 40
3.10 Same as figure 3.6 for Fe 5335. This index displays a quite similar behavior to that of Fe5270. 41
3.11 Analytical vs grid Mg_2index. 42
3.12 Analytical vs grid Mg_2index after flattening of the ripple was done. 43
3.13 Plot of indices versus empirical values. Vertical bars connect the points referring to different determinations of atmospheric parameters given in C91 for the same star. 45
3.14 Differences between Mg_2 indices computed from WFGB94 fitting functions and our grid for different metallicities and gravities as functions of $\theta_{\rm eff}$. The values [M/H] and log g are given in parenthesis in each panel. 46

4.1 Distribution of the observed stars in terms of the atmospheric parameters. 50
4.2 Subset of observed supergiant stars. It is evident from these spectra the opposite behavior of Hβ with respect to those of magnesium and iron. 51
4.3 Same as figure 4.2 for giant stars. 52
4.4 Same as figure 4.2 for dwarf stars. 53

4.5 a)- Mg_2 vs Mg_s. b)- Fe5270 vs $Fe52_s$. The indices were computed from theoretical spectra by considering the stellar parameters assigned to the observed stars (see text). 62
4.6 Mg_b index from observed spectra as a function of $\theta_{\rm eff}$. Symbols are explained in the box. Note that dwarf stars are well separated from giants and supergiants. In both trends the index increases with decreasing temperature (increasing $\theta_{\rm eff}$) reaching a maximum at 5300 K ($\theta_{\rm eff}$=0.95) for high gravity stars and 4600 K ($\theta_{\rm eff}$=1.1) for giants and supergiants. The turnover in the index behavior is less pronounced in low gravity stars. Compare this to Fig. 3.8. The two most deviating points correspond to determinations for the stars HD 109511 and HD 73710. 63
4.7 Mg_s index from observed spectra as a $\theta_{\rm eff}$. Symbols have the same meaning as in figure 4.6. Effects of gravity are also distinguishable in this index. The most deviating points correspond to the same determinations as for Mg_b. 64
4.8 $Fe52_s$ index from observed spectra as a function of effective temperature. Symbols have the same meaning as in figure 4.6. The most deviating points correspond to the same determinations as in previous figures. 65
4.9 Comparison between observed and computed Mg_b indices. Vertical bars connect the points corresponding to different determinations of atmospheric parameters for a given star. 67
4.10 Comparison between observed and computed Mg_s indices. Vertical bars connect the points corresponding to different determinations of atmospheric parameters for a given star. 68
4.11 Comparison between observed and computed $Fe52_s$ indices. Vertical bars connect the points corresponding to different determinations of atmospheric parameters for a given star. 69
4.12 Standard deviation of the residual spectra for the 114 determinations as a function of $\theta_{\rm eff}$. The starred symbol and dotted line correspond to the solar value. Primary and secondary data are represented by solid and empty dots respectively. Note that the deviations seem to increase towards low temperatures. 71
4.13 Mg_s of selected stars as a function of effective temperature. 73
4.14 Mg_s of selected stars as a function of effective temperature. Symbols are as in figure 4.13. 74
4.15 $Fe52_s$ of selected stars as a function of effective temperature. Symbols are as in figure 4.13. 75

5.1 Diagram representing the population synthesis technique 79
5.2 Isochrones of different ages for solar metallicity, Z=0.02. The inner box illustrates the parameter space covered by the synthetic stellar fluxes. 81

5.3 Iron and Magnesium indices as a function of age for a SSP of solar metallicity. The upper and lower panels display the indices measured in magnitudes and equivalent widths. For populations older than 18 Gyr the there is a turnover of the trend of the indices. 82
5.4 Mg_2 index as a function of age for different metallicities. Note that over the whole age range the index values never overlap. 83
5.5 a)- Cumulative flux in the pseudocontinuum bandpass in a SSP of 15.84 Gyr and Z=0.02. The contribution of of the different types of stars to the visual luminosity can be estimated if we separate stellar type using the gravity sale on the right. b)- Zoomed region to illustrate the contribution of advance stellar stages. 87
5.6 a)- Mg_2 index vs initial mass in individual stars along an isochrone of age 15.84 Gyr and solar metallicity. b)- Zoomed region to display the contribution of advanced stellar stages 88
5.7 a)- Cumulative Mg_2 index vs initial mass in a SSP of 15.84 Gyr and Z=0.02. The integrated Mg_2 index starts with very high values (stars of the lower MS) then stars at the turnoff and stars in the MS near the turnoff cause an abrupt decrease of the index. b)- The index is slightly increased by stars in the RGB and the AGB to reach the final value of 0.387. 89
5.8 The Mg_2 index as a function of age in three galaxies of different mass. 92

Chapter 1

Introduction

1.1 On stellar populations

The concept of stellar populations was first introduced by Walter Baade in 1944 (Baade 1944), when he succeeded in resolving into individual stars the central regions of our companion spiral galaxy M31, as well as its satellite elliptical galaxies M32 and NGC 205. The only information that Baade had about these stars was their location in the Color-Magnitude diagram (CMD). At that time, the theory of nucleosynthesis was not yet well established and with the instrumentation available it was not possible to obtain kinematical data for stars in external galaxies. Baade noted that the upper cutoff of the luminosity function of the resolved stars was quite sharp, in marked contrast to that for systems in the Magellanic Clouds and in the arms of spiral galaxies. From this limited information Baade developed a simple scheme: Population I stars are those whose HR diagram resembled that of open clusters in the disk of the Galaxy, and Population II stars are those located on the same regions in the HR diagram as the galactic globular cluster giants. Baade assigned to Population II stars outside the thin disks of spiral galaxies-globular clusters, stars in elliptical galaxies, and stellar halo components of disk galaxies.

In the late 40's and early 50's a great body of literature came along with evidence pointing out the need of a revision of the scheme proposed by Baade. Keenan and Keller (1953) compared the HR diagram of field high velocity stars with a typical globular cluster diagram far from expecting to see any differences between them. Instead, they obtained an almost normal Population I diagram resembling the one for the old galactic cluster M67 (Johnson and Sandage 1955). The chemical *homogeneity* of the prototype objects of Population II was also brought into question by Mayall (1946) and Morgan (1956, 1959) who found that the composite spectral type of the integrated light of globular clusters varies from early F to late G, a dispersion that was also confirmed by Deutch (1955).

Mayall (1946) and Morgan (1956) had previously shown that the G-type clusters were concentrated towards the galactic center while the F-type were more widely distributed. Observations carried out by Kinman (1959) on southern stars demonstrated that the kinematics of the globular clusters was dependent on the strength of metallic lines present in the spectra of these systems.

The famous Vatican Conference held in 1957 (O'Connell 1958) brought together all the problems encountered since the introduction of the idea of stellar populations invoked by Baade. In this conference arose the present concept of various populations subsystems that have changing characteristics. Five types (proposed by Oort in that conference) were suggested, types I and II became Populations I (extreme and intermediate) and II (intermediate and halo), and disk population. Each subsystem being characterized by different types of objects.

Eventhough at present people still use these subsystems to describe different stellar components in galaxies, there seems to be no agreement on what are the exactly limiting stellar types connecting them. Modern data has revealed that the Galaxy is a complicated system. We know that the different stellar populations are not a one parameter system, as had been suggested by the smooth correlations that were evident between kinematics and chemistry, and between chemistry and time.

In the IAU symposium on Stellar Populations held in Holland last year (IAU symposium 164), Dr. Jeremy Mould closed the meeting with words that *"clearly"* describe the current status of the population concept:

"It seems that no two people agree on a definition of a stellar population, but everyone uses the term"

In the proceedings of the same symposium, Dr. Ivan King also quoted

"Populations are not I and II; they are manifold (age and metallicity), and they should be described in the right way not in the wrong way"

1.1.1 The stellar content of elliptical galaxies

Numerous studies since the early works of Spinrad & Taylor (1971), followed by the contributions of Tinsley and collaborators (Tinsley 1980), indicate that elliptical galaxies have metal abundance [Fe/H][1] ranging from solar to about twice the solar value and that are old, but probably not as old as globular clusters as

[1]It is a universal practice to specify the chemical abundance in terms of the logarithmic abundance of iron, related to hydrogen, and this ratio relative to the solar values, thus [Fe/H]=log(N_{Fe}/N$_H$)-log(N_{Fe}/N$_H$)$\odot$. In this dissertation the abundance of metals (any element heavier than helium) will be specified using either [M/H] or [Fe/H] notations. All metals are considered to vary in lock-step.

indicated by measurements of Hβ (Burstein et al. 1984).

In the classical view, ellipticals formed stars in the early universe and their populations could, in principle, be modelled by a single stellar burst followed by a passive evolution. (e.g. Larson 1974). Recent observational evidence has shown that the classical picture is far too simple and that, in order to have a realistic picture of elliptical galaxy formation and evolution, well established constraints should be considered.

For example, the metal rich population dominating the integrated light in giant ellipticals suggests that star formation has continued for a long time in those galaxies. Moreover, the metallicity gradients measured for different elements indicate more metal rich populations in the inner regions than in the outskirts.

Eventhough elliptical galaxies might look rather simple objects if compared to spirals or irregulars, there are some "complications" in understanding their stellar content and thus their evolution as a whole.

1.2 Recent results and open problems

1.2.1 The ultraviolet excess in elliptical galaxies

An important issue in our understanding of the underlying stellar populations in elliptical galaxies is the well established ultraviolet upturn seen shortward of 2000 Å (see Dorman, O'Connell & Rood 1995 for an excellent review). The rise in the spectral energy distribution was first recognized in observations of the M31 bulge from the OAO-2 satellite (Code 1969; Code and Welsh 1979). The first interpretation to the phenomenon was given by Hills (1971) who pointed out that this UV upturn had a hot thermal origin, and he suggested as the probable source the Post-Asymptotic Giant Branch (P-AGB) stars during their high luminosity transit towards the White Dwarf cooling branch. Since these early works, a large amount of theoretical as well as observational material has shown up in the main journals of astrophysical matters.

Observational properties of the UV-excess in galaxies

The vast majority of the observational data comes from the highly successful *IUE* satellite (Burstein et al. 1988) and, below the IUE cut off, by the Hopkins Ultraviolet Telescope (HUT). UV observations have revealed that the main characteristics of this phenomenon are:

- Almost all normal ellipticals and S0's bulges observed so far emit detectable far UV radiation. By normal it is understood those galaxies which are neither AGN's nor show signs of recent star formation.

- The strength of the UV-excess, as measured by the ultraviolet color index (1500-V), defined as the difference between the average flux in the band

1250-1850 Å and the visual magnitude, varies from galaxy to galaxy reaching in some cases differences of about one order of magnitude (e.g. Bertola, Capaccioli & Oke 1982), much greater than that found in optical and near IR broad band colors.

- The UV flux positively correlates with metallicity (or the Mg_2 absorption line index) as first pointed out by Faber (1983). This correlation was confirmed by Burstein et al. (1988) using IUE observations of the nuclear regions of M31 and of bright elliptical galaxies. It also correlates with velocity dispersion and with luminosity (mass).

- The slope of Far-UV spectral energy distribution is found to be constant from object to object and indicates that the radiation should be dominated by stars with $T_{\rm eff} \leq 25000$ K. Recently, the observations of NGC 1399 and M31 carried out by HUT in the wavelength band 900-1800 Å (Ferguson et al. 1991 and Ferguson & Davidsen 1993) have put important constraints on the possible source of the UV-excess. It was found that in both objects different populations give rise to the UV upturn, but also in both cases massive stars are to be excluded as the main source of this radiation because of the turn over of the energy distribution at around 1000 Å and the weak C IV line at 1550 Å which is expected to be strong in massive stars (spectral types B2 and earlier) with high metallicity (Rountree & Sonnenborn 1991).

What produces the UV rise?

The numerous papers devoted to the theoretical considerations based on observational constraints mentioned above have given light in unmasking the main contributors to the UV flux in elliptical galaxies. The next few lines list the sources proposed and/or analyzed to date.

i)- Massive hot stars ($T_{\rm eff} \geq 25000$ K) that are part of a minority star-forming Population. Observational data indicate that at least in the two objects observed by HUT massive OB stars do not contribute to the UV flux. NGC 1399 is the galaxy with the strongest UV upturn found to date. Its Far-UV spectral shape and the weak CIV absorption feature at 1500 Å are inconsistent with massive metal-rich OB stars as the source of the UV flux. The HUT spectrum of M31 differs significantly from that of NGC 1399. Again features expected from massive metal-rich OB stars are very weak. The shape of the ISED (Integrated Spectral Energy Distribution) in both galaxies do not match, M31 being hotter for $\lambda <$ 1200 and cooler for longer wavelengths. There have been proposed two distinct populations of low mass stars to produce the UV flux in M31. Recently HST has resolved M31 and found no massive stars, but stars that seem to be P-AGB stars (some of them surrounded by PN).

ii)- Low mass stars at different advanced evolutionary stages

- Post-Asymptotic Giant Branch stars (P-AGB). This type of stars are the most widely discussed in the literature. The 'normal' P-AGB stars are stars with exhausted helium cores evolving to the white dwarf cooling track after the loss of their envelopes at the tip of the AGB. Since P-AGB stars are inevitable products of stellar evolution, their UV flux represents at least a lower limit. It is important to note that the strong decrease of the life span with increasing core mass and hence the UV flux emitted by P-AGB stars will be lower for brighter and more massive objects (important for intermediate-age population rather than for old populations). The mass of these objects depends in turn on the mass-loss at the tip of the RGB which normally is considered as a free parameter in population studies since the underlying physics is poorly known. Observational evidence in favour and against these stars as primary contributors to the UV excess has been published, however, at least for the most UV-bright galaxies these stars cannot account for the bulk of the observed radiation.

- Hot Horizontal Branch stars (HHB) and their progeny, the subdwarf (O, OB, and B), P-EAGB (Post-Early Asymptotic Giant Branch) and AGB-manqué stars. It was until recently when people turn to look at other possible candidates on the basis of theoretical considerations. Indeed, it was confirmed that the lifes of the less massive P-AGB stars were too short to produce sufficient UV flux to account for the strongest UV galaxies. Brocato et al. (1990) and Greggio & Renzini (1990) studied the evolution of stars which suffered different degrees of mass loss at the RG stage. They found that these stars with low enough envelope mass would leave the AGB before reaching the thermally pulsing regime (P-EAGB) or will never reach the AGB stage at all if stronger mass-loss is incorporated (AGB-manqué stars).

iii)- Different kinds of binary systems in which either one component is close to become a WD or a WD component is accreting material and burning nuclear fuel. These scenarios have not been extensively explored. To our knowledge, the only somewhat detailed listing of the possible circumstances in which binary star evolution can result in strong Far-UV emitters has been given by Greggio & Renzini (1990). They proposed the following schemes: a)- post-red giant products of close binary systems in which extreme mass transfer prevents the red giant component from reaching the He core flash; b)- mass transfer binaries in which one star does reach the He flash; c)- white dwarfs burning accreted hydrogen in their outer layers; d)- mergers between low mass white dwarfs forming He-stars.

1.2.2 The age and chemical composition of old stellar systems

For a long time it was thought that the spectroscopic properties of old stellar populations were regulated by one parameter, namely the mean metallicity of the system. In the 70's a new view came into play and the mean age of the system was suggested as a second parameter. At present it is well established that, even if these two parameters were the only ones governing the photometric characteristics of ellipticals, the dissociation of their effects on the ISED represents a difficult task not yet fully overcome Worthey 1992, Faber et al. 1995). Photometric properties of the stellar contents of ellipticals respond in a very similar way to changes in age and metallicity.

It results that young stellar systems of high metallicity mimic the ISED of a less metallic but older system (See figures 1 and 2 of Worthey 1992). The age-metallicity *degeneracy* is estimated to be a 3 to 2 relationship. This is, if two populations have $\Delta\log(\text{age})/\Delta\log Z$=-3/2, then their ISED (and colors) will be nearly the same.

The problem of univokely estimating age and metal content can be tackled with some confidence in globular clusters, provided that a Color-Magnitude diagram can be constructed from the observations of single stars. Nonetheless, there are cases in which a single cluster has quite contrasting age determinations (see Renzini & Buzzoni 1986). For most galaxies stars cannot be resolved, so that we can retrieve information only through their integrated properties.

Many investigations have been directed towards disentangling these age and metallicity effects using different techniques of population synthesis. These techniques are known as "evolutionary population synthesis" (Barbaro and Olivi 1986, Renzini & Buzzoni 1986, Buzzoni 1989) and "optimized synthesis" (O'Connell 1986 and references therein). In many instances these two methods have yielded results in net disagreement.

In view of these age-metallicity degeneracy in broadband colors, we should look into more detail the ISED, i.e. move to higher spectral resolution in search of conspicuous spectral features easily observable also in distant stellar systems. The different sensitivity of the strength of these features to changes in age and metallicity would, in principle, provide a powerful tool for the analysis of the underlying mixture of stellar populations in old stellar systems, and consequently give clues on their evolutionary status.

Narrow band spectral indices have been defined in a wavelength interval from the UV to the IR (Faber et al. 1985; Gorgas et al. 1993; Worthey et al. 1994). Studies in the visible range are of particular importance because this is the region where old stellar populations radiate most of their energy and because it contains the most prominent features in cool star and galaxian spectra. Among the indices in the visible range, Mg_2, which measures Mg b and MgH lines at about 5170 Å, is the most popular one and its relationship with the fundamental stellar parameters has been widely investigated from both the theoretical and observational points of view.

In order to optimize the use of spectral indices in dating stellar systems several authors have abandoned the use of individual indices and defined combinations of them (e.g. Jones & Worthey 1995a, Bressan, Chiosi & Tantalo 1995 and Worthey, Trager & Faber 1995).

1.3 Goals and Description of this Dissertation

Previous sections gave a very general view of some of the current problems associated to old stellar populations. As we shall see below the material regarding the detailed analysis of integrated properties, as treated in this work, is still very preliminary, but conforms a strong base for later detailed studies.

The main objective of the material contained in this dissertation is to offer an alternative approach for the analysis of the integrated spectra of stellar systems. The proposed approach consists on the use of theoretical stellar spectra as templates in the evolutionary population synthesis technique. To attain this goal, several important intermediate steps have to be carefully treated, steps that conform the body of this thesis.

The remainder of this dissertation is composed of four chapters which are interconnected by the leading motivation, but which can be considered as independent entities. For that reason chapters 2 to 5 have their own introductory remarks, and this *introductory* chapter was left to give a more general description of some problems associated to stellar populations.

The contents of this work can be outlined as follows:

Chapter 2 is concerned with some details on the stellar spectrum synthesis technique. Models and numerical codes developed by Dr. R. Kurucz are used to compute a theoretical solar spectrum and to compare it with an observed spectrum (Solar Atlas by J. Brault-see details in Kurucz 1992). Through this comparison we intend to improve the principal agents affecting the spectral line's strengths and profiles, i.e. oscillator strengths and damping constants. The improvement is done by modifying these parameters and re-computing the solar spectrum until a satisfactory match between observed and computed spectra is attained. In this chapter we also present a grid of synthetic spectra computed with the line list based on revised atomic and molecular parameters. This grid represent an important tool to be used not only in populations synthesis, but also in other branches of astrophysics such as the determination of stellar atmospheric parameters.

In chapter 3 we present from both a qualitative and quantitative points of view the relationships between the line strength of important features, measured as spectral indices (Faber et al. 1985) and the stellar atmospheric parameters. The quantitative calibration is done through a multiregression analysis and presented in the form of fitting functions.

Chapter 4 gives a detailed analysis of a sample of SMR stars for which we do a revision of the chemical composition. We selected from the literature and observed at moderate resolution a sample of stars catalogued as SMR. For some of the stars in our sample there were several determinations of metallicity from high resolution spectra. For those stars that were found to have more than one determination of atmospheric parameters (*primary data*) we have selected, by means of a comparison with synthetic spectra, the set of parameters that best fit the observed spectrum. Such comparison was done in the following way: For each star with two or more sets of atmospheric parameters we computed the corresponding synthetic spectra. Then we divided the theoretical spectra by the observed ones and look for the synthetic spectra that produced the smaller dispersion, taking into account that the dispersion is mainly due to the intensity of spectral lines (and hence metallicity). Many stars lack either or both gravity and effective temperature (*secondary data*) so we searched in other sources in the literature or derived the atmospheric parameters from their spectral types to fill up the gaps and proceeded in the same way as with the primary data. The important output of this chapter is the set of revised parameters for some the observed stars.

Chapter 5 is devoted to briefly describe the application of the theoretical grid of spectra into the population synthesis method. A sub-set of isochrones computed by the Padova Group (see Bressan, Chiosi & Fagotto 1994 and references therein) are used to derive integrated spectral indices in simple stellar populations and elliptical galaxies. The approach presented here is still in its early stages, but represents indeed a solid starting point to carry out the *task list* given in chapter 6 to illustrate the major scientific goals in a project that we will attack in the near future.

Chapter 2

Building up a Theoretical Spectral Library

This chapter is devoted to give a simplified description of the necessary steps towards creating a theoretical stellar flux library. The details of some of these steps, particularly those regarding the computation of synthetic stellar spectra, have been described elsewhere (Kurucz & Avrett 1981; Bonifacio 1991; Gulati 1991) therefore, for the sake of completeness, we briefly present here the way to compute a synthetic spectrum with emphasis on the part regarding the description of the atomic and molecular data used in the computations.

A comprehensive spectrophotometric stellar library is an important tool for many branches of astronomy, in particular when it serves as a basis to understand and discriminate the underlying stellar populations seen only through their integrated spectra.

Bica (1992) reviewed spectral libraries of stars and star clusters and the use of these libraries in the context of stellar population synthesis. Over the years numerous stellar libraries, empirical or theoretical, have been used to study the integrated spectra of ensembles of stars.

The justification for the need of a theoretical stellar spectra library is two fold. First, although there are extensive collections of observed spectra (e.g Worthey et al. 1994, Jones and Worthey 1995b), stars with some particular characteristics can be accounted by only through the use of theoretical spectra, for example the metal poor stars of low luminosity or the metal rich stars for which the metallicity (as well as other atmospheric parameters) are still highly uncertain (see chapter 5). Second, an important advantage of theoretical spectra is that they are naturally "labelled" with the atmospheric parameters of the model used to compute them. As we shall discuss in more detail later on, in the case of observed spectra one is forced to label the spectra with the parameters available in the literature or to derive them from observed quantities. This may introduce non-negligible

errors when using these data bases to study the integrated properties of stellar systems.

Theoretical libraries have been built in the past (see Gulati 1991, Gulati, Malagnini & Morossi 1991, 1993 hereafter GMM93, Barbuy, Erdelyi-Mendes & Milone 1992). GMM93 computed a grid of synthetic spectra based on the model atmospheres and codes to compute theoretical spectra developed by Kurucz (1992, hereafter K92), however, both the model atmospheres and numerical codes have been revised and improved, therefore the need to re-compute the spectra and test the new results by comparing them with high resolution, high S/N stellar observations.

We have mentioned before that one of the ultimate goals of the present study is the analysis of absorption spectral features in stars and stellar systems. This analysis is feasible only through the study of high resolution synthetic spectra. The existing libraries of stellar fluxes provided by Dr. Kurucz are computed at a resolution (10 to 25 Å in the ultraviolet and visible respectively) which is suitable for the analysis of the general shape of the spectral energy distributions or to carry out the computation of broad and intermediate band photometric indices, but not for the analysis of absorption spectral features.

The material contained in this chapter was mostly done at the Harvard- Smithsonian Center for Astrophysics in November of 1994. It was later continued in Trieste.

2.1 Spectrum Synthesis: an overview

Much of the study of stellar atmospheres has been done through the analysis of the curve of growth. This method, which gives the equivalent width in terms of the number of absorbing atoms that produce a spectral line, has been widely used because it can provide a quick estimation of stellar parameters from equivalent widths alone. Nevertheless, the curve of growth approach is based on a large number of approximations (see for example Aller 1963) which introduce serious inaccuracies in the results (e.g. Mihalas 1978). An alternative approach for a more careful analysis of a stellar atmosphere is provided by the use of model atmospheres that include the depth-variation of all physical quantities (e.g. temperature and density). This approach is called spectrum synthesis technique[1].

The starting point in this technique is to choose a model that most closely represents an observed spectrum, assuming that the star under study has good preliminary estimates of surface gravity, effective temperature (T_{eff}) and chemical composition.

[1]Spectrum synthesis has actually several meanings depending on the astrophysical context. The definition adopted in this chapter and in chapters three and four, refers to the calculation of a theoretical stellar spectrum. In order to avoid confusion with the spectrum synthesis described in chapter 5, we will always explicitly say synthetic *integrated* spectrum when referring to the output of population synthesis technique

Extensive grids of model atmospheres for cool stars are currently in use (see for example the comprehensive review by Gustaffson & Jorgensen 1994). Among the most used grids of model atmospheres, are those developed by Gustaffson et al. (1975) and Kurucz (1979). Kurucz's grids have proved to faithfully reproduce the spectra of real stars in the visible and ultraviolet spectral regions for early B to K stars (see Malagnini et al. 1992, Morossi et al. 1993; Chavez, Stalio & Holberg 1995).

Kurucz's model atmospheres are continuously upgraded in the treatment of some physical mechanisms (see below) which greatly affect the calculation of surface fluxes. The atomic (and recently also molecular) data is updated with better energy level determinations. The atmospheric parameters coverage of the most recent grid of Kurucz's models (Kurucz 1993, hereafter K93), the one we will use in this work, supersede any of the existing grids and the number of atomic and molecular lines that can be included in the computations is about 5.8×10^7.

The detailed explanation of the physical basics for computing a classical model atmosphere is given in Kurucz (1970, 1979). Here let us just repeat the basic assumptions considered in these computations:

- Plane parallel layers
- non-moving atmospheres: hydrostatic equilibrium
- Steady State
- Horizontally homogeneous atmospheres
- Local Thermodynamic Equilibrium (LTE)
- Convection: Mixing length parameter = 1.25
- Radiative and convective equilibrium
- Line blanketing

Kurucz model atmospheres are now available for a range in temperatures that spans from 3500 to 50000 K, metallicities, [M/H], from -3.5 to +1.0 and surface gravities (log g) from 0.0 to 5.0 dex (see Table 1 of Gustafsson & Jorgensen 1994). As we shall see in following chapters, some of the assumptions written above will prevent us from computing (realistically) models for certain types of stars.

A model provides the temperature and density stratification throughout the atmosphere and the list of atomic and molecular line parameters to calculate the intrinsic spectrum (intensity or flux). This spectrum can be subsequently degraded by including different types of mechanisms that give rise to line broadening (rotation, macroturbulence, microturbulence) or filtered with, say, a gaussian function to simulate an instrumental degradation. After computing a theoretical spectrum for the model one proceeds to test, by comparison with observed spectra, the reliability of the basic physics behind it as well as to interpret the

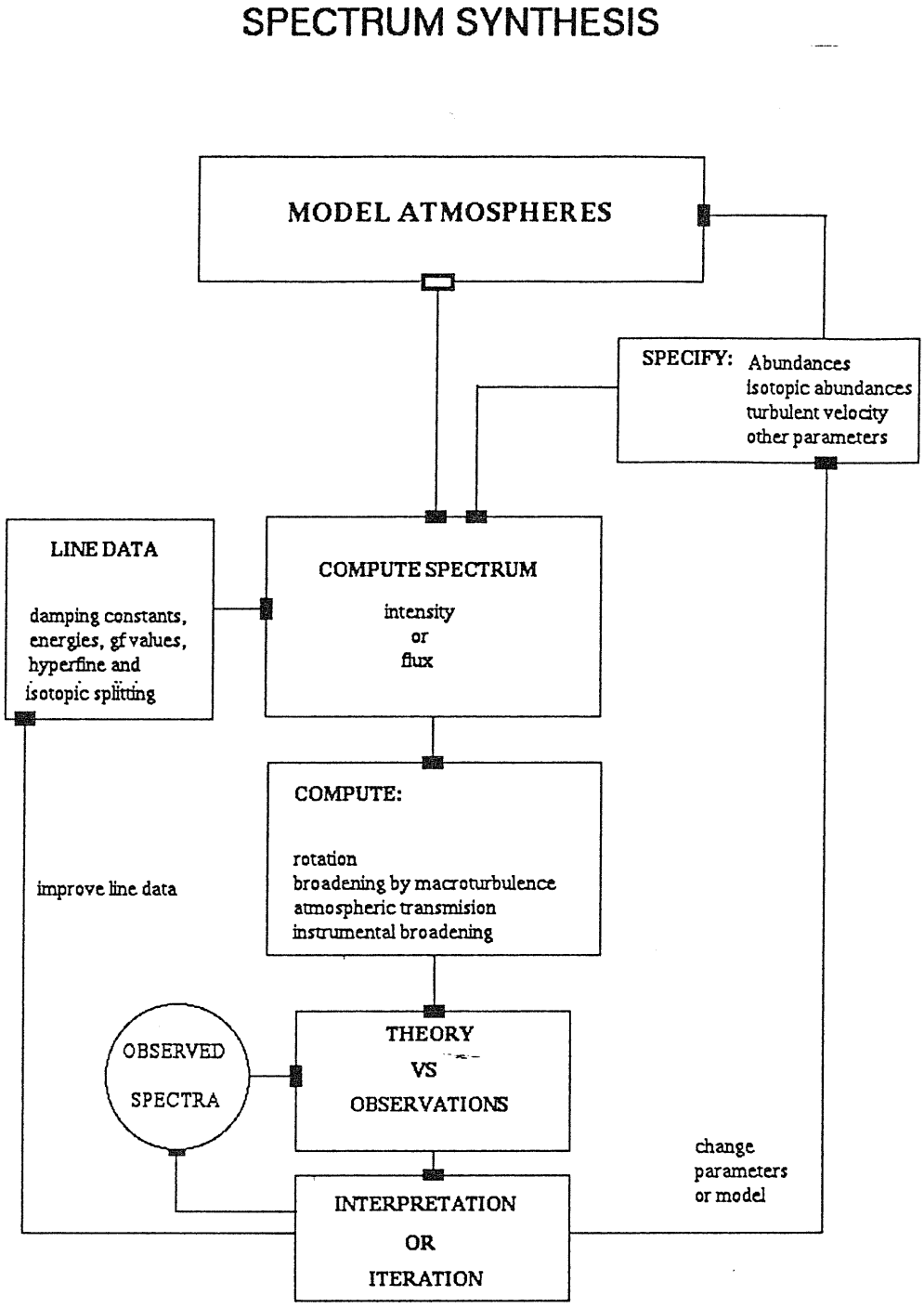

Figure 2.1: Schematic representation of the process of computing a synthetic spectrum

overall physical condition in the atmosphere. The process of computing theoretical spectra is displayed in Fig. 2.1.

Gulati (1991) and Bonifacio (1991) gave a concise description of the spectrum synthesis method from the analytical point of view so we refer the reader to those works. For the interested reader in appendix A we shortly describe the main codes used for computing a theoretical high resolution spectrum.

2.1.1 Recent improvements

The newest grid of Kurucz models (K93) contains a number of improvements and changes with respect to K92 models. Let us only enumerate some of the principal changes:

- New models contain 72 depth points starting at Rosseland optical depth of 10^{-7} instead of 64 starting at 10^{-6}. This improvement removes the abrupt temperature drop that appeared in earlier models, reduces the molecular abundances near the surface, and decreases the central depth of strong lines.
- A bug in the Fe I continuous opacity at low temperatures was present in both the model atmospheres and spectrum synthesis programs. In K93 the bug was corrected.
- The new SYNTHE series of programs to compute synthetic spectra include a detailed treatment of scattering in the source function by default; in previous versions the default was a fast approximation based on a small scattering fraction that led to trouble if scattering was large.

The iron bug would produce an error that correlates both with temperature and abundances. In Figure 2.2a we illustrate the T(τ) structure of the new and K92 model for T_{eff}=4000 K, log g=1.5 and [M/H]=0.0. In Figure 2.2b we show two synthetic spectra computed from the same model, the same set of atomic and molecular lines, but with the old and new numerical codes. After making several tests we realized that the effect of the different T(τ) structure is in general negligible in the visible and that the bug in the iron opacity and the scattering term in the source function produce large differences with respect to previous computations at low temperatures and gravities (Fig. 2.2 represents the case where the largest discrepancies were found).

2.2 The Atomic and Molecular Data

One of the most important ingredients needed in the computation of theoretical spectra is the absorption line list to be considered in the spectral interval of interest. In order to check the reliability of the parameters governing the strength

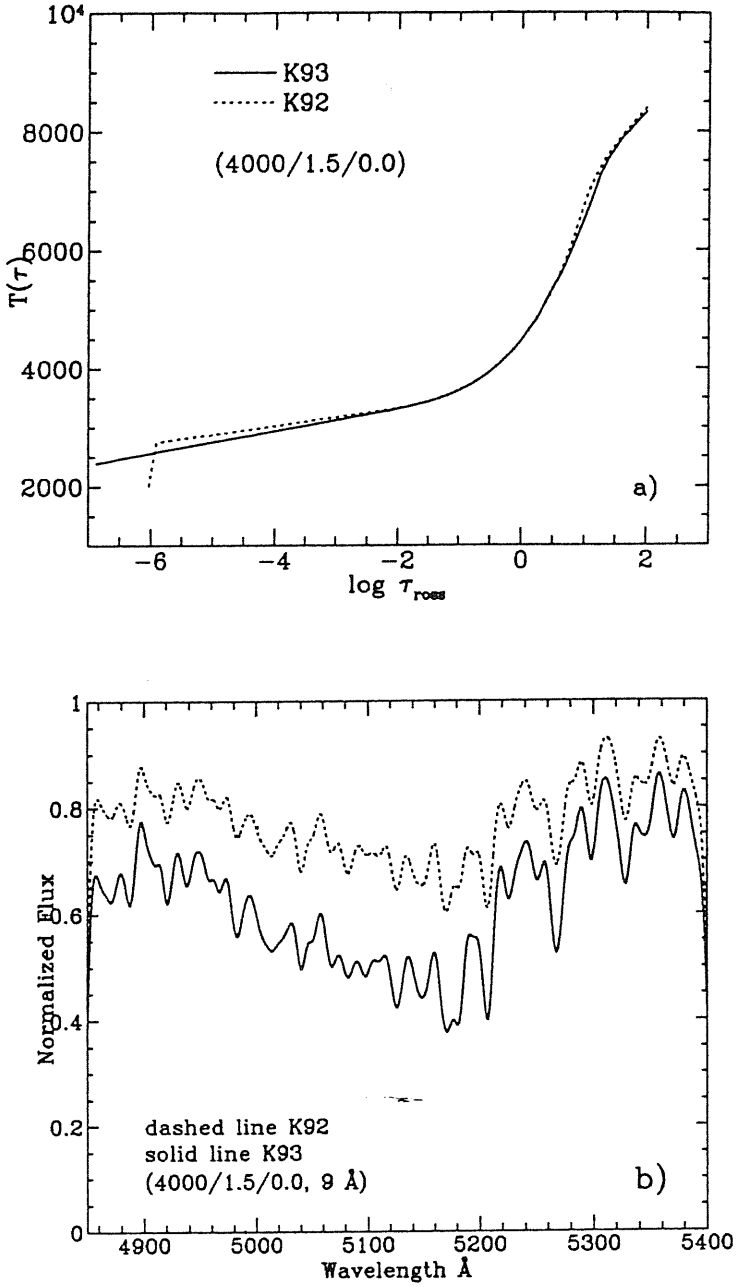

Figure 2.2: a) Differences in the temperature structure of the model atmospheres in the newest model version and K92. b) Synthetic spectra computed from the same model atmospheres and the line list of Gulati (1991), but different numerical codes. The model fluxes have been computed for the following set of atmospheric parameters: T_{eff} = 4000 K, log g = 1.5 and [M/H] = 0.0, and have been convolved with a gaussian profile of FWHM=9 Å.

and the shape of the lines, the line list adopted should be compared with the lines observed in high resolution stellar spectra.

The line list to be included in our computations has been extracted from the most updated atomic and molecular line lists compiled by Kurucz and colleagues. The original lists contain the information of nearly 58 million lines of atoms up to the tenth stage of ionization and of diatomic molecules.

Over 45000 lines for the 4850–5400 Å spectral interval have been taken into account. Molecules considered in our computations are CN, C_2, MgH, SiH and CH, and account approximately for 85% of the lines. As indicated by Kurucz (1995), two calculation have to be done; one for the lines with good laboratory wavelength determinations and one with the lines having wavelengths in the spectral interval of interest from theoretically *predicted* energy levels. The first set of lines is important to preserve the wavelength detail and the second is needed to preserve the spectral energy distribution.

Table 3.1 list the atomic and molecular species and the corresponding number of lines used in our computations. Column one list the element or molecular species. Column 2 indicates the code used in the programs to identify the species. In this code the ionization stage is given by the number after the point; .00 means neutral and .01 once ionized. The third column gives the number of lines. In the last column we tabulate the number of lines that are so weak that they do not play any role in the solar spectrum, but are important in the spectrum of cool stars. The additional line list was derived from a cross-correlation between the line lists currently used by Dr. Kurucz for the analysis of the solar spectrum and the line list used by Gulati (1991). In Table 2.2 we tabulate the *predicted* lines considered, all of them molecular.

Before computing a synthetic spectrum with the material described so far, there is one important factor to be taken into account; the limited accuracy of the agents affecting the line profile and strength. Kurucz (1995) pointed out "*very few gf values are known more accurately than 1%, few of them are known better than 10% and the vast majority only to within a factor of two. The accuracy of the damping constants goes from 10 to 1000%*". We will follow the left branch of figure 2.1 to improve, when possible, the current estimates of these parameters, particularly in strong lines. In order to carry out the improvement we have to specify which observed spectrum we will use and the corresponding starting model. The best laboratory for testing the line data is the Sun because there are high resolution, high signal-to-noise observations. The next two sections describe the solar model adopted and the procedure followed to modify the line parameters.

Table 2.1: Atomic and molecular species included in the computations

atom or molecule	code	number of lines	additional lines	atom or molecule	code	number of lines	additional lines
H	1.00	1		Ag	47.00	1	
He	2.00	3		Cd	48.00	1	
	2.01	2		Ba	56.00	5	
Li	3.00		2		56.01	2	
C	6.00	160		La	57.00	35	1
	6.01	30			57.01	39	
N	7.00	157		Ce	58.00	257	
O	8.00	26			58.01	60	
Na	11.00	5		Pr	59.00	37	
Mg	12.00	7			59.01	61	
Al	13.00	4		Nd	60.00	72	
Si	14.00	53			60.01	97	
	14.01	17		Sm	62.00	48	7
P	15.00	28			62.01	62	
	15.01	5		Eu	63.00	10	37
S	16.00	3		Gd	64.00	100	1
	16.01	10			64.01	52	
Cl	17.00	1		Tb	65.01	4	
K	19.00	18		Dy	66.00	27	2
Ca	20.00	106			66.01	27	
	20.01	27		Ho	67.00	6	1
Sc	21.00	141	28	Er	68.00	24	
	21.01	9	9		68.01	30	
Ti	22.00	609	61	Tm	69.00	3	9
	22.01	52	54		69.01	25	
V	23.00	406	75	Yb	70.00	9	
	23.01	121			70.01	18	
Cr	24.00	753		Lu	71.00	7	3
	24.01	146			71.01	1	
Mn	25.00	284		Hf	72.00	28	
	25.01	33			72.01	14	
Fe	26.00	862		Ta	73.00	62	
	26.01	508			73.01	2	
Co	27.00	433		W	74.00	60	
	27.01	33			74.01	8	
Ni	28.00	218		Re	75.00	20	
	28.01	72		Os	76.00	31	
Cu	29.00	18		Ir	77.00	12	
Zn	30.00	1		Pt	78.00	7	
As	33.00	7		Tl	81.00	1	
Rb	37.00		8	Pb	82.00	2	
Sr	38.00	15		Th	90.00	33	28
	38.01	2			90.01	85	
Y	39.00	30		U	92.00	2	20
	39.01	13			92.01	40	
Zr	40.00	57		CH	106.00	609	
	40.01	8		MgH	112.00	1195	2045
Nb	41.00	85		SiH	114.00		204
Mo	42.00	177	3	C_2	606.00	1810	
Ru	44.00	64		CN	607.00	1122	
Rh	45.00	36					
Pd	46.00	9					

Table 2.2: Molecular species in the auxiliary line list

molecule	code	number of lines	additional lines
CH	106.00	1867	102
MgH	112.00	6148	7175
SiH	114.00	972	2475
C_2	606.00	9282	
CN	607.00	13251	

2.3 The Solar Model

There are two types of solar models that can be used to carry out the comparison with the observed solar spectrum. These two types are called "semi-empirical" and "theoretical" models. Semi-empirical models are constructed in such a way that the temperature structure adopted permits to reproduce the observed solar intensity, and generally include the chromosphere and its effects (chromospheric heating) on the upper layers of the photosphere. These models consider a turn over in the temperature structure after reaching a minimum temperature (T_{min}) towards the surface due to the presence of the chromosphere. It also includes a depth dependent microturbulent velocity.

On the other side there are several computed solar models, which as the rest of the models in Kurucz's grid, have the same microturbulent velocity throughout the atmosphere and the temperature decreases monotonically with depth.

Figure 2.3 displays the $T(\tau)$ structure of the theoretical solar model of Kurucz (1993) and the semi-empirical solar model of Maltby et al. (1986).

Several tests we have done revealed that the high temperatures at the surface in the semi-empirical solar model by Maltby et al. (1986) produce emission in the computed cores of the strongest lines. This emission is not present in the observed solar spectrum.

One way to overcome this difficulty is to modify one of the parameters which modulate the contribution of scattering to the formation of a spectral line. This parameter (in the numerical codes written as *RHOXJ*) is the mass-depth variable, ρ_x, above which the line is formed in scattering so that the source function and the mean intensity are equal, S=J. This modification keeps the line from seeing the local temperature. The starting value *RHOXJ* was 0.01 and it was varied until the emission went away for several lines. We found that the stronger the line (with emission) the higher the value of *RHOXJ* needed to remove the emission. For the case of the strong Mg lines at 5170 Å, *RHOXJ*=1.0 removes completely the emission, but the line saturates and more important, the profile near the core is modified in a non negligible way as shown in Fig. 2.4. Note also in this figure that the core of the nearby lines decreased. This may produce little effects in the

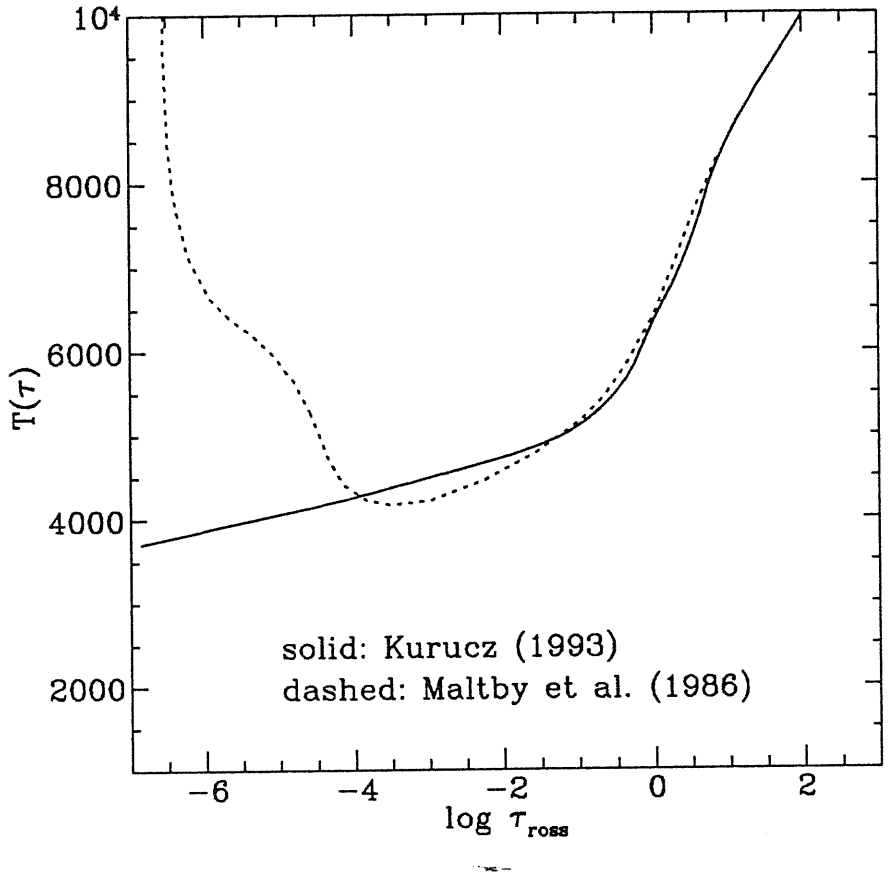

Figure 2.3: Temperature variation in the solar atmosphere as considered by the K93 theoretical model (solid line) and a semi-empirical one (Maltby et al. 1986, dotted line). Note in the semi-empirical model the rise in temperature above τ_{ross}=2×10^{-4} (log τ_{ross} = -3.6).

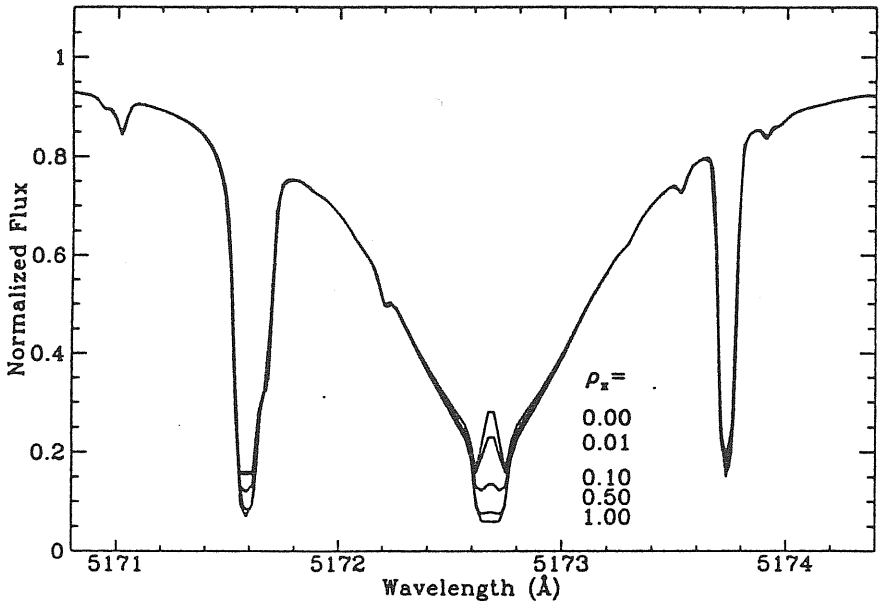

Figure 2.4: Effects of changing the mass-depth variable to eliminate the emission in the strong Mg feature at 5170 Å.

solar spectrum, but important ones in cooler stars where the line is stronger.

The theoretical solar model do not show this problem. It seems that the low temperatures at the surface in this model mimics the NLTE effects that are expected to be present in strong lines due to their sensitivity to the solar chromosphere. No differences between semi-empirical and theoretical models in weaker lines.

In brief, we have decided to use theoretical solar model for the comparison with the observed solar spectrum because:

- The synthetic solar spectra computed from this model do not show emission in strong lines, in agreement with the observed spectrum. Treatment of these lines in NLTE would be important.

- The temperature structure of the model is similar to the one considered in the rest of the models in Kurucz's grid.

We would like to remark that the comparison between observed and synthetic solar spectra has been done in the past to test and improve line parameters. However, every time an improvement is included in the starting model atmospheres or in the numerical codes a new test is required.

2.4 Observed and Computed Solar Central Intensity Spectrum

In order to check the reliability of the theoretical material, we have computed the solar central intensity spectrum and carried out a line by line comparison with intensity spectrum of the solar disk center observed by J. Brault, and reduced and digitized by Kurucz (Kurucz 1991).

The model we have used to carry out the comparison has the following atmospheric parameters: T_{eff}=5777, log g=4.43770 and element abundances from Grevesse and Anders (1989). The micro and macro turbulent velocity values adopted are 1 and 1.5 km s^{-1} respectively (see Thévenin 1989 and references therein). The spectrum was computed at a spectral resolution of $\lambda/\Delta\lambda$ =522,000, in correspondence to the observed spectrum.

2.4.1 Adjusting the line parameters

The main physical agents affecting the structure of the line absorption coefficient are:

- The damping constant for natural broadening
- Stark and van der Waals damping constants
- Oscillator strengths (log *gf* values)

The fitting is a trial and error procedure (see for example Peterson et al. 1993) in which one has to modify the line parameters and compare the spectra until a satisfactory match has been obtained. Gulati (1991) presented the line fitting in the region 4900-5400 Å only where the spectral bands of the Mg_2 index are defined. We have worked in this same region to account for the bands defining 4 more magnesium and iron indices (Mg_b, Mg_1, Fe5015 and Fe5270) plus some improvement in the Mg_2 and Fe5335 bands, since the previous fitting was done using the semi-empirical solar model.

We started by modifying the log *gf* values for the strongest lines and then move to the weakest. While for the Sun and solar like stars the inclusion of these weak lines (say, of residual intensity ≥ 0.9) are not expected to contribute substantially to the indices at the resolution at which the observations are available, for cooler stars they might be important so we have tried to fit even this weak lines. In general we have considered a satisfactory fitting in the log *gf* values when the difference in residual intensity between the observed and theoretical spectrum was less than 0.05.

Regarding the damping constants, van der Waals pressure broadening affects most of the lines specially for cool stars while Stark broadening is more important in hot stars (Quadratic) or affect only the hydrogen lines (Linear). We have modified the van der Waals damping constant to match the line wings of the strongest lines. Very few weak line constants were modified since in most of the

cases weak features in the solar spectrum correspond to blends and even at the very high working resolution it was not possible to distinguish the lines forming the blends.

A total of about 2000 modifications were performed on the main parameters of some 1500 lines. Figure 2.5 shows the the regions around a strong magnesium feature at 5170 Å (panel a) and iron and chromium features at 5330 Å (panel b). The thick solid line corresponds to the observed solar central intensity spectrum, the dotted line indicates the model spectrum without modifying the line parameters and the thin solid line after modifications have been made. In general lines of Cr I needed a slight correction in wavelength. We have done this manually, but it is recommended to revise the energy level giving rise to this wavelength problem.

In order to illustrate the importance of these corrections, in figure 2.6 we show two histograms of the differences, computed minus observed spectra (both normalized to the continuum), before and after making the modifications of the line parameters. The spectra were rebinned the a wavelength step of 2.5 Å.

The standard deviation of the distribution decreased by 30% from 0.09 to 0.06 in the modified line list. The negative residuals below the -0.2 level that appear in the unmodified list histogram are no longer present in the histogram after the modifications. Negative residuals correspond to spectral lines in excess (or stronger) in the theoretical spectrum, thus, these residuals can be reduced by properly modifying the log *gf* values.

On the other side, positive residuals indicate lines which are weaker in the theoretical spectrum. Again, the residuals can be reduced by changing the log *gf* values, but only if the line in question has been identified. In some cases it was not possible to identify the line(s). As an example we see the large positive residual at the +0.5 level. It is worthwhile to mention that there is little room for further improvement in our line list because the largest differences in the modified list histogram correspond to unidentified lines. This will have important implications in the calculation of spectral indices presented in the next chapter where a more quantitative comparison between observed and computed solar spectra is given.

2.5 The new grid of synthetic Spectra

We have computed nearly 700 synthetic spectra covering the effective temperature range between 4000-6000 K at a step of 250 K plus the spectra for 7000 and 8000 K. Surface gravity from 1.0 to 5.0 dex at a step of 0.5 dex and the following metallicities: [M/H]=-1.0,-0.5, 0.0, 0.1, 0.2, 0.3, and 0.5. For [M/H] $\geq$ 0.0 the spectra have been computed considering finer steps in metallicity than in previous theoretical grids because such results will be used to give insight on a long standing problem regarding absolute metallicity scale of the so-called super-metal rich stars to be discussed in chapter 4.

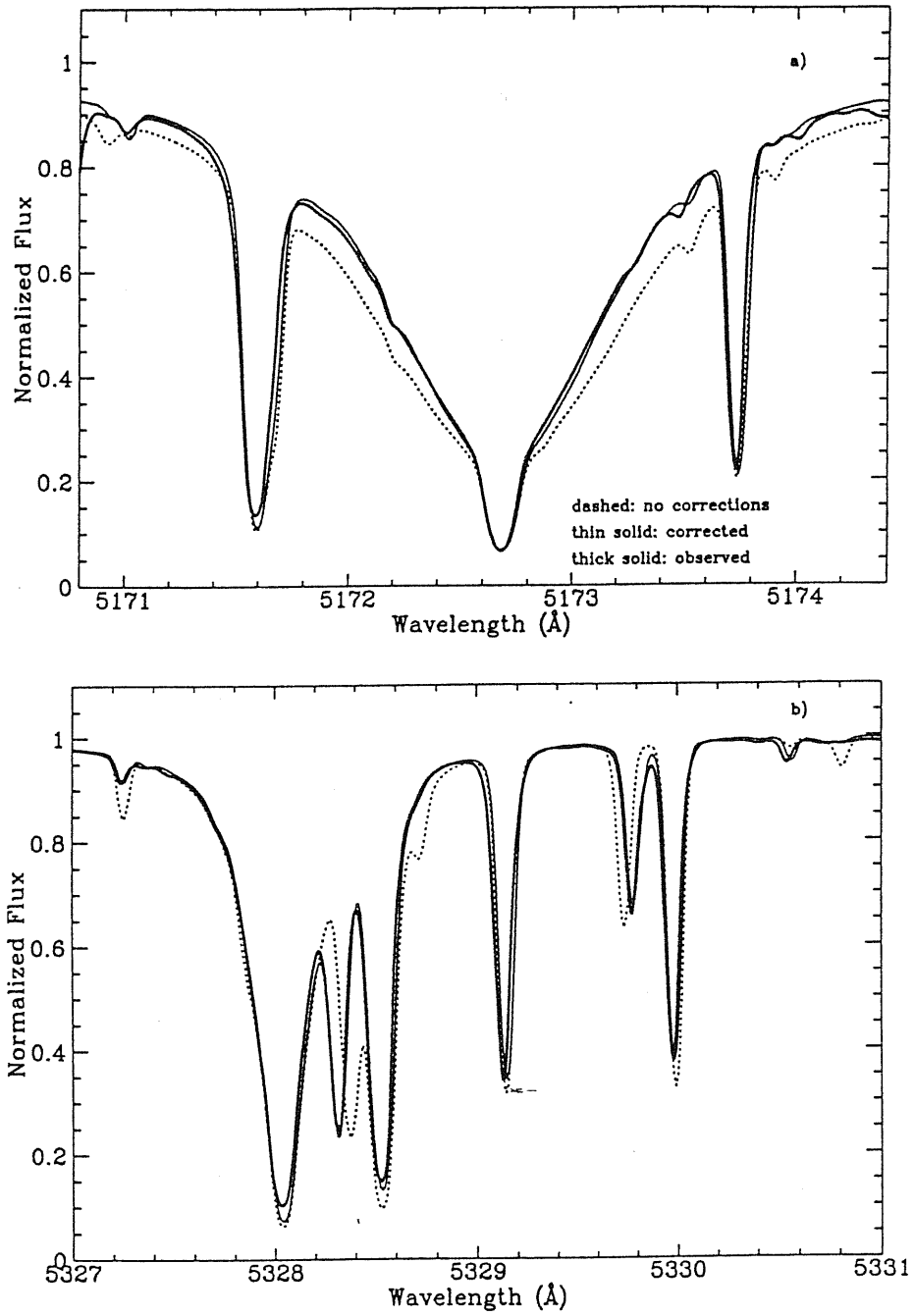

Figure 2.5: a)- Magnesium feature in the interval 5171–5174 Å. b)- Iron and Chromium features in the region 5327–5331 Å. In both panels the thick solid line corresponds to the observed spectrum and the thin solid and dotted lines indicate the theoretical solar intensity spectra computed with and without adjusting line parameters, respectively.

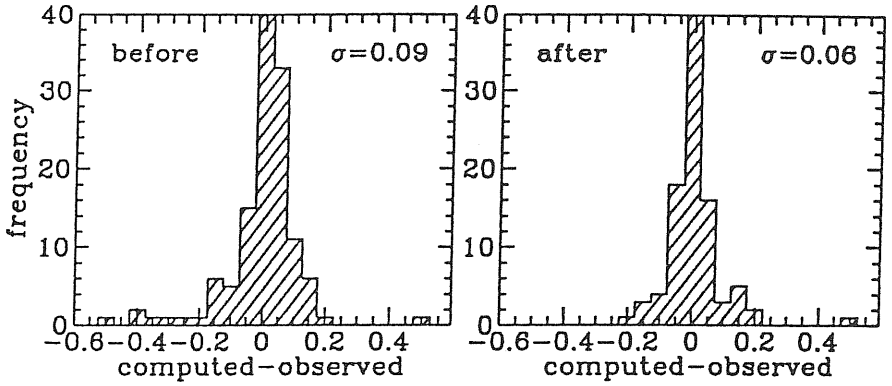

Figure 2.6: Histograms of the differences between the computed spectrum and the observed solar central intensity spectrum, before and after performing the modifications to the line parameters.

The main computational characteristics of the synthetic spectra are the following:

1.- microturbulence velocity $\xi = 2$ km s^{-1}

2.- resolving power $(\lambda/\Delta\lambda) = 250{,}000$

3.- rotational velocity of 0 km s^{-1}

Two important issues that have to be taken into account are:

i)- The fact that the assumptions of plane parallel atmosphere and hydrostatic equilibrium prevent us from computing models for supergiant stars with gravities in the range log g=0.0-1.0.

ii)- Triatomic molecules are not considered here and more over, since the opacity for TiO is still of low quality (Kurucz 1995), models (and synthetic spectra) for M type stars cannot be computed realistically. According to Bell & Gustaffson (1989), below 4000 K the TiO molecule becomes one of the most important contributors to opacity.

The grid presented here is, to our knowledge, the most comprehensive ever computed at high resolution. The applications of the grid of synthetic spectra described above is multiple. Two of these applications will be implemented in this dissertation. On one side, in the context of stellar populations it provides an alternative approach in which complete control on the stellar atmospheric

parameters is gained. The fact that the spectra are computed at high resolution permits to compute spectral indices (Faber et al. 1985) widely used in population synthesis and investigate in detail their behavior in terms of the atmospheric parameters. By properly degrading the synthetic spectra one can match high or low resolution observations.

On the other side, the spectra can be a valuable tool for deriving stellar atmospheric parameters (often ill determined) of stars through the comparison with their observed spectra (at high or low resolution). Quantitative methods has been described for example in Malagnini & Morossi (1983), Thévenin & Foy (1983), Laird (1985) and Cayrel de Strobel et al. (1992).

The grid of synthetic spectra just presented will be soon available in a CD-ROM (Malagnini, Chavez & Morossi 1995).

Chapter 3

Iron and Magnesium Indices: The calibration

Narrow band spectral indices computed from intermediate and low resolution spectra provide a powerful tool for the study of the integrated spectra of ensembles of stars in the Galaxy and in other galaxies.

The application of a wide variety of indices in the study of stellar populations has led to a deeper understanding in the relative contributions of different types of stars to the composite spectrophotometric characteristics of globular clusters, and the most probable combination of stellar populations that give rise to the observed integrated properties of external galaxies.

We have stated in the introductory chapter that one of the leading objectives in the study of absorption line indices is to get a useful combination of the spectral indices that permits to single out the effects of the different agents governing the characteristics of an integrated spectrum, particularly to dissociate the effects of metallicity from those of age (Jones & Worthey 1995a; Bressan, Chiosi & Tantalo 1995), effects that cannot be disentangled from photometric information alone.

The starting step before using spectral indices in the study of stellar populations is to investigate and determine the relationship between the indices and stellar atmospheric parameters. These investigations have been carried out from the analysis of both observed spectra (Faber, Burstein & Dressler 1977; Faber et al. 1985; Buzzoni, Gariboldi & Mantegazza 1992; Gorgas et al. 1993; Worthey et al. 1994-hereafter WFGB94; Buzzoni, Mantegazza & Gariboldi 1994;) or by using model atmospheres to calculate theoretical spectra (Mould 1978; Barbuy 1989, 1994; Gulati, Malagnini & Morossi 1991; GMM93; McQuitty et al. 1994). Much of the material found in the literature has concentrated in one index, Mg_2, mainly because of its potential as a metallicity indicator and because it measures the most prominent feature in the optical spectra of normal galaxies and Galactic cool stars.

Buzzoni, Gariboldi & Mantegazza (1992) carried out the quantitative calibration of the Mg_2 index and studied the dependence of the index in terms of stellar atmospheric parameters. Their stellar data base, after normalization to the standard (Lick) system (see below) was later applied to population synthesis (see chapter 5) to study the effects of changes in the initial mass function (IMF), age and metallicity on the integrated indices of simple stellar populations. Their analysis was later expanded to include iron indices plus Hβ (Buzzoni, Mantegazza & Gariboldi 1994).

Among the empirical libraries of stellar spectra and indices, the most extensive to date is the one by WFGB94. It is convenient to spend a few words to summarize this work: their data base contains about 460 stellar spectra in the 4000-6400 Å region and complement the material catalogued by Faber et al. (1985), and Gorgas et al. (1993). The resolution of the spectra was estimated to be 9 Å.[1] They present a collection of 21 absorption spectral indices that conform the Lick system, 11 of which were firstly defined by Faber et al. (1985) and a set of 10 new indices. The indices were calibrated through multivariate polynomial fitting functions giving the relationship between each index and the stellar atmospheric parameters. The parameters assigned to each index were obtained from the literature or derived from observable quantities available, such as the *V-K* color for deriving effective temperature.

Theoretical work initiated by Mould (1978) and continued by Barbuy (1989, 1994), Barbuy, Erdely-Mendes, & Milone (1992) and GMM93 has complemented and sometimes substituted empirical ones. It is important to stress that the main advantage of using theoretical calibrations relies on the fact that synthetic spectra can be computed for almost any combination of atmospheric parameters allowing the inclusion of poorly observed stellar types. In addition, the set of atmospheric parameters for each synthetic spectrum is directly attached from the parent model while for empirical calibrations the parameters are generally extracted from various sources in the literature and quite often several different determinations are available for a single star.

In the previous chapter we have computed an extensive grid of synthetic spectra using the updated material provided by Dr. R. Kurucz. The grid coverage in parameter space is the largest so far computed (nearly 700 spectra). In this chapter we present the grid of new spectral indices and comparison of the new Mg_2 indices with previous theoretical computations based on Kurucz's models and recent empirical calibrations. The core of this chapter is presented at the end where we illustrate qualitatively and quantitatively index strengths as functions of effective temperature, surface gravity and metallicity. After Gorgas et al. (1993) and WFGB94 polynomial fitting functions are used to establish the parameters-indices relationship.

The following sections deal with the computation of the indices in the spectral

[1]The reader will find in this chapter that the theoretical spectra have been convolved with a gaussian profile of FWHM=9 Å or rebinned to have a wavelength step of 0.83 Å. These choices respond to the characteristics of the empirical data of WFGB94 and the observational material presented in chapter 4.

region we have synthetised. We start from the indices definitions and proceed to compute indices from solar spectrum to estimate quantitatively the effects on the indices of the residuals described in section 2.4 of previous chapter. We then explore the effects of broadening in the form of microturbulence and instrumental response in the Sun and a model for a cooler star. After these preliminary tests we compute indices for all the synthetic spectra in our grid.

A final remark. We partially transcribe here the paper by Chavez, Malagnini & Morossi (1995). This paper has been appended at the end of this dissertation.

3.1 Spectral index definitions

We have followed the definition given by Worthey (1992) and WFGB94, but used the revised bands extrema from the latter reference. An index is measured according to the following procedure. Two *pseudo*continua are defined on either side of the central bandpass which includes the feature(s) to be measured. The average flux on these side bands, F_1 (red) and F_3 (blue), is interpolated to the midpoint of the central bandpass. The difference between the interpolated *pseudo*continuum and central bandpass flux, F_2, defines the index. In Figure 3.1 we show a synthetic spectrum for the model with T_{eff}=4000 K, log g = 1.5 and [M/H]=+0.0. The spectrum has been convolved with a gaussian profile of FWHM = 9 Å. The three bands defining the Mg_2 index and the pseudocontinuum are superimposed to the spectrum.

If the index measures an equivalent width (in Å) then its analytical description will be given by

$$Index(EW) = \Delta\lambda \left[1 - \frac{F_2}{F_1 + (F_3 - F_1)B}\right] \tag{3.1}$$

and if the index is measured in magnitudes then

$$Index(mag) = -2.5log\frac{F_2}{F_1 + (F_3 - F_1)B} \tag{3.2}$$

where the factor B depends on the bands defining each index.

The wavelength interval covered by our grid of synthetic spectra permits us to calculate 6 of the 21 indices defined by Faber et al. (1985) and WFGB94. This indices are listed in Table 3.1 where columns (1) to (5) give the name of the index, the feature(s) it measures, the bandpasses that define the index and whether it is an equivalent width or measured in magnitudes. In order to compute the indices from the grid of synthetic spectra presented in the previous chapter, we followed the relationships described above.

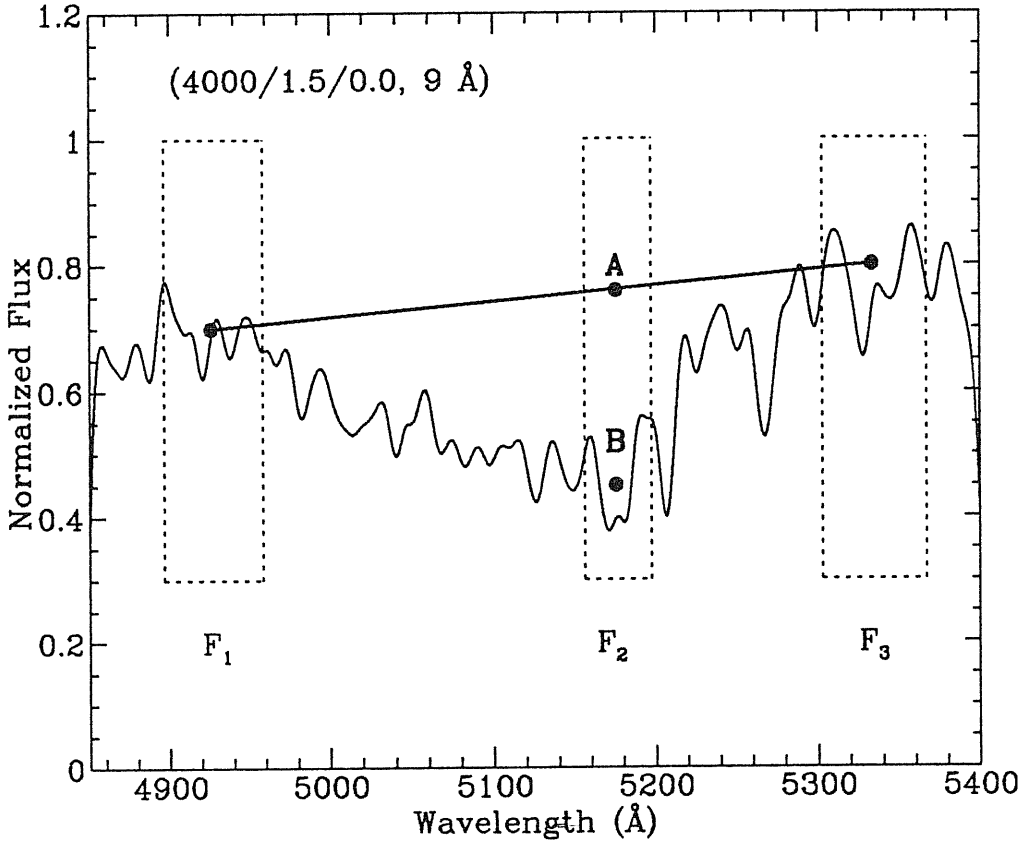

Figure 3.1: Definition of a spectral index. The three bands defining the Mg_2 index are shown inside the dotted boxes; the straight solid line represents the pseudo-continuum. An index is measured by comparing the flux in the pseudocontinuum (A) and the average flux in the central bandpass (B).

Table 3.1: Index definitions

Index	Features Measured	Index Bandpass	Continua Bandpasses	Units
Mg_1	MgH, Fe I, Ni I	5069.125-5134.125	4895.125-4957.625	mag
			5301.125-5366.125	
Mg_2	MgH, Mg_b, Fe I	5154.125-5196.625	4895.125-4957.625	mag
			5301.125-5366.125	
Mg_b	Mg_b	5160.125-5192.625	5142.625-5161.375	Å
			5191.375-5206.375	
Fe5015	Fe I, Ni I, Ti I	4977.750-5054.000	4946.500-4977.750	Å
			5054.000-5065.250	
Fe5270	Fe I, Ca I	5245.650-5282.650	5233.150-5248.150	Å
			5285.650-5318.150	
Fe5335	Fe I	5312.125-5352.125	5304.625-5315.875	Å
			5353.375-5363.375	

3.2 Spectral indices for the Sun

We have seen in section 2.4 of previous chapter the importance of working on the atomic and molecular line list before using it to compute synthetic spectra. In this section we illustrate the same results more quantitatively. We have computed two solar central intensity spectra using the starting model as in section 2.4, and the same computational characteristics, this is, spectral resolution of 522,000, macroturbulence of 1.5 km s^{-1} and microturbulent velocity of 1.0 km s^{-1}. The only difference between the spectra is the input line list used in the computations. In one case the unmodified line list was used while in the other, a line list with corrections included. The spectral indices derived from these spectra are listed in Table 3.2. Columns 2 and 3 give the indices using the line list before and after the corrections. As a reference we tabulate in column 4 the indices computed from the solar observed spectrum (Kurucz 1991). In column 5 we list the residuals obtained by subtracting computed (with modified list) minus observed indices and in column 6 the RMS error per observation for stars as reported in WFGB94.

The improvement is clear in all but one of the indices, Fe5015. A comparison between columns 5 and 6 of Table 3.2 yields the following results. For Mg_1, Mg_2 and Fe5270 our residuals are about one half of WFGB94's RMS errors, while for Fe5335 is less that one fourth. This result greatly favours the use of our line list for the computation of synthetic spectra and spectral indices.

Regarding Fe5015, it appears that before corrections the index was in good agreement with the observed one. However, the reason for this result is most probably the fact that in the spectral region defining this index, numerous lines are predicted in excess by the models or, conversely, present in the solar observed

Table 3.2: Spectral Indices for the Sun

Index	Without Corrections	Modified List	Observed	Δ(Index)	RMS WFGB94
Mg_1	0.195	0.015	0.011	+0.004	0.007
Mg_2	0.146	0.130	0.124	+0.006	0.008
Mg_b	3.445	3.017	3.061	-0.042	0.23
Fe5015	4.257	3.701	4.316	-0.615	0.46
Fe5270	2.625	2.356	2.485	-0.129	0.28
Fe5335	2.673	2.114	2.183	+0.069	0.26

spectrum, but not accounted by the models. These features will compensate each other when computing the index when using the unmodified line list. In the modified list we have eliminated all non-observed features in such a way that when calculating the residual solar spectrum (theoretical minus observed spectra normalized to the continuum) negative residuals rarely exceed 0.2. This situation is clearly displayed in Figure 3.2. Both observed and theoretical spectra were rebinned to have a step in wavelength of 0.83 Å. Note in this figure that the largest positive residual (0.5) lies in the feature bandpass of Fe5015 while the region covered, for example, by the Fe5335 index, residuals are very small. A positive residual would imply a stronger feature in the theoretical spectrum and therefore a grater index in agreement with our measurement reported in Table 3.2. The Fe5015 index will not be included in further analysis in this thesis.

3.2.1 Dependence of solar indices on microturbulence

Although there is still debate on what microturbulence, ξ, assign to a solar model (if considered constant), it might be important to address the question of the effects of ξ on the spectral features we measure. Barbuy (1994) claims that the effects of ξ in the computations of the indices are not negligible and assigned a value of $\xi = 1.0$ km s^{-1} for stars with gravities log g ≥ 2.0 and $\xi = 1.8$ km s^{-1} for stars with log g < 2.0.

We have computed the grid of synthetic spectra from model atmospheres all of which consider $\xi = 2$ km s^{-1}. Therefore, it is necessary to quantify these effects and give an estimate of the corrections that would be needed for the grid of indices presented in this chapter.

We computed the solar central intensity spectrum considering $\xi = 0.0$, 0.5,

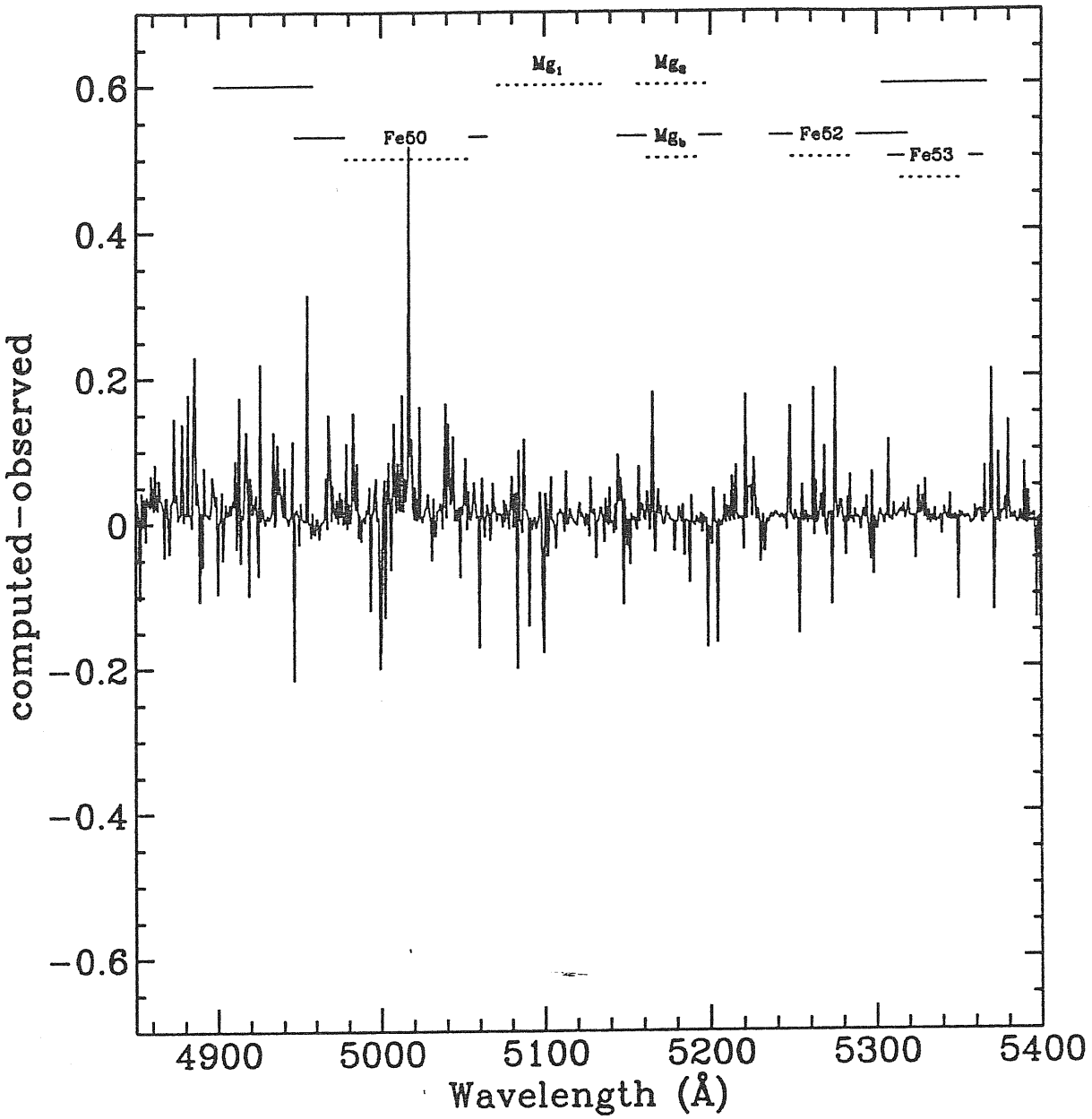

Figure 3.2: Differences between the computed and observed solar spectra. Both spectra were normalized to the continuum. Fluxes are given at a wavelength step of 0.83Å. Note that the largest positive residuals appear in the region where the index Fe5015 is defined.

1.0, 1.5 and 2.0 km s^{-1}. The results for the indices measured as equivalent widths and those measured in magnitudes are displayed in Figure 3.3

From these figures it is evident that all indices but one, Mg_b, increase with increasing microturbulent velocity. Error bars for each index correspond to the values given in column 5 of Table 3.2. Assuming that the real stellar ξ has a value located somewhere in the interval 1-2 km s^{-1} depending on the surface gravity, -(and assuming that these differences will be the same at low temperatures)-, we can safely say that only slight correction would be necessary to the data presented here.

3.2.2 Dependence of solar indices on instrumental profile

Another important test to carry out is to see the variation of stellar indices with the instrumental response. This step is necessary if we want to properly compare synthetic spectra and features measured from them with observations. This is also particularly important when using stellar templates (observed or theoretical) to study integrated spectra of galaxies, spectra intrinsically degraded due to the velocity dispersion of the components.

We have convolved the solar central intensity spectrum presented in previous sections and the spectrum for the model 4000/1.5/0.0 with seven different gaussian profiles. We chose the 4000/1.5/0.0 model in order to also explore the effects in the coolest edge of our grid. The 10 panels displayed in Figure 3.4 summarize the behavior of five spectral indices with respect to the FWHM of the gaussian profile used to convolve the spectra, in the solar (top five panels) and 4000/1.5/0.0 models (lower panels). In general the behavior is similar in both models, but note that the differences of the indices computed from non-degraded spectra and those computed from the spectra convolved with the 11 Å profile, are larger in the 4000/1.5/0.0 model. We also note that the indices defined with the broadest bands turned out to be less affected by the instrumental profile.

3.3 Comparison with previous theoretical grids

This and next section are based on results reported in Chavez, Malagnini & Morossi (1995). Having in mind that improved model atmospheres and numerical codes yield better estimations of all indices for the Sun, we present here a detailed analysis for Mg_2, which is the index most thoroughly studied. Figure 3.5 shows the comparison of GMM93 results with the present ones in 9 panels, each panel refers to one gravity and one metallicity.

The general trend of the differences between the two sets of data, illustrated in this figure, is the following: (i) new Mg_2 indices tend to be higher than in GMM93 at low temperatures and gravities, and at high metallicities; (ii) the temperature above which old and new results do not differ significantly, irrespective of gravity,

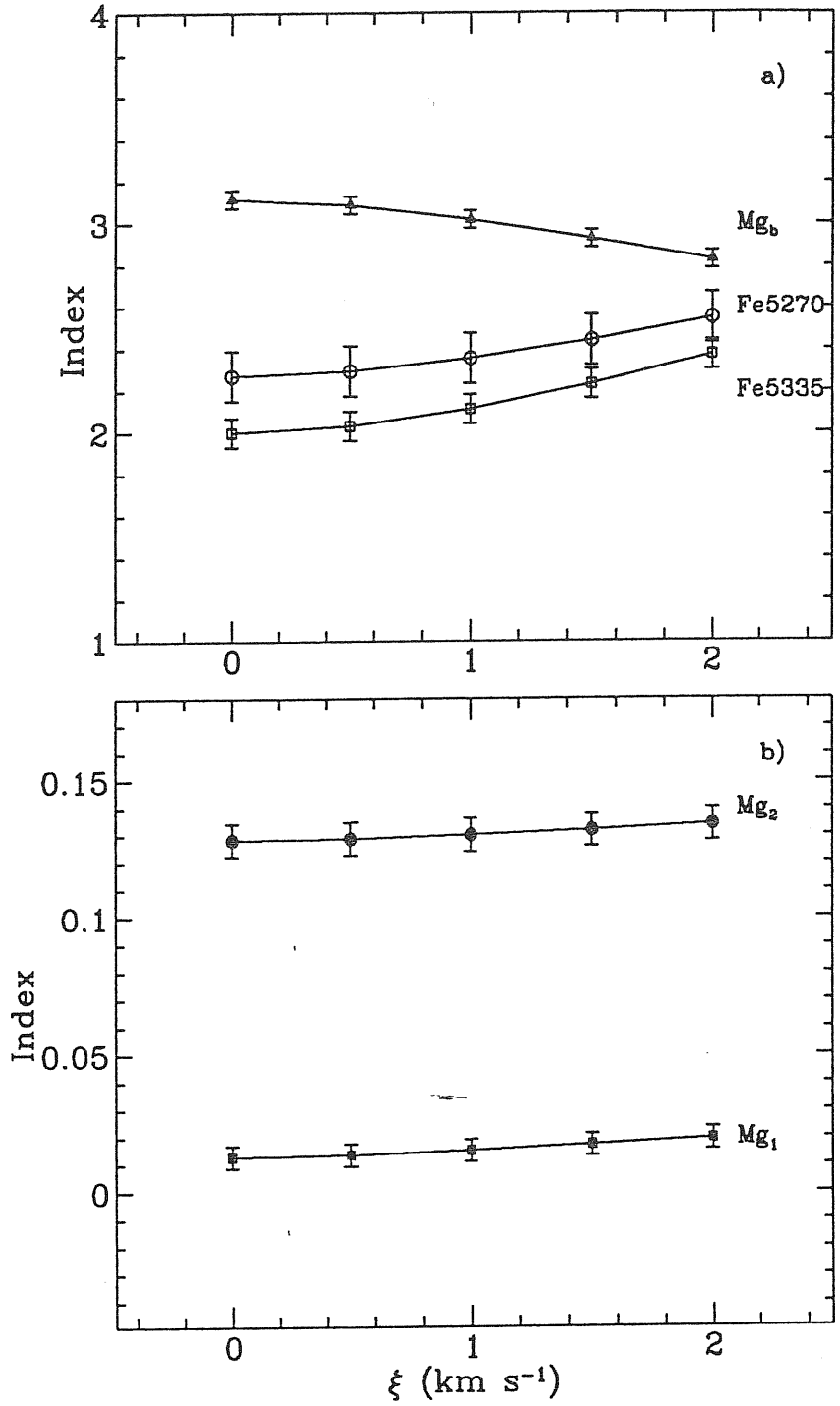

Figure 3.3: Spectral indices from the solar spectrum as a function of microturbulent velocity, ξ.

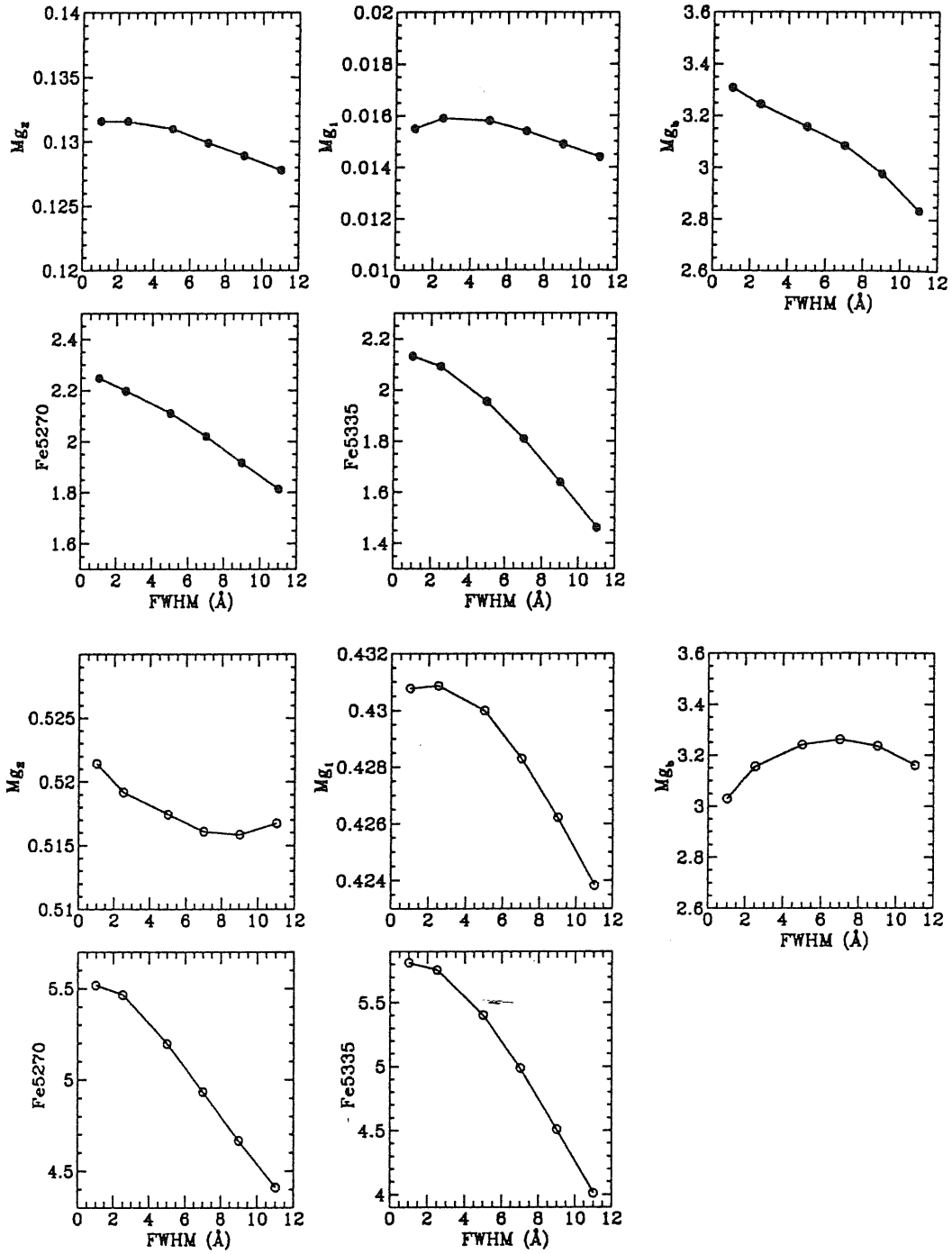

Figure 3.4: Trend of the indices in terms of the FWHM of the gaussian profile used to convolve the solar (filled dots) and 4000/1.5/0.0 (empty dots) models. Note that Mg_1 and Mg_2 vary very little while iron indices change drastically.

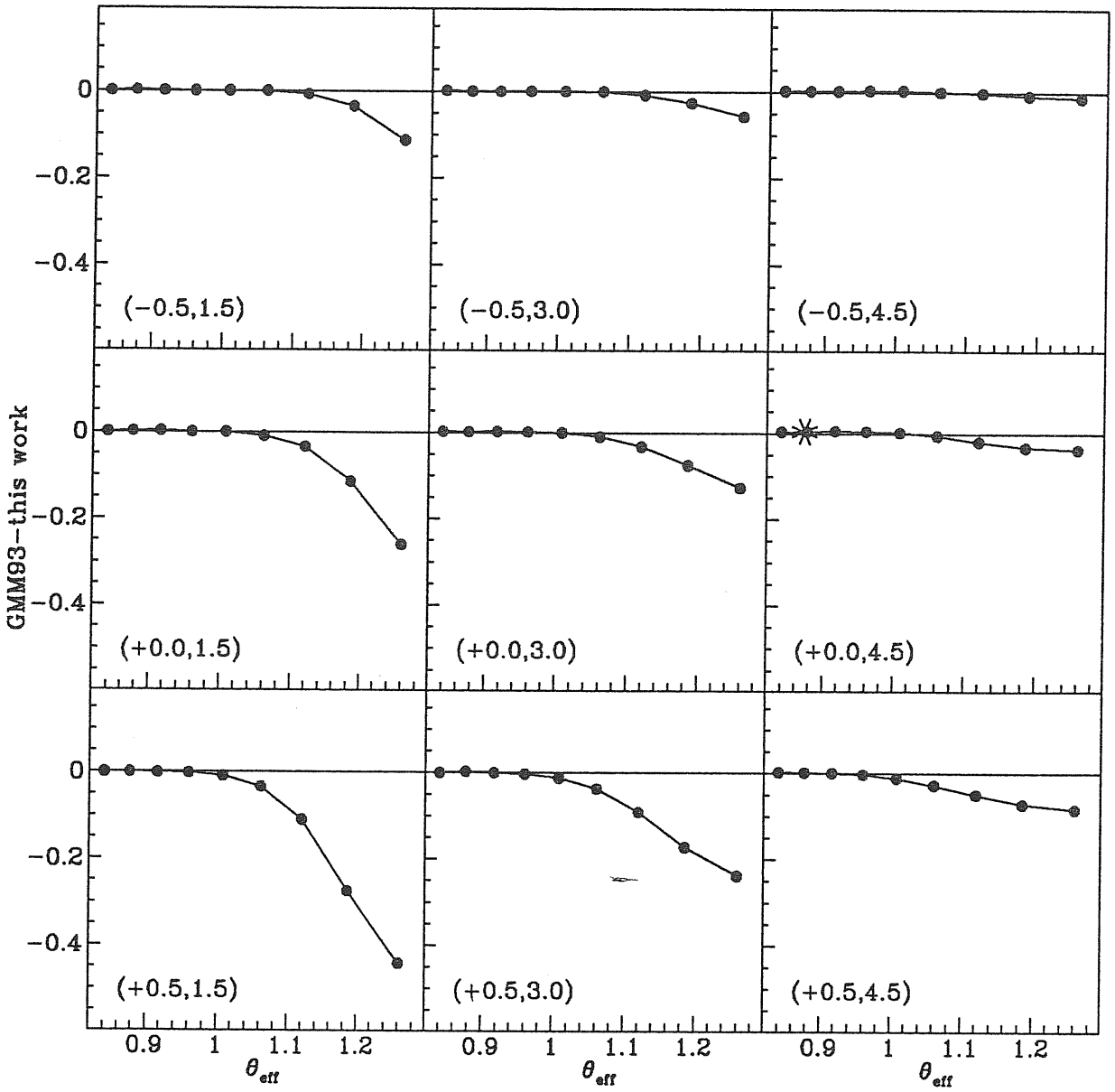

Figure 3.5: Differences between Mg_2 indices computed reported by GMM93 and our grid for different metallicities and gravities as functions of $\theta_{\rm eff}$. The values [M/H] and log g are given in parenthesis in each panel.

depends on metallicity. It goes from T_{eff} = 4500 K, for [M/H] = -0.5 up to 5000 K, for [M/H] = +0.5 dex.

In order to illustrate the effect of these differences in the interpretation of stellar data, we chose the case (4000/1.5/0.0), for which the differences are the highest. The use of new SYNTHE code starting from the same model as in GMM93 produced Mg_2 = 0.5196, to be compared with the new value (Mg_2 = 0.5251), and with the old one (Mg_2 = 0.260). It results that the differences in the models do not produce a significant difference in the index.

By comparing the new values for T_{eff} = 4000 K, log g = 1.5 dex, and different metallicities to the old ones, it results that new Mg_2 values are close to GMM93 ones reported for gravities higher than 1.5 dex: the difference in gravity goes from 0.75 dex for [M/H] = -0.5 up to 2.5 dex for [M/H] = 0.5. The net result is that Mg_2 values previously attributed to low temperature dwarfs are now obtained for giants.

From these results and other tests, we conclude that the major differences in the indices are due to the different treatment of the scattering in the codes, while only minor effects are due to differences in the models.

3.4 Indices and Atmospheric Parameters

The core of this chapter is to present the theoretical relationships between indices and stellar atmospheric parameters (the indices computed for the whole grid of spectra are presented in tabular form in appendix B). In this section these relationships are illustrated with reference to a selected subset of parameters. In Figures 3.6 to 3.10 we show the trend of each index with effective temperature for 3 surface gravities and four metallicities. Each figure contains 3 panels, where we plot the index values versus the effective temperature parameter θ_{eff} ($\equiv$ 5040/T_{eff}). Each panel refers to one surface gravity value (1.5, 3.0, and 4.5 dex, respectively), and four different metallicities; filled circles represent the indices computed for eleven T_{eff} values, from 4000 K to 6000 K, at a step of 250 K plus the indices for T_{eff} = 7000 and 8000 K.

From the figures illustrated above or from the grid, index values for atmospheric parameters within the limits of the grid can be easily derived and directly interfaced with population synthesis codes.

In this context, polynomial fitting functions derived from empirical libraries of spectral indices have been used by several authors. Eventhough some of them extensive, such libraries do not cover homogeneously the parameter space, and therefore, fitting functions provide the only tool to account for sections in the library with coarse coverage. In order to illustrate the effects due to the utilization of fitting functions, we chose as an example the case of Mg_2.

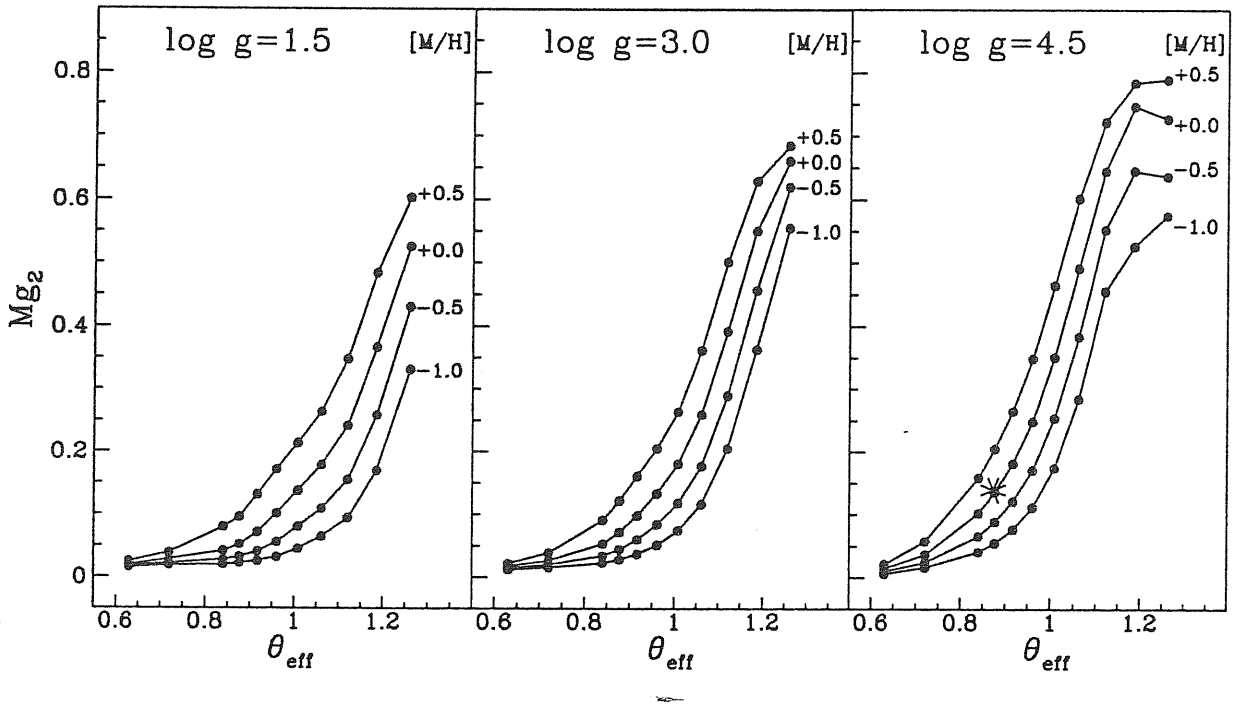

Figure 3.6: Mg_2 indices for different metallicities and gravities as a function of θ_{eff} =5040/T_{eff}. The trend of the index with θ_{eff}, at fixed gravity, is quite similar when varying metallicity, while a clear difference is present at low temperature between giant and dwarf models. Indeed, for dwarfs a plateau is reached, while it is not for giants. In the panel referring to log g = 4.5 dex, the value computed for the solar model (5777/4.43770/0.00) is also plotted (starred symbol).

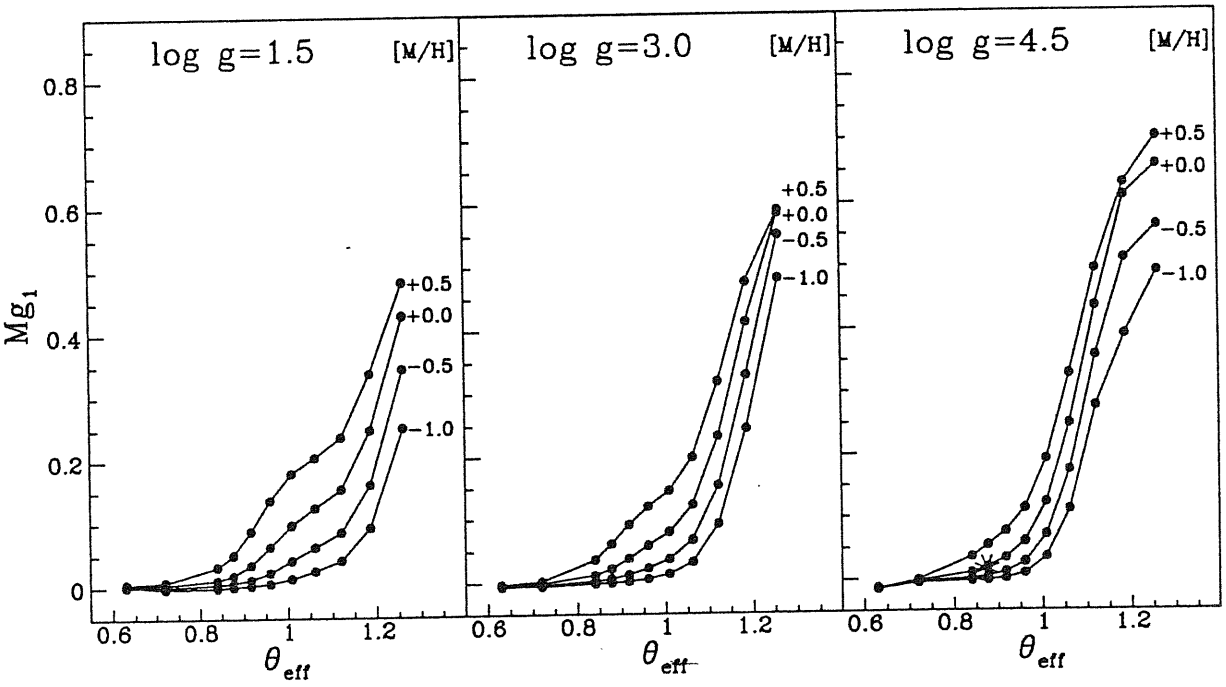

Figure 3.7: Same as figure 3.6 for Mg_1. This index increases monotonically till the lowest temperatures considered. Worthey (1992) found that there is a turnover at 4000 K, for both giant and dwarf stars.

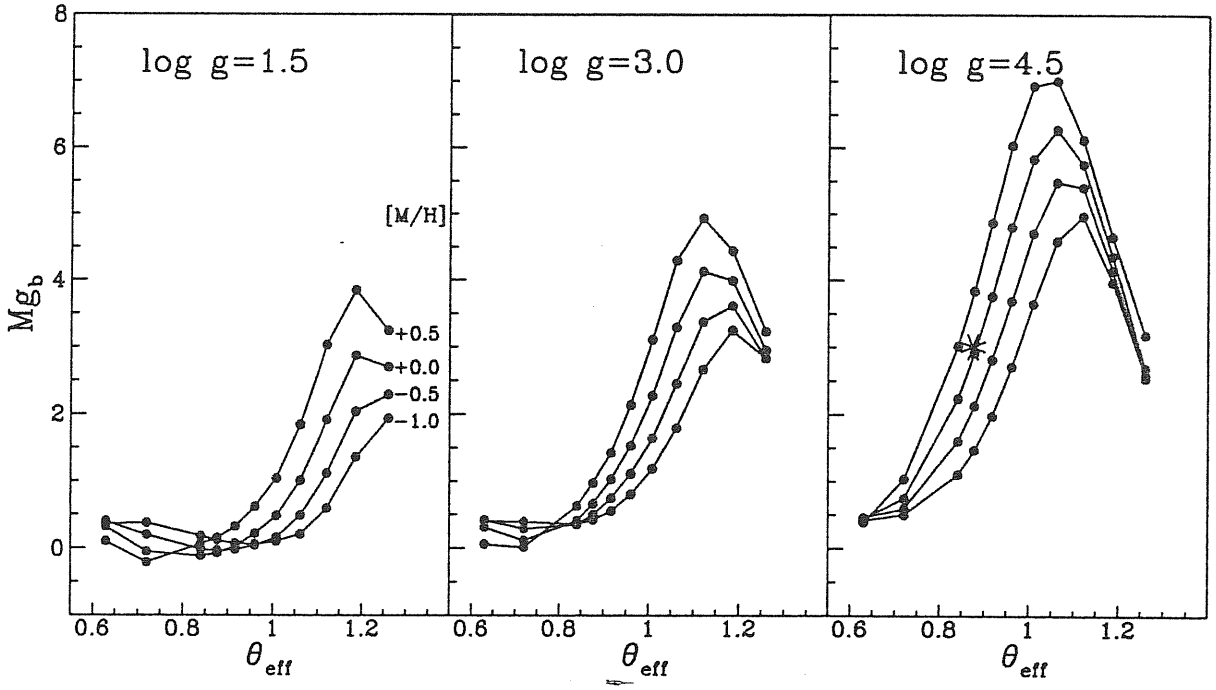

Figure 3.8: Same as figure 3.6 for Mg_b. Note that the maximum of the index strength is displaced towards lower temperatures with decreasing gravity. At the temperature where the maximum is reached differences due to metallicity are enhanced.

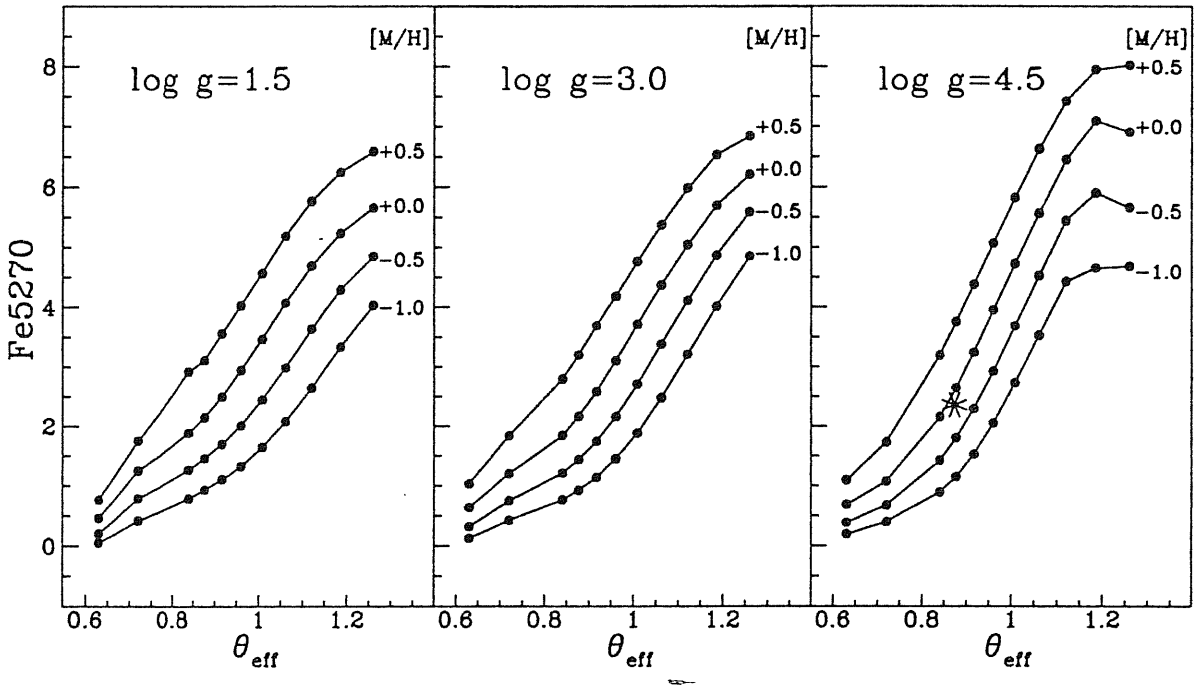

Figure 3.9: Same as figure 3.6 for Fe5270. As in the case of Mg_2, the trend of this index with respect to θ_{eff}, at fixed gravity, respond in a similar way to metallicity changes. It is also clear that a plateau is reached at the lowest temperatures for log g = 4.5.

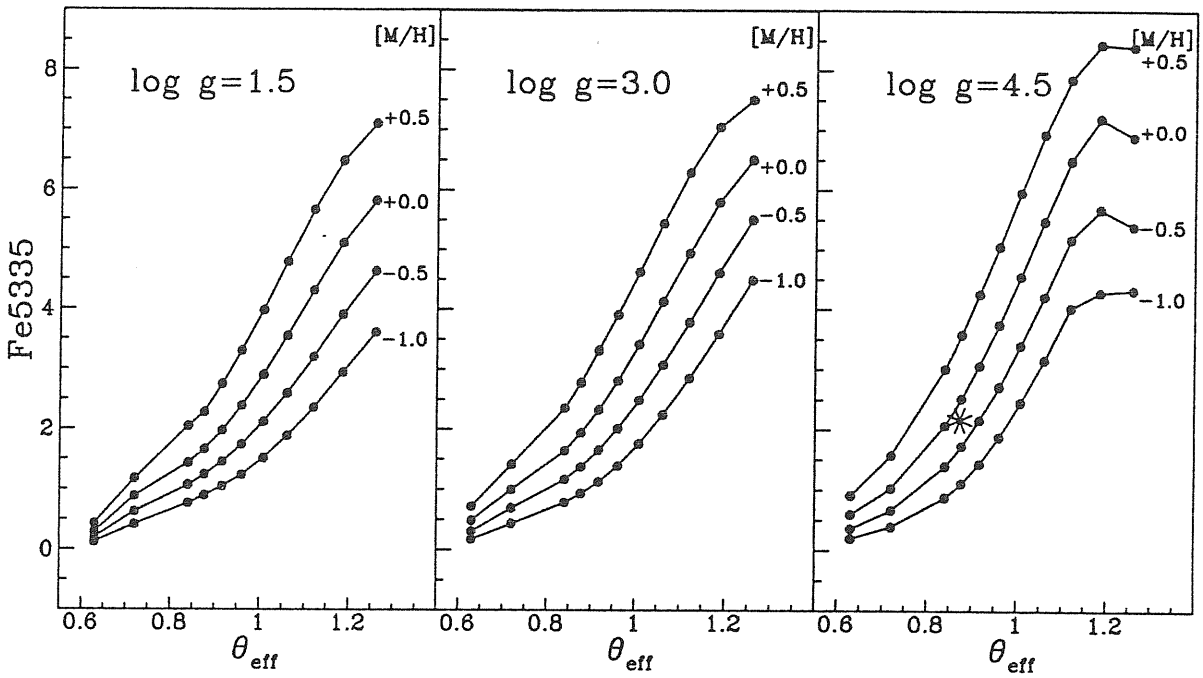

Figure 3.10: Same as figure 3.6 for Fe 5335. This index displays a quite similar behavior to that of Fe5270.

The theoretical calibration of the Mg_2 index as a function of the stellar atmospheric parameters has been derived by carrying out a multivariate regression analysis following the same procedure as in Malagnini et al. (1994), by assuming a polynomial function we have started by considering all possible combinations of the independent variables (i.e. the atmospheric parameters) including terms up to the third degree. Terms with partial correlation coefficients less that 0.1 were then rejected. Tests we have done revealed that including a larger number of terms did not improve in an appreciable way the quality (RMS) of the fit. The final fit is represented by the expression:

$$\begin{aligned} Mg_2(cal) \;=\; & 0.1225 + 1.8342(log\ \theta_{\rm eff}) + \\ & 10.0393(log\ \theta_{\rm eff})^2 + 0.1236[M/H] + \\ & 0.0110(log\ g)^2 + 0.6486([M/H](log\ \theta_{\rm eff})) + \\ & 0.4051(log\ g)(log\ \theta_{\rm eff}) \end{aligned} \qquad (3.3)$$

with a RMS of 0.0414. Note that no cross terms including log g and [M/H] appear in the resulting function pointing out that gravity weakly couples with the index strength.

As already noted by Malagnini et al. (1994), fitting functions introduce ripples that affect in a significant way the analytical index. This situation in illustrated in figure 3.11 where we plot the index obtained from equation 3.3, Mg_2(calc), versus the index from our grid, Mg_2(mod). Large discrepancies appear at the

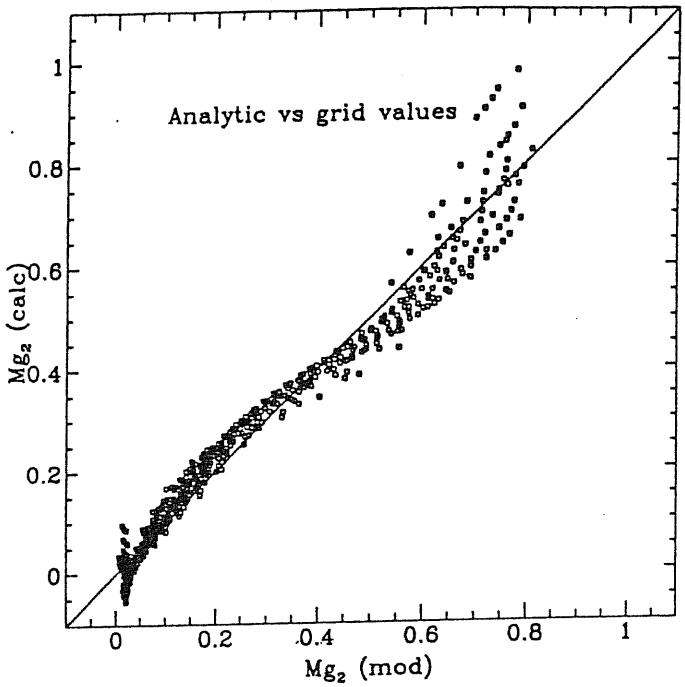

Figure 3.11: Analytical vs grid Mg_2index.

highest and lowest values of the index with residuals that can reach up to 0.2 magnitudes.

We further corrected the s-shaped behavior shown in Fig. 3.11 by fitting a third order polynomial and re-computed the analytical index, Mg_2(out). The problem was somewhat solved (see Fig. 3.12), the largest residual being now of the order of 0.1 magnitudes, however, a large spread is still present for high values of the index.

In view of the problems just described, and taking into account that even in our grid of indices, homogeneously distributed in the parameter space, such problems are found, we strongly recommend to use the indices tabulated in appendix B or directly interpolate, when necessary, within the grid, instead of deriving indices from equation 3.3.

3.5 Comparison with empirical data

In order to compare two astronomical quantities it is necessary that they are either both referred to the same reference system or that one of the two is suitably transformed according to the instrumental system of the other. The same is true when comparing theoretical data with observations.

This concept is particularly relevant in the present situation, in which we remark that our grid of indices does not necessarily reproduce any instrumental system. However, in this section we shall present the comparison between our

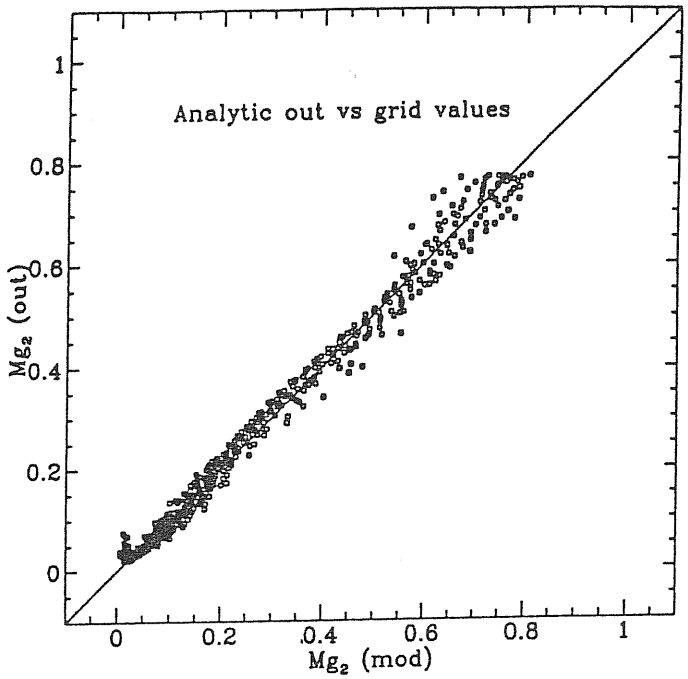

Figure 3.12: Analytical vs grid Mg_2index after flattening of the ripple was done.

indices and indices measured from observed spectra in order to point out their differences.

To compare with observational data, we chose the most homogeneous collection of measured Mg_2 indices, presented by the Lick group (WFGB94) and kindly made available to us in a computer–readable form by the authors. It is important to note here that their indices were computed directly from spectra given in count/pixel and divided by the response of a quartz lamp, thus modifying the spectral shape (Faber 1994-private communication) while our grid of indices was computed from theoretical absolute fluxes. We also bear in mind that the wavelength scale of the Lick spectra might be potentially off by 1-2 Å.

To establish the link between theoretical predictions and empirical data, the knowledge of atmospheric parameters, which naturally label the synthetic values, is required for the stars. We chose the most complete collection of ($\theta_{\rm eff}$, log g, [Fe/H]), with [Fe/H] derived from high resolution analysis, i.e. A catalogue of [Fe/H] determinations: 1991 edition (Cayrel de Strobel et al. 1992, hereafter C91). In the models, all metals are scaled by the same factor, thus the observed [Fe/H]'s correspond to the theoretical [M/H]'s. The cross-check of the stars present in WFGB94 and of the determinations given in C91 produced a list of 501 entries. Out of this set, we extracted the determinations falling in the parameter ranges of our grid, leading to a final list of 141 determinations, referring to 67 stars.

The C91 atmospheric parameters were used to obtain synthetic Mg_2 indices from our grid by interpolating linearly in the three–dimensional space ($\theta_{\rm eff}$, log g,

[M/H]) (see Table 2 of Chavez, Malagnini & Morossi 1995).

The comparison between observed and synthetic indices is illustrated in Fig. 3.13, where synthetic values from different determinations for the same star are connected by vertical bars.

In general, the points cluster around the 45 ° line with perhaps a small shift, however, it is clear that a large spread is present. The amplitude of the spread is much larger not only than the observational errors but also than the uncertainties expected in the synthetic values. By looking at different determinations for the same star, we can attribute most of the spread to uncertainties in the atmospheric parameters. This effect strongly affects the reliability of any empirical Mg_2 calibration based on heterogeneous and/or non statistically unbiased datasets.

Fitting functions computed by the Lick group have been used to study the integrated properties of old stellar populations (Bressan, Chiosi & Tantalo 1995). To have insight into the differences between the theoretical indices and those computed from these fitting functions we present in figure 3.14 the index residuals for Mg_2 in a similar way as in figure 3.5. It is evident from this figure that strong discrepancies exist at high temperatures and low gravities and at low temperatures regardless of gravity.

It is important to stress that these discrepancies will be better understood once a transformation of the theoretical and empirical data to the same reference system is done.

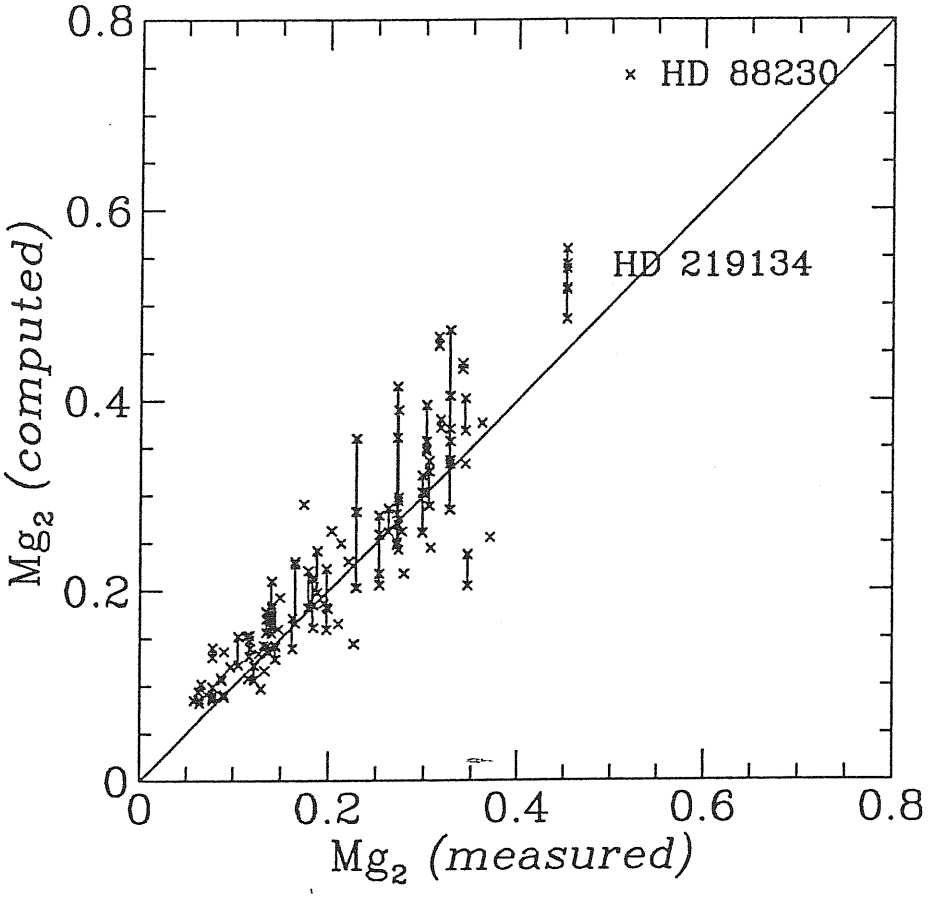

Figure 3.13: Plot of indices versus empirical values. Vertical bars connect the points referring to different determinations of atmospheric parameters given in C91 for the same star.

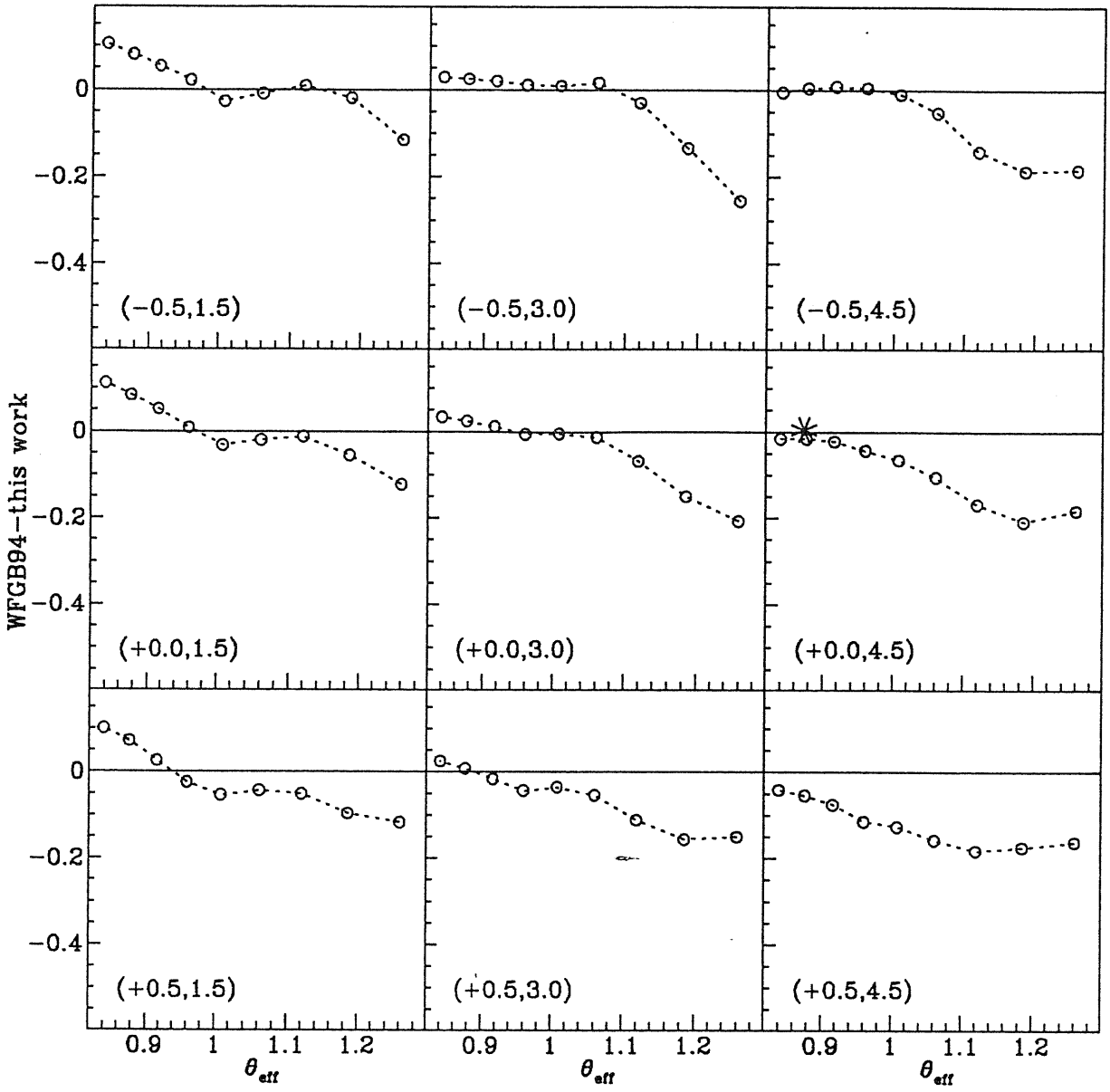

Figure 3.14: Differences between Mg_2 indices computed from WFGB94 fitting functions and our grid for different metallicities and gravities as functions of $\theta_{\rm eff}$. The values [M/H] and log g are given in parenthesis in each panel.

Chapter 4

Observed and Synthetic Spectra of Super Metal-Rich Stars

In this chapter we present recent work and steps towards the determination of the metallicity scale for super-metal rich (SMR) stars. This calibration is intended to be done by quantitatively comparing observed and synthetic spectra of a selected sample of stars. Characteristics of the observational material collected so far are given.

4.1 The super metal-rich phenomenon

SMR stars (for a recent review on the subject see Taylor 1991) were first identified as a group by Spinrad & Taylor (1969). They found, when analysing a sample of G and K stars, that some giants presented line absorptions stronger than those observed in their standard stars. They argued that these stars have a global metal overabundance confirmed by the stronger line blanketing in the Johnson UBV colors. In a subsequent paper (Spinrad et al. 1970), the same enhancement in metal lines was seen in dwarf stars observed in M67 and NGC 188.

Another explanation for the SMR phenomenon was provided by Peterson (1976). After a detailed high resolution analysis of three K giants, one of which was metal rich (μ Leo), she suggested as a possible explanation for the SMR stars the difference in physical conditions at the surface of normal and SMR stars. The strong lined appearance of the spectrum was due to a drop in temperature caused by enhanced CN absorption just above the continuum-forming region (see also Desikachary & Gray 1978). A similar explanation was previously given by Strom, Strom & Carbon (1971), but they also considered anomalous microturbulence as the underlying agent producing the SMR appearance. Campbell (1986) gave one

further explanation for the SMR stars. He claimed that SMR stars may result from the coalescence of close binaries with the envelope contaminated by material processed in the core of the secondary.

More recently, Gratton & Sneden (1990) re-analyzed the metallicity of μ Leo. They concluded, from high resolution high S/N analysis, that this star is indeed metal rich ([Fe/H]=+0.34) and that this determination cannot have an error (due to continuum tracing and uncertainties in atmospheric parameters) larger than 0.15 dex.

Despite the great efforts and numerous papers devoted to the analysis of SMR stars, their nature as well as their true metallicity is far from being a settled question. As an example, μ Leo, has metallicity determinations from high quality data (C91) which differ by up to a factor of 3!.

The lack of a reliable metallicity scale for these stars not only limits our understanding of the origin of the SMR phenomenon, but also, from a more general point of view, our understanding of stellar systems where metal rich stars are thought to be present (giant ellipticals and spiral bulges). In section 3.5 of last chapter we saw that the uncertainties associated with the atmospheric parameters of stars used to produce fitting functions for studying stellar populations, strongly affect the reliability of any empirical calibration of spectral indices in terms of stellar atmospheric parameters.

Thus, the analysis presented here turns out to be of fundamental importance for several reasons:

i) identification of true SMR stars to complement current empirical data bases;

ii) to give insight on the absolute metallicity scale of super-solar stars

iii) to create a grid of synthetic spectra to complement existing stellar spectral libraries.

4.2 Observations and reductions

We have selected 201 stars of spectral types F to M that are catalogued in Taylor (1991) or in C91 or in WFGB94 as having super-solar abundances ([Fe/H]$\geq$ 0.10).

The observations were carried out by A. Buzzoni in March 1994 using a Boller & Chivens Cassegrain Spectrograph coupled with the 2.1 m telescope at the Guillermo Haro Observatory, México. A total of 91 stars were observed in two overlapping spectral intervals that cover the region 3750–5300 Å .

The spectra were reduced using the MIDAS reduction package (version 1992) following the standard reduction procedure:

- The bias was subtracted from each frame and the pixel-to-pixel variations of intensity were corrected by dividing each frame by a normalized average

flat field. The dark current turned out to be very small compared to stellar fluxes, so that we did not carry out any correction for dark current.

- The sky background image was subtracted from each frame. To create the sky background image, two windows adjacent to the stellar image in each frame were extracted. The filtered average on these windows along the direction perpendicular to the dispersion was grown to produce a 2-D image covering also the positions of stellar data.

- One dimensional stellar spectra were extracted by averaging the rows where the stellar spectrum was present. To establish the rows over which the average should be carried out, we fitted a gaussian function to the stellar profile and took the central row $\pm$ 1.5$\times$FWHM.

- Atmospheric extinction was corrected for by using the extinction curve derived for Kitt Peak, since Cananea has very similar atmospheric conditions and both observatories are very close to each other. Typical airmasses are $X = 1.0$ to 1.2; in very few cases the airmasses exceeded $X = 1.2$.

- The wavelength calibration and the determination of the resolution were performed using an He-Ar comparison lamp. The resolution in the two spectral ranges (FWHM), 3750-4650 Å and 4450-5300 Å , has been estimated to be 3.2$\pm$0.2 and 2.5$\pm$0.1 Å , respectively.

- The shape of the observed spectra was recovered by dividing each spectrum by a mean instrumental response function derived from the spectrophotometric information of six standard stars from Kiehling (1987) and Gutierrez-Moreno et al. (1988).

- The S/N has been estimated to be on the order of 50 or better.

Figure 4.1 shows the distribution of the observed stars in terms of the three atmospheric parameters, effective temperature, surface gravity and metallicity ([Fe/H]). The number written at the top left of each panel indicates the total number of determinations of the corresponding parameter. Note that some of the determinations are below the metallicity limit we imposed to select our stars. These determinations correspond to stars from WFGB94 that in the other two sources are reported to have [Fe/H] < 0.10. In these histograms we have included all determinations available in the three sources. From the numbers in figure 4.1, it is clear that for many stars more than one determination, for at least one of the atmospheric parameters, is available, in particular for [Fe/H].

In figures 4.2, 4.3 and 4.4 we show some of the observed spectra. In order to illustrate the behavior in terms of effective temperature of the most prominent spectral features in this spectral region, we have plotted the stellar spectra for luminosity classes I, III and V and selected spectral types. At the top of each figure we indicate the position of the strongest spectral lines of iron and magnesium. The spectra are, from top to bottom, roughly in order of increasing temperature.

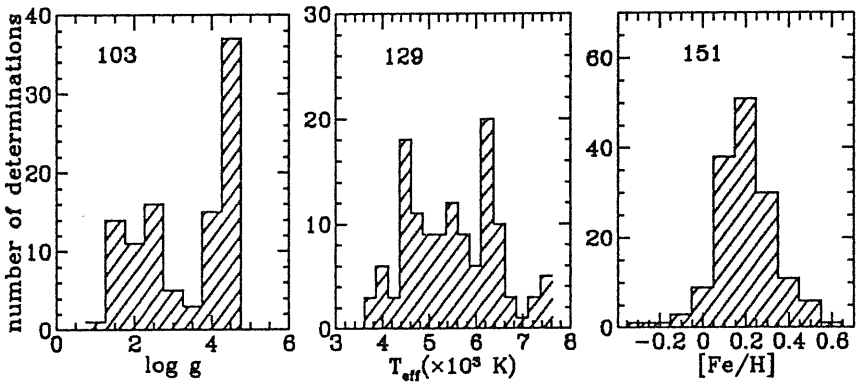

Figure 4.1: Distribution of the observed stars in terms of the atmospheric parameters.

A short note before continuing. On what follows we will refer only to the observations carried out with the second instrumental set up (4450–5300 Å). The reason is that the atomic and molecular data to compute synthetic spectra for the spectral interval covered by the first set up (and part of the second one) has not yet been tested by comparison with the solar spectrum as we did for the region 4850–5400 Å in chapter 2.

4.3 Iron and magnesium indices in SMR stars

The comparison between the observed and synthetic spectra will be done in two ways. On one side through the comparison of spectral indices computed from the observed and theoretical spectra, and on the other through the direct comparison of the spectral energy distributions. In this section we concentrate on spectral indices.

The red-edge cut off of the observed spectra prevented us from computing the indices Mg_2, Mg_1, Fe5270 and Fe5335, the last one being completely out of range. The spectral index computable according to the definitions in WFGB94 in the wavelength interval in which theoretical and observed spectra overlap is, Mg_b. To account for the indices for which we have partial coverage, we introduce

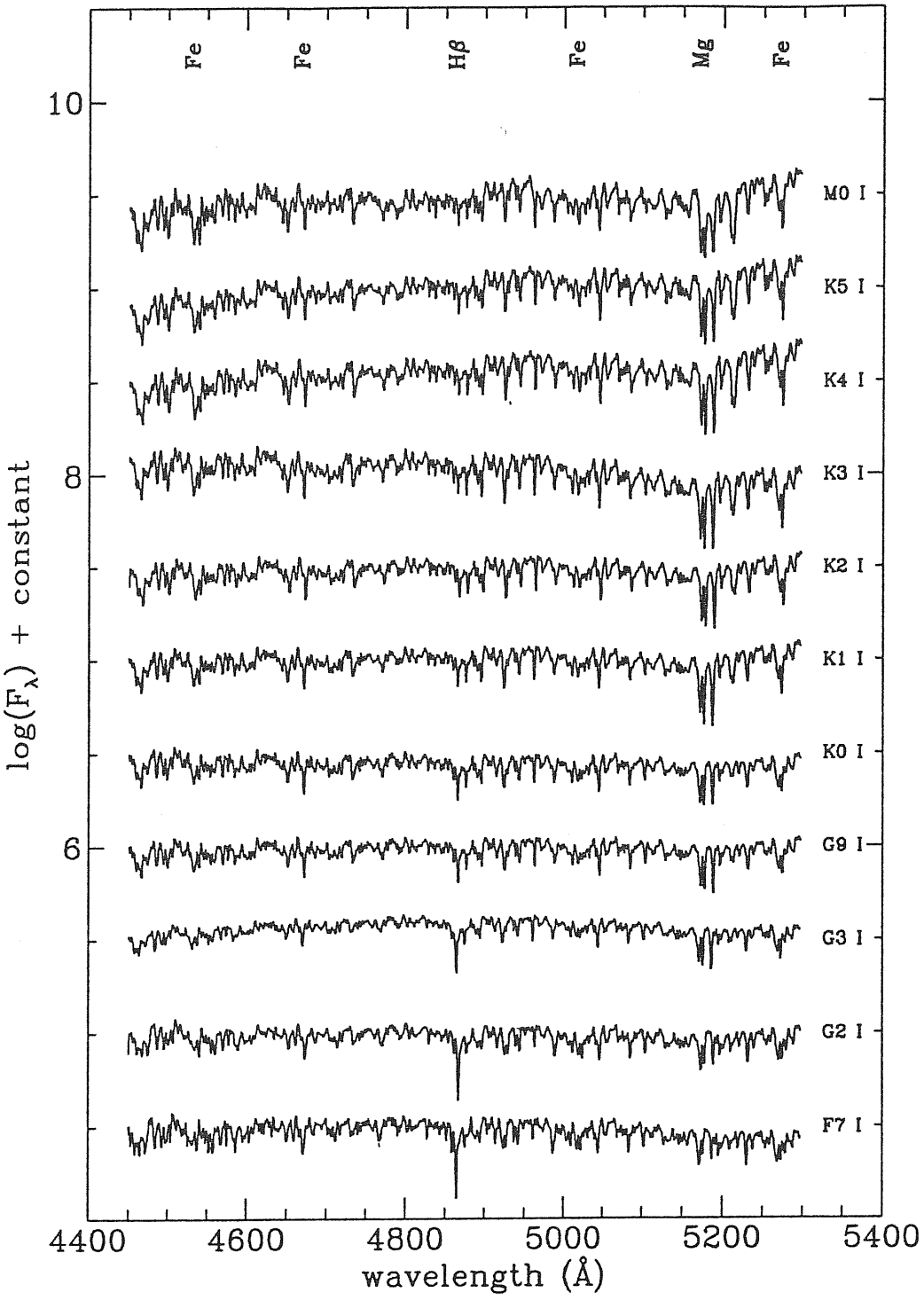

Figure 4.2: Subset of observed supergiant stars. It is evident from these spectra the opposite behavior of Hβ with respect to those of magnesium and iron.

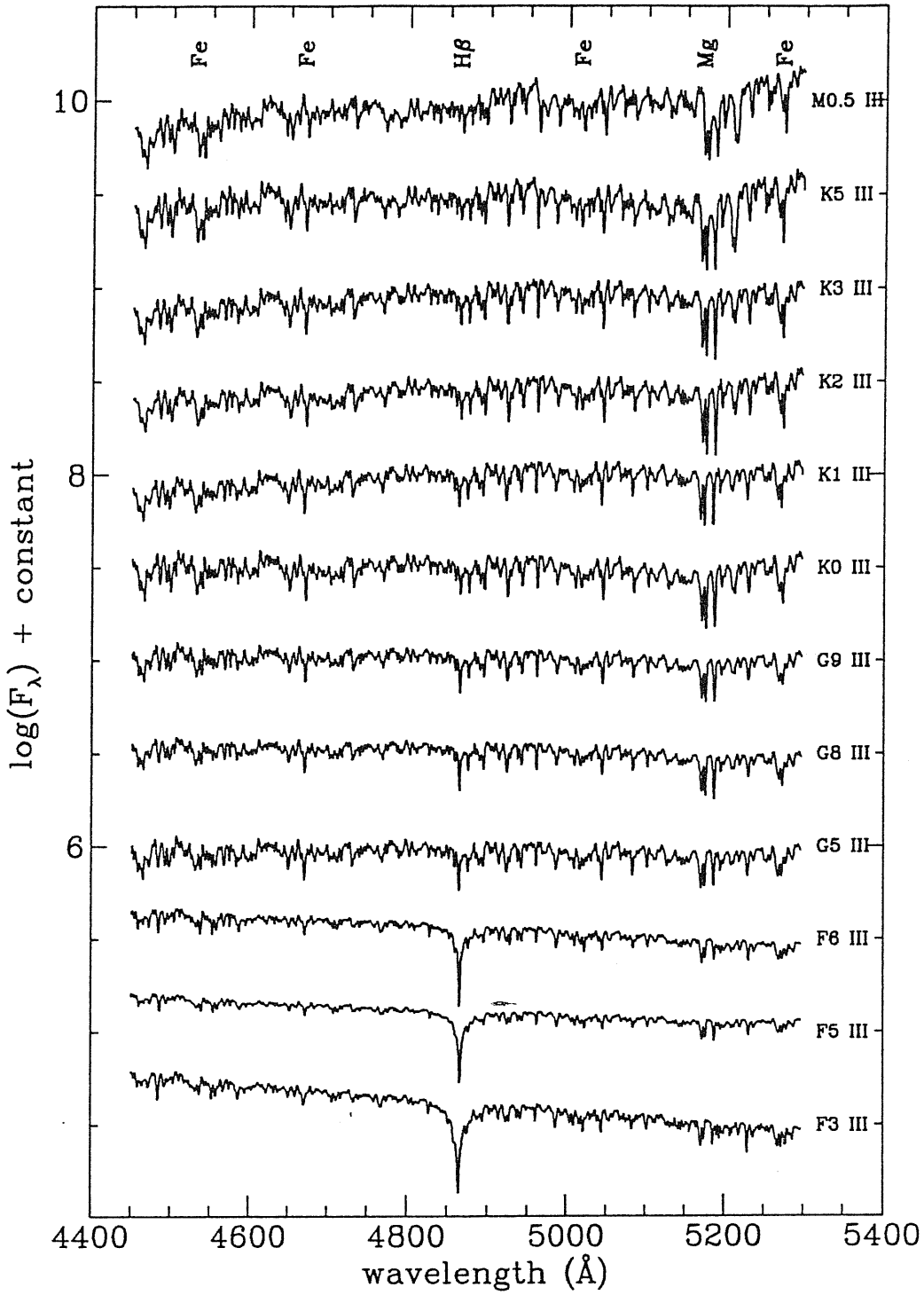

Figure 4.3: Same as figure 4.2 for giant stars.

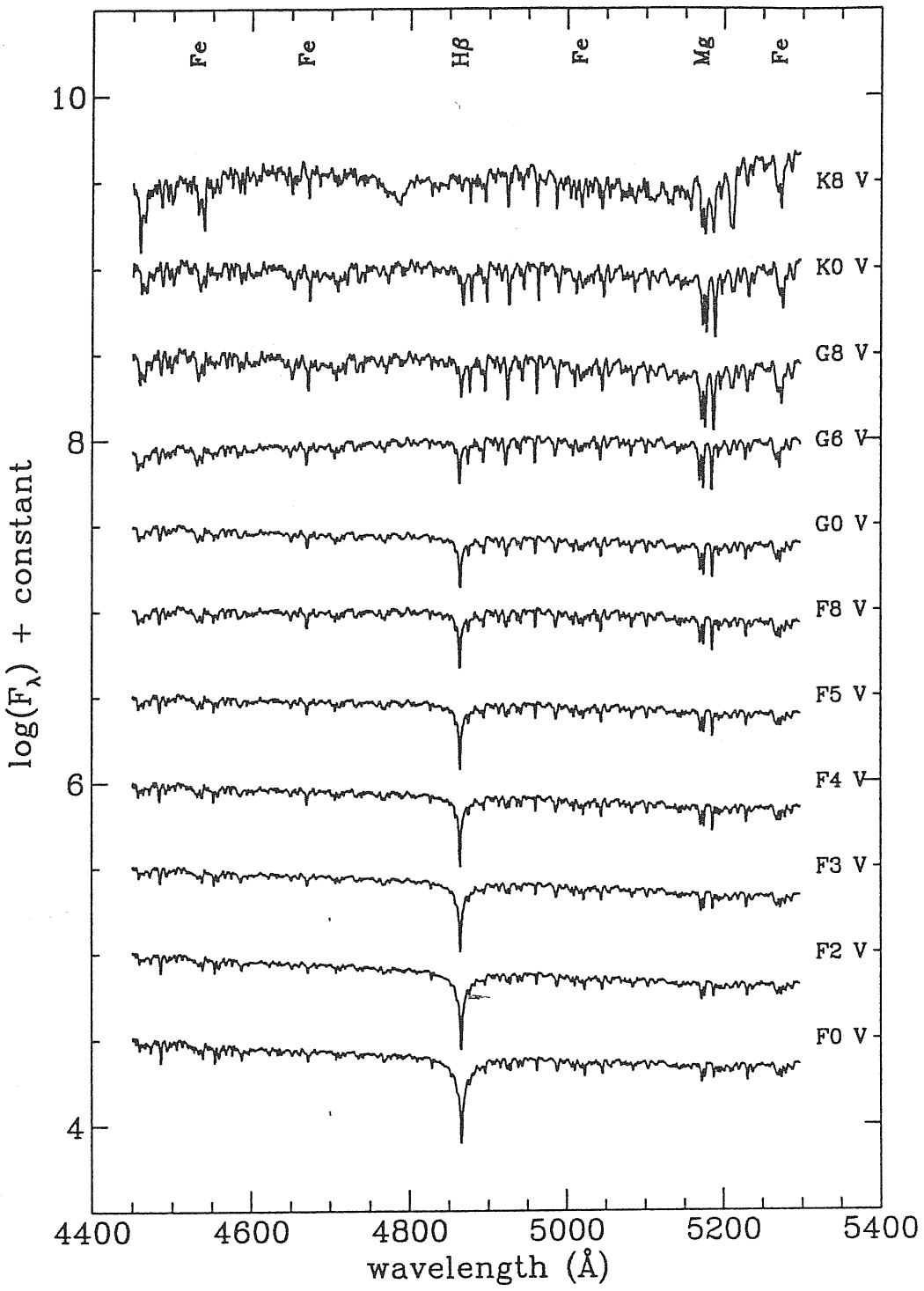

Figure 4.4: Same as figure 4.2 for dwarf stars.

Table 4.1: Additional index definitions

Index	Features Measured	Index Bandpass	Continua Bandpasses	Units
$Fe52_s$	Fe I, Ca I	5245.650-5278.000	5233.150-5248.150	Å
			5278.000-5289.000	
Mg_s	MgH, Mg_b	5154.125-5196.625	4895.125-4957.625	mag
			5235.180-5260.000	

the definition of two indices, that we call Mg_s and $Fe52_s$ which measure (almost) the same features as Mg_2 and Fe5270, respectively. The blue and central bands for Mg_2 and Mg_s are the same. The red side band for Mg_s was chosen so as to avoid as much as possible the presence of features defining other indices, with special care in avoiding very strong iron lines. Fe5270 and $Fe52_s$ share the same blue bandpass while the central bandpass of $Fe52_s$ is slightly narrower than that of Fe5270. Table 4.1 list the definitions of these newly defined indices. The use of these two new indices is validated after a few tests that demonstrated that the new and parent indices have a very similar behavior in terms of the stellar atmospheric parameters (see discussion below), and present some interesting properties with respect to gravity.

Information on the observed stars as well as the set of indices computed from their spectra are summarized in Table 4.2 (the table refers only to stars observed in the second instrumental setup). A few stars not reported in the table were rejected from further computations because their spectra appeared contaminated by nearby companions. HD numbers followed by an asterisk indicate the flux calibration standards. Two of the six standard stars were used only for flux calibration purposes, HD 84971 (B2 V) and HD 149382 (B5), however, we have computed the indices also for these hot stars. Visual magnitudes and spectral types were collected from the sources of metallicity or from SIMBAD data base.

Table 4.2: Observed SMR stars and spectral indices

STAR (HD)	V	ST	Mg_b	$Fe52_s$	Mg_s
48682	5.24	G0 V	3.147	1.257	0.114
49161	4.77	K4 I	4.930	3.851	0.260
52973	3.73	F7 Ib	1.684	2.312	0.070
57727	5.03	G8 III	3.721	2.104	0.132
58207	3.79	G9 IIIb	3.693	2.468	0.153
60522	4.06	M0 I	5.814	3.768	0.354
61064	5.13	F6 III	1.835	0.979	0.065
63700	3.33	G3 Ib	3.118	1.926	0.115
65714	5.83	G8	3.486	2.609	0.130
72184	5.90	K2 I	5.193	3.017	0.243
72324	6.36	G9 I	3.633	2.472	0.140
72505	6.28	K0 III	4.845	3.165	0.252
72561	5.87	G5 III	2.960	2.622	0.117
73665	6.39	K0 I	3.654	2.598	0.135
73710	6.44	K0 III	1.225	0.322	0.049
74739	4.03	G7.5 IIIa	2.987	2.402	0.104
75732	5.94	G8 V	6.643	2.628	0.297
78249	7.10	K1 IV	5.521	2.690	0.236
81029	7.31	F0	1.529	0.665	0.062
81873	5.71	K0 III	4.141	2.655	0.176
83951	6.14	F3 V	1.814	0.657	0.062
84971*	8.63	B2 V	0.761	-0.377	0.015
85503	3.88	K0 III	5.364	3.461	0.283
87822	6.24	F4 V	2.175	0.708	0.077
88230	6.60	K8 V	5.575	4.004	0.494
90277	4.74	F0 V	1.570	0.807	0.058
92125	4.71	G2 IIa	2.281	1.913	0.086
93257	5.49	K3	5.283	3.137	0.268
95849	5.95	K3 III	4.725	3.332	0.205
100563	5.78	F5 V	2.465	0.793	0.074
101013	6.14	K0p+B3	3.087	2.401	0.162
102328	5.27	K3 I	5.385	3.528	0.278
102634	6.14	F8 V	2.766	1.175	0.097
102870*	3.61	F8 V	2.890	1.126	0.073
109511	5.03	K2 III	4.121	2.912	0.179
110014	4.66	K2 II-III	5.030	3.477	0.245
113022	6.20	F6 V	2.284	0.806	0.006
114710	4.26	G0 V	3.384	1.205	0.120
115604	4.73	F3 III	1.635	0.936	0.054
115617*	4.74	G6 V	4.939	1.685	0.171
116976	4.76	K1 III	4.272	2.785	0.167

Table 4.2 (Continued)

STAR (HD)	V	ST	Mg_b	$Fe52_s$	Mg_s
120136	4.50	F7 V	2.688	0.997	0.090
121370*	2.68	G0 IV	2.980	1.455	0.106
124425	5.91	F7 V	2.116	0.806	0.070
124570	5.55	F6 IV	2.565	1.098	0.093
127227	7.48	K5 III	5.851	3.871	0.380
129989	2.70	K0 II-III	3.500	3.102	0.144
130948	5.86	G2 V	3.464	1.174	0.097
135482	5.33	K0 III	3.983	2.978	0.188
136028	5.89	K5 I	4.802	3.801	0.288
137391	4.31	F0 V	1.602	0.595	0.065
137759	3.29	K2 I	4.929	3.145	0.241
139357	5.97	K4	4.993	3.257	0.222
139669	4.96	K5 III	5.197	4.263	0.321
140573	3.62	K2 III	4.964	3.196	0.242
142980	5.54	K1 I	5.583	3.010	0.275
144284	4.01	F8 IV	2.460	1.080	0.089
145000	6.25	K1 III	4.673	3.042	0.211
145148	5.97	K0 I	5.947	2.784	0.284
145675	6.65	K0 V	6.696	2.848	0.304
146051	3.73	M0.5 III	6.203	3.691	0.350
147677	4.85	K0 III	4.012	2.477	0.164
148513	5.39	K4 I	4.982	3.965	0.329
149382*	8.90	B5	0.934	-0.281	-0.014
150680	2.81	G0 IV	3.275	1.425	0.124
153956	6.01	K1	4.802	3.120	0.245
156283	3.16	K3 II	4.256	3.745	0.193
159181	2.80	G2 Ib-IIa	2.029	2.285	0.110
159925	6.10	G9 III	3.527	2.375	0.140
160922	4.80	F5 V	2.300	0.859	0.080
161096	2.77	K2 III	5.090	3.196	0.252
161797*	3.42	G5 IV	4.258	1.877	0.175
162917	5.77	F4 IV-V	2.264	0.757	0.078
163770	3.86	K1 II	3.405	3.888	0.167
163993	3.70	K0 II	3.675	2.300	0.147
166208	5.00	G8 III	3.635	2.136	0.105
166229	5.48	K2 III	5.128	3.191	0.267
167858	6.62	F2 V	1.691	0.603	0.062
169916	2.82	K0 II	4.299	2.530	0.153
171802	5.39	F5 III	1.731	0.446	0.068

We have compiled a total of 114 atmospheric parameters determinations for 69 stars; among this set, 42 stars have 87 determinations in the catalogue of C91 (herafter, referred to as *primary data.* For those stars not having effective temperature and/or surface gravity reported in C91 (*secondary data*), the parameters are adopted from Brown et al. (1989), McWilliam (1990) and Clariá, Piatti & Lapasset (1994). We decided to preserve the metallicity determination reported in C91 even if in these references a different value of [Fe/H] was given.

For the purposes of the comparison between theoretical and observed indices we made use of the grid of synthetic spectra described in the previous chapter. The spectra were degraded to the same instrumental resolution and rebinned to get the same wavelength step as the observational material, i.e. FWHM = 2.5 Å and $\Delta\lambda = 0.83$ Å respectively. Since in general the atmospheric parameters for a given star did not match those available within the theoretical grid, we derived a theoretical spectrum by linearly interpolating in the three–dimension parameter space. From the resulting theoretical spectra we computed the spectral indices reported in Table 4.3. Columns 1 to 12 give the HD number, the corresponding set(s) of atmospheric parameters and the seven spectral indices computed. Last column list the reference for the effective temperature and/or surface gravity.

Table 4.3: Spectral indices from theoretical spectra

STAR HD	$\theta_{\rm eff}$	log g	[M/H]	Mg_2	Mg_1	Mg_b	Fe5270	Fe5335	$Fe52_s$	Mg_s	ref
48682	0.88	4.38	0.15	0.158	0.020	4.176	2.915	3.305	1.776	0.164	1
49161	1.24	1.85	0.23	0.518	0.402	4.326	5.703	6.662	4.536	0.465	1
52973	0.88	1.50	0.21	0.077	0.024	1.310	2.444	2.446	1.662	0.069	1
52973	0.88	1.50	0.49	0.103	0.045	1.483	2.945	2.782	2.036	0.090	1
52973	0.88	1.90	0.33	0.091	0.035	1.454	2.668	2.697	1.782	0.082	1
58207	1.06	2.92	0.16	0.279	0.129	4.662	4.494	4.938	3.138	0.254	2
58207	1.14	2.92	0.16	0.436	0.270	5.443	5.288	5.942	3.921	0.406	3
61064	0.79	3.21	0.44	0.070	0.010	1.562	2.041	2.266	1.162	0.069	1
63700	1.01	1.15	0.24	0.172	0.126	1.866	3.795	3.751	2.694	0.145	1
65714	1.05	1.50	0.24	0.204	0.141	2.454	4.203	4.387	2.979	0.168	4
72184	1.08	2.65	0.34	0.319	0.173	4.690	4.893	5.464	3.460	0.281	1
72324	1.04	1.60	0.17	0.186	0.123	2.325	3.948	4.124	2.782	0.156	1
72324	1.07	2.25	-0.20	0.184	0.086	3.071	3.666	3.999	2.578	0.165	1
73665	1.01	2.35	0.16	0.179	0.098	2.730	3.737	4.015	2.550	0.158	1
73710	1.04	2.10	0.24	0.210	0.125	2.937	4.134	4.449	2.876	0.178	1
74739	1.04	2.00	0.20	0.199	0.120	2.740	4.036	4.321	2.813	0.169	1
75732	0.97	4.40	0.11	0.277	0.066	6.157	4.232	4.563	2.764	0.282	1
75732	0.97	4.50	0.24	0.314	0.081	6.735	4.604	4.962	3.012	0.317	1
75732	0.97	4.50	0.30	0.326	0.088	6.879	4.734	5.108	3.100	0.327	1
81873	1.06	2.13	0.16	0.221	0.123	3.256	4.243	4.589	2.983	0.189	6
83951	0.75	4.00	0.14	0.053	-0.003	1.671	1.351	1.776	0.615	0.058	1
85503	1.07	2.82	0.11	0.275	0.131	4.485	4.443	4.876	3.123	0.250	1
85503	1.11	2.30	0.35	0.348	0.206	4.669	5.116	5.752	3.696	0.302	1
85503	1.11	2.35	0.48	0.381	0.230	4.990	5.378	6.110	3.874	0.330	1
85503	1.13	2.40	-0.01	0.324	0.184	4.484	4.678	5.160	3.436	0.291	1
85503	1.14	2.30	0.03	0.337	0.200	4.438	4.786	5.305	3.540	0.301	1
85503	1.14	2.30	-0.11	0.310	0.179	4.227	4.538	5.005	3.351	0.279	1
85503	1.17	2.20	0.31	0.446	0.302	4.897	5.504	6.314	4.153	0.396	1
87822	0.77	4.20	0.19	0.067	-0.002	2.045	1.564	1.995	0.773	0.072	1
88230	1.26	4.50	0.28	0.743	0.668	4.190	7.488	8.213	6.423	0.757	1
90277	0.68	3.46	0.19	0.036	-0.007	1.217	1.008	1.344	0.338	0.038	1
92125	0.96	2.12	0.13	0.131	0.070	1.913	3.116	3.299	2.106	0.117	3
93257	1.11	2.30	0.11	0.299	0.166	4.240	4.664	5.150	3.378	0.263	4
100563	0.79	4.30	0.12	0.075	-0.001	2.323	1.654	2.107	0.841	0.082	1
101013	1.19	2.50	-0.33	0.409	0.282	4.501	4.743	5.231	3.648	0.387	5
102328	1.13	2.35	0.41	0.405	0.250	5.116	5.431	6.190	3.971	0.355	1
102634	0.83	4.30	0.14	0.105	0.006	3.026	2.156	2.593	1.225	0.111	1
102634	0.83	4.30	0.50	0.139	0.023	3.480	2.827	3.176	1.685	0.142	1
102870	0.82	4.20	0.10	0.090	0.003	2.634	1.916	2.364	1.051	0.095	1
102870	0.82	4.29	0.26	0.105	0.008	2.936	2.207	2.619	1.252	0.111	1
102870	0.82	4.30	0.20	0.101	0.006	2.883	2.109	2.536	1.184	0.107	1
102870	0.82	4.40	0.14	0.101	0.004	2.958	2.045	2.491	1.134	0.107	1
102870	0.83	4.10	0.18	0.099	0.008	2.759	2.148	2.568	1.230	0.104	1
102870	0.83	4.12	0.28	0.109	0.012	2.901	2.331	2.724	1.355	0.113	1
102870	0.84	4.30	0.29	0.130	0.015	3.478	2.603	2.994	1.546	0.135	1

Table 4.3 (Continued)

STAR HD	$\theta_{\rm eff}$	log g	[M/H]	Mg_2	Mg_1	Mg_b	Fe5270	Fe5335	$Fe52_s$	Mg_s	ref
109511	0.64	2.50	0.42	0.039	0.001	1.048	0.949	1.145	0.313	0.035	2
109511	1.12	2.50	0.42	0.410	0.246	5.332	5.428	6.191	3.943	0.362	3
110014	1.15	2.46	0.16	0.398	0.250	4.865	5.136	5.789	3.824	0.359	3
113022	0.79	4.20	0.10	0.071	-0.001	2.198	1.605	2.057	0.809	0.077	1
114710	0.82	4.52	0.06	0.099	0.001	3.022	1.952	2.418	1.059	0.107	1
114710	0.85	4.40	0.02	0.116	0.006	3.404	2.247	2.699	1.293	0.124	1
114710	0.85	4.47	0.27	0.146	0.016	3.935	2.767	3.162	1.653	0.152	1
115604	0.64	3.80	0.32	0.033	-0.011	1.203	0.960	1.278	0.294	0.036	1
115604	0.67	4.10	0.44	0.040	-0.011	1.364	1.200	1.526	0.484	0.045	1
115604	0.70	3.00	0.18	0.040	-0.003	1.147	1.185	1.460	0.480	0.041	1
115617	0.90	4.00	-0.03	0.131	0.018	3.456	2.586	3.003	1.575	0.136	1
115617	0.90	4.50	-0.02	0.165	0.017	4.495	2.910	3.303	1.773	0.174	1
115617	0.92	4.52	0.22	0.228	0.041	5.548	3.779	4.117	2.383	0.234	1
116976	1.08	2.66	0.11	0.275	0.139	4.301	4.462	4.905	3.159	0.247	3
120136	0.78	4.30	0.00	0.064	-0.003	2.094	1.405	1.886	0.651	0.070	1
120136	0.78	4.30	0.28	0.079	0.001	2.328	1.784	2.201	0.933	0.085	1
120136	0.79	3.80	0.30	0.072	0.004	1.935	1.818	2.181	0.976	0.075	1
120136	0.79	4.30	0.14	0.077	0.000	2.340	1.682	2.130	0.862	0.083	1
121370	0.81	3.80	0.16	0.074	0.004	2.073	1.805	2.209	0.979	0.078	1
121370	0.83	3.72	0.38	0.102	0.018	2.439	2.409	2.740	1.428	0.102	1
124570	0.81	4.20	0.00	0.076	0.000	2.360	1.642	2.116	0.841	0.082	1
124570	0.81	4.20	0.12	0.084	0.002	2.487	1.829	2.274	0.982	0.090	1
124570	0.81	4.20	0.13	0.085	0.002	2.497	1.844	2.287	0.993	0.090	1
127227	1.26	1.73	0.12	0.543	0.445	3.968	5.657	6.624	4.598	0.492	7
129989	1.06	2.24	0.13	0.222	0.118	3.381	4.207	4.561	2.954	0.192	3
130948	0.88	4.43	0.20	0.167	0.023	4.367	3.046	3.425	1.862	0.174	7
135482	1.11	2.77	0.21	0.369	0.208	5.125	5.026	5.619	3.638	0.335	3
136028	1.25	1.90	0.14	0.530	0.426	4.133	5.629	6.570	4.531	0.481	1
137391	0.70	4.14	0.28	0.045	-0.008	1.516	1.212	1.598	0.499	0.050	1
137759	1.12	2.05	0.12	0.299	0.169	4.138	4.751	5.247	3.471	0.257	1
139357	1.13	2.20	0.13	0.330	0.193	4.409	4.868	5.414	3.576	0.289	4
140573	1.09	2.39	-0.07	0.238	0.120	3.734	4.130	4.514	2.944	0.213	1
140573	1.10	2.00	0.17	0.267	0.154	3.692	4.586	5.030	3.303	0.227	1
140573	1.10	2.90	0.37	0.393	0.222	5.450	5.263	5.944	3.772	0.356	1
140573	1.11	2.10	0.25	0.309	0.181	4.195	4.878	5.419	3.533	0.265	1
140573	1.11	2.50	0.23	0.341	0.194	4.746	4.935	5.521	3.568	0.302	1
142980	1.12	2.55	0.10	0.347	0.194	4.838	4.861	5.401	3.548	0.312	1
144284	0.81	3.70	0.23	0.076	0.006	2.019	1.893	2.268	1.046	0.079	7
145000	1.10	2.20	0.10	0.269	0.148	3.868	4.501	4.938	3.239	0.234	4
145148	1.04	3.45	0.13	0.290	0.118	5.230	4.451	4.869	3.058	0.276	1
145675	0.93	4.50	0.31	0.255	0.054	5.904	4.097	4.445	2.606	0.258	1
145675	0.94	4.55	0.27	0.271	0.058	6.198	4.221	4.566	2.703	0.275	1
145675	0.96	4.57	0.35	0.330	0.085	7.044	4.798	5.176	3.122	0.331	1
145675	0.97	4.40	0.18	0.290	0.073	6.316	4.383	4.727	2.865	0.293	1
145675	0.97	4.50	0.22	0.310	0.079	6.687	4.561	4.912	2.983	0.313	1

Table 4.3 (Continued)

STAR HD	$\theta_{\rm eff}$	log g	[M/H]	Mg_2	Mg_1	Mg_b	Fe5270	Fe5335	$Fe52_s$	Mg_s	ref
147677	1.03	2.98	0.11	0.225	0.096	4.003	4.025	4.398	2.750	0.206	3
148513	1.24	1.00	0.20	0.449	0.320	4.145	5.685	6.482	4.510	0.385	1
150680	0.87	2.85	0.07	0.079	0.016	1.758	2.150	2.478	1.322	0.077	2
150680	1.02	2.85	0.26	0.229	0.109	3.830	4.167	4.555	2.837	0.205	2
153956	1.12	2.30	0.12	0.324	0.183	4.500	4.818	5.344	3.517	0.285	1
159181	0.94	1.35	0.29	0.124	0.070	1.574	3.158	3.074	2.213	0.107	1
159181	0.94	1.35	0.30	0.125	0.072	1.581	3.177	3.088	2.226	0.108	1
159181	0.94	1.60	0.10	0.104	0.050	1.497	2.802	2.872	1.932	0.092	1
159181	0.96	1.60	0.14	0.125	0.071	1.621	3.110	3.164	2.158	0.109	1
159925	1.04	2.70	0.11	0.219	0.102	3.683	4.035	4.400	2.782	0.197	4
160922	0.75	4.33	0.40	0.072	-0.001	2.128	1.727	2.117	0.889	0.078	7
161096	1.09	2.44	0.14	0.278	0.148	4.122	4.529	4.992	3.231	0.245	1
161797	0.91	3.91	0.16	0.159	0.035	3.770	3.074	3.443	1.928	0.160	1
161797	0.93	3.83	0.23	0.184	0.050	4.079	3.441	3.795	2.196	0.181	1
161797	0.93	4.10	0.30	0.215	0.054	4.821	3.759	4.114	2.397	0.213	1
161797	0.93	4.10	0.32	0.218	0.057	4.859	3.803	4.161	2.426	0.216	1
162917	0.79	4.10	0.10	0.069	0.000	2.092	1.585	2.031	0.798	0.074	1
163770	1.16	1.28	0.11	0.306	0.195	3.657	4.970	5.421	3.743	0.255	3
163993	1.01	2.50	0.27	0.200	0.110	3.057	3.979	4.306	2.707	0.175	1
166208	1.01	2.76	0.10	0.188	0.084	3.287	3.735	4.054	2.529	0.171	3
166229	1.11	2.58	0.12	0.328	0.181	4.681	4.772	5.296	3.454	0.295	3
167858	0.72	4.33	0.17	0.051	-0.006	1.738	1.257	1.703	0.537	0.058	7
169916	1.06	2.92	0.11	0.270	0.122	4.571	4.399	4.820	3.071	0.246	1
171802	0.78	4.20	0.10	0.067	-0.002	2.086	1.524	1.976	0.746	0.073	1

REFERENCES 1: $T_{\rm eff}$ and gravity from C91
2: $T_{\rm eff}$ from C91 and gravity from McWilliam (1990)
3: $T_{\rm eff}$ and gravity from McWilliam (1990)
4: $T_{\rm eff}$ and gravity from Brown et al. (1989)
5: $T_{\rm eff}$ from C91 and gravity from Brown et al. (1989)
6: $T_{\rm eff}$ and gravity from Clariá, Piatti & Lapasset (1994)
7: Gravity estimated from the luminosity class (Schmidt-Kaler 1982)

Before proceeding with the comparison between indices computed from observed and theoretical spectra, let us comment on the two new indices. In figure 4.5 we show the index-index comparison Mg_2 vs Mg_s (a) and Fe5270 vs $Fe52_s$ (b). The comparison is done by using the values listed in Table 4.3. For the case of the magnesium indices we see an almost one-to-one correlation. However, an interesting behavior was found. It results that two well defined trends dependent on surface gravity are visible; for dwarf stars (log g $\geq$ 3.5) Mg_2 and Mg_s have the same value while for lower gravity stars Mg_2 tend to have higher values than Mg_s, a difference that increases with decreasing temperature. After applying a linear regression to the low gravity data we found that the Δ(index)=Ms_2-Mg_s at T_{eff}=4000 K is estimated to be about 0.15 magnitudes.

For iron indices it results that Fe5270 values are about 1 Å higher than the values of $Fe52_s$. Note, however, that the comparison between these two indices yielded similar results as for magnesium indices in the sense that stars are well separated in two gravity trends which, once again, appear to diverge towards low temperatures. Note also that, since the indices depend on the width of their central bands, in order to make the indices comparable we have multiplied $Fe52_s$ by the ratio of their central bandpasses, $\Delta\lambda$ (Fe5270)/$\Delta\lambda$ ($Fe52_s$).

The analysis of these indices as gravity indicators is envisaged for a future research.

Figures 4.6-4.8 display the behavior of the spectral indices listed in Table 4.2 in terms of θ_{eff} (Table 4.3). Each point corresponds to one determination of θ_{eff}, (different determinations for the same star are connected by a solid line). We have also separated stellar data according to the source of the atmospheric parameters. Points of interest in each figure are indicated in the captions.

The comparison between observed and theoretical indices is depicted in figures 4.9–4.11. In these three figures we have separated stars into primary (solid dots) and secondary data (open dots). Comments on each index follow.

Mg_b (Fig. 4.9). A remarkable good agreement is seen for Mg_b. Points spread around the one-to-one relationship. The scattering appears enhanced at intermediate values of the index. Stars with several determinations indicate that the spread can be attributed mainly to uncertainties in the parameters. The two determinations for the stars HD 109511 (0.64/2.50/0.42) and HD 73710 (1.01/1.60/0.17) repeat the anomalous behavior seen in figures 4.6–4.8. The temperature assigned to HD 109511 in C91 is in clear disagreement (too hot) with the spectral type (K2 III). HD 73710 is a K0 III star in agreement with the temperature determination, however, after an inspection to its observed spectrum, we noticed a strong Hβ line and very weak iron and magnesium lines. This star was most probably misidentified in the observations.

Mg_s (Fig. 4.10). For this index we found that points also cluster around the reference 45^0 line. The point with the highest index values correspond to HD 88230. Notice the similarities between Fig. 3.13 and Fig. 4.10

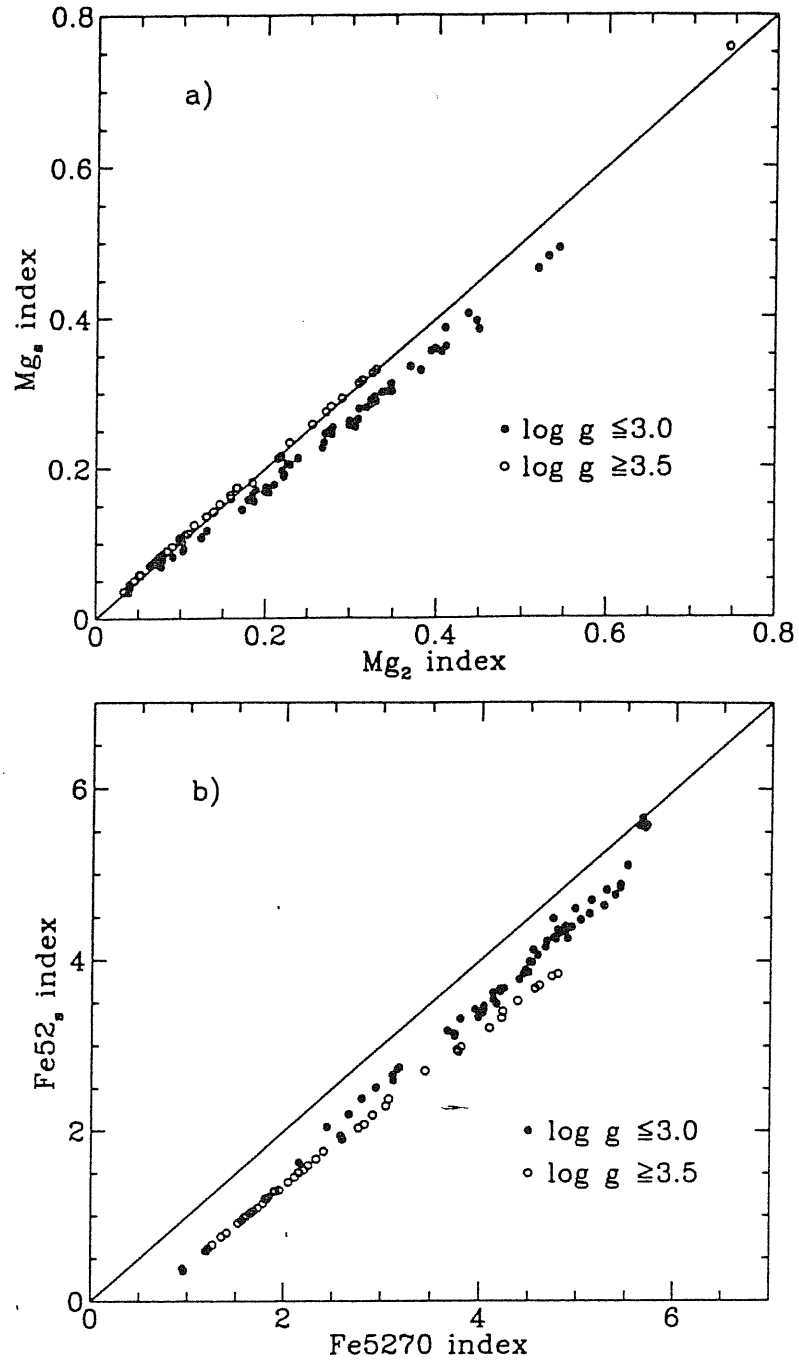

Figure 4.5: a)- Mg_2 vs Mg_s. b)- Fe5270 vs $Fe52_s$. The indices were computed from theoretical spectra by considering the stellar parameters assigned to the observed stars (see text).

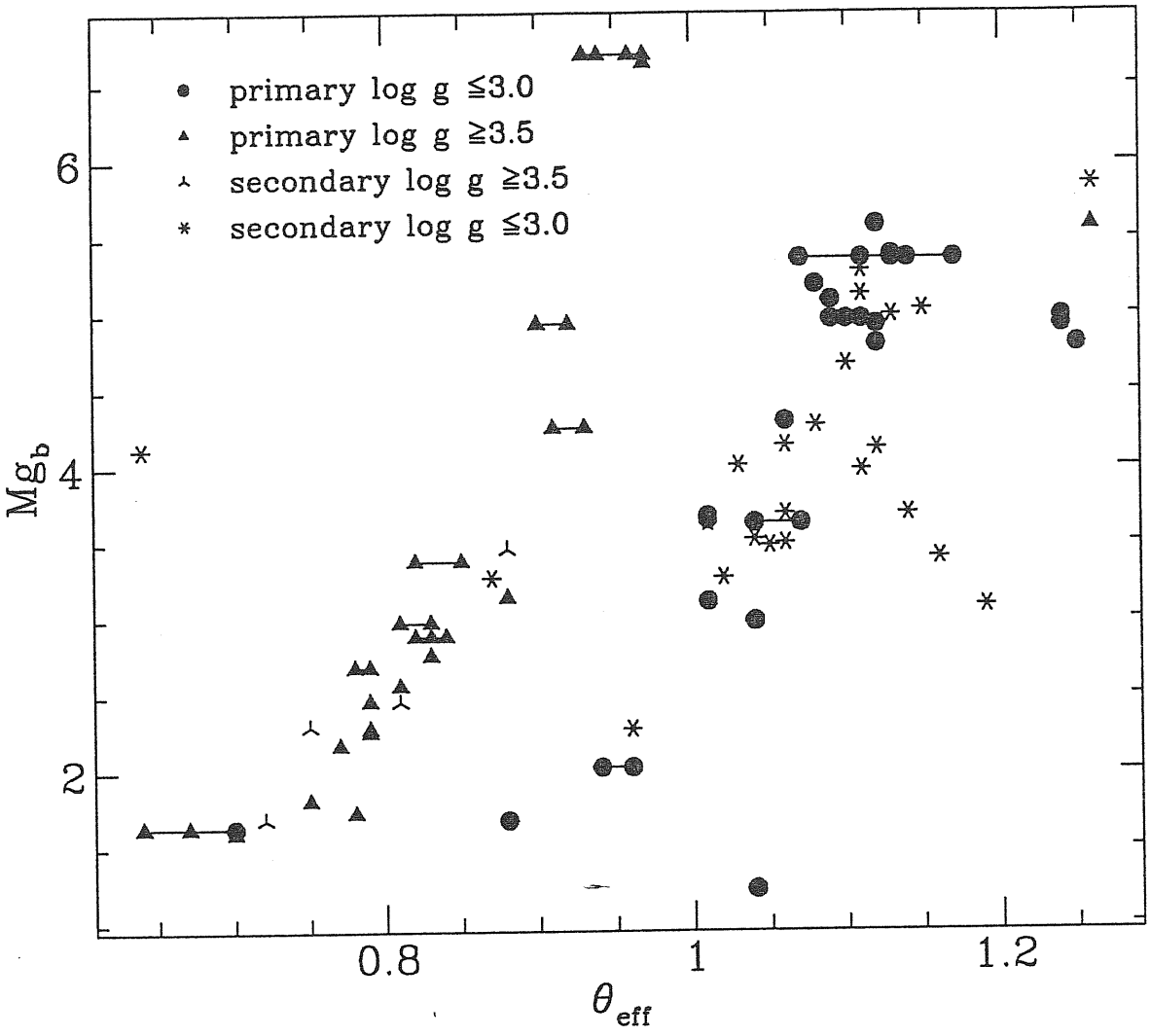

Figure 4.6: Mg_b index from observed spectra as a function of $\theta_{\rm eff}$. Symbols are explained in the box. Note that dwarf stars are well separated from giants and supergiants. In both trends the index increases with decreasing temperature (increasing $\theta_{\rm eff}$) reaching a maximum at 5300 K ($\theta_{\rm eff}$=0.95) for high gravity stars and 4600 K ($\theta_{\rm eff}$=1.1) for giants and supergiants. The turnover in the index behavior is less pronounced in low gravity stars. Compare this to Fig. 3.8. The two most deviating points correspond to determinations for the stars HD 109511 and HD 73710.

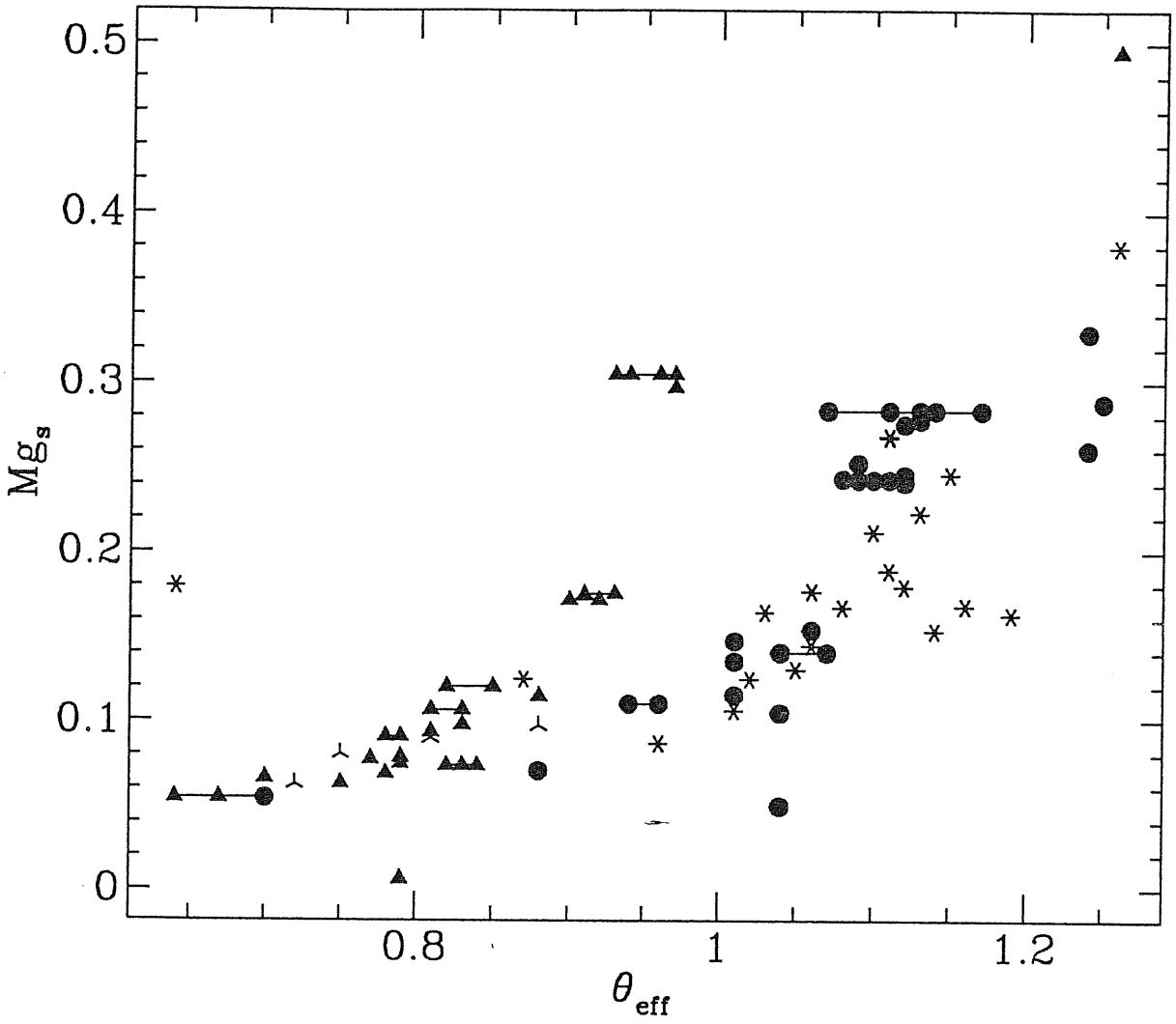

Figure 4.7: Mg_s index from observed spectra as a θ_{eff}. Symbols have the same meaning as in figure 4.6. Effects of gravity are also distinguishable in this index. The most deviating points correspond to the same determinations as for Mg_b.

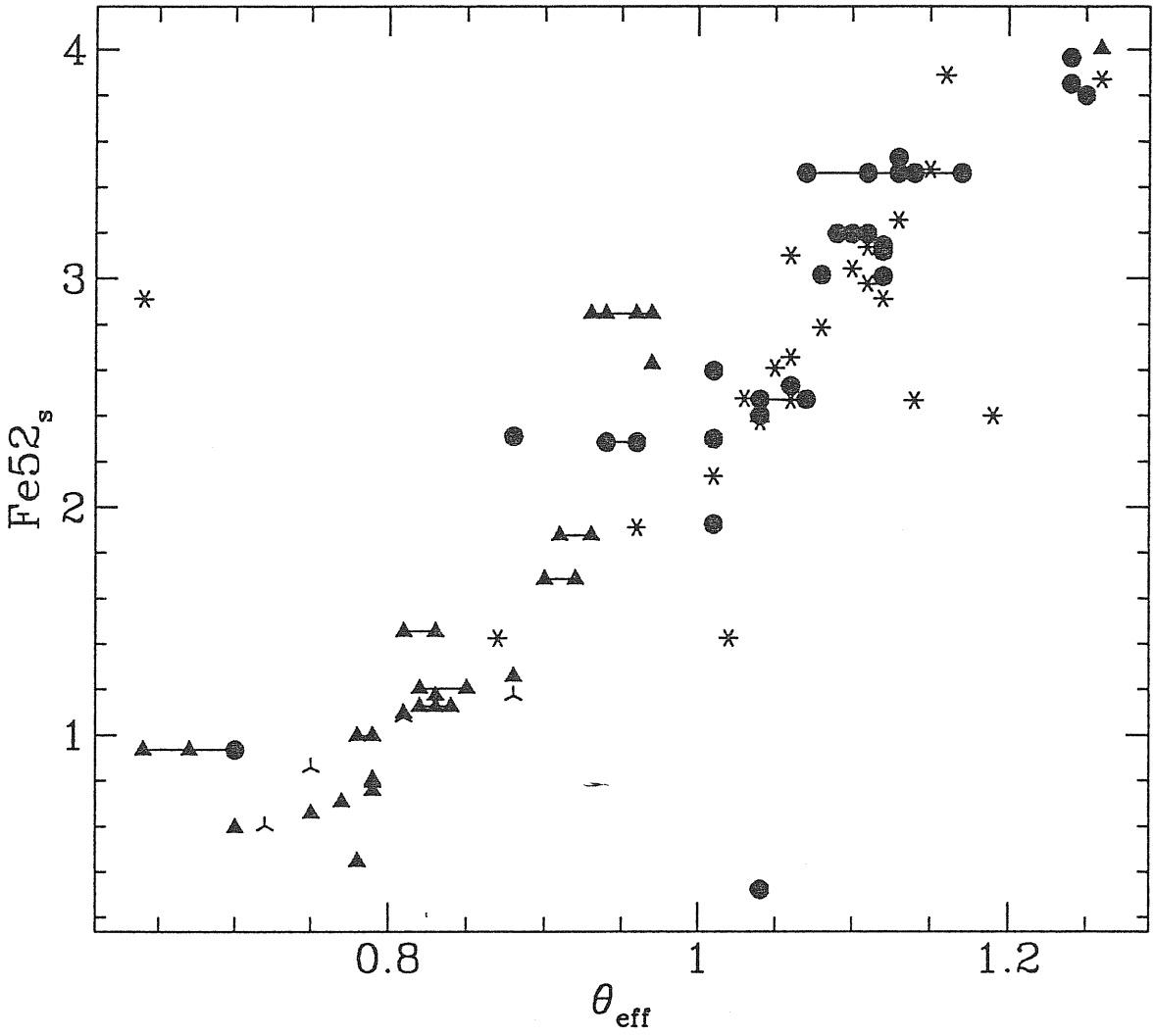

Figure 4.8: Fe52$_s$ index from observed spectra as a function of effective temperature. Symbols have the same meaning as in figure 4.6. The most deviating points correspond to the same determinations as in previous figures.

$Fe52_s$ (Fig. 4.11). The behavior of this index is essentially the same as for Mg_s. The discrepant points correspond to the determinations mentioned above.

From the comparison of the three indices we conclude that in general there is good agreement between theoretical and observed indices. We noted three *extreme* cases clearly deviating from the trends seen for each index. A wrong set of atmospheric parameters can explain two of these cases. Whether HD 88230 is an intrinsically anomalous case or the discrepancies are due to the inadequacy of the atmospheric models at low temperatures will be investigated when the complete sample of SMR stars will be analyzed.

4.4 Observed versus computed spectra

The comparison between observed and synthetic spectra was carried out according to the steps described as follows:

i)- All spectra, observed and theoretical, were normalized to the mean flux in the spectral interval 4900–5290 Å. The blue-edge of the interval was chosen so as to avoid the region in which the wings of the Hβ line are still present in the spectra of the hottest stars in our sample.

ii)- We then computed the ratio between the theoretical normalized spectrum (or spectra, when more than one determination was available) to the corresponding observed one.

iii)- Finally, we calculated the mean and the RMS deviation from the ratios of normalized spectra. The RMS deviation provides a direct measurement of the agreement between theoretical and observed spectra.

For reference we have applied the procedure just described to the solar observed flux (Kurucz et al. 1984) and a theoretical model interpolated from our grid using the solar parameters (5777/4.43770/0.0) Both the observed and the theoretical fluxes were degraded and rebinned to make the results compatible with the stellar spectra. The deviation found for the Sun is σ=0.0109, which we consider as the best attainable value, according to the analysis presented in chapter 2.

The results are listed in Table 4.4. The two columns list the HD number, and the RMS deviation. Stars with multiple determinations are ordered as in Table 4.3.

A clear illustration of the results is presented in figure 4.12. Over the temperature range 4400-7750 K (1.15-0.65 in $\theta_{\rm eff}$) and excluding the four heavily deviating points, σ displays a quite flat behavior. Many of the determinations have a σ very close to the solar value represented by the starred symbol, particularly at temperatures near the solar one. The four points with the largest σ correspond to the stars already commented in the previous section plus the star HD 113022.

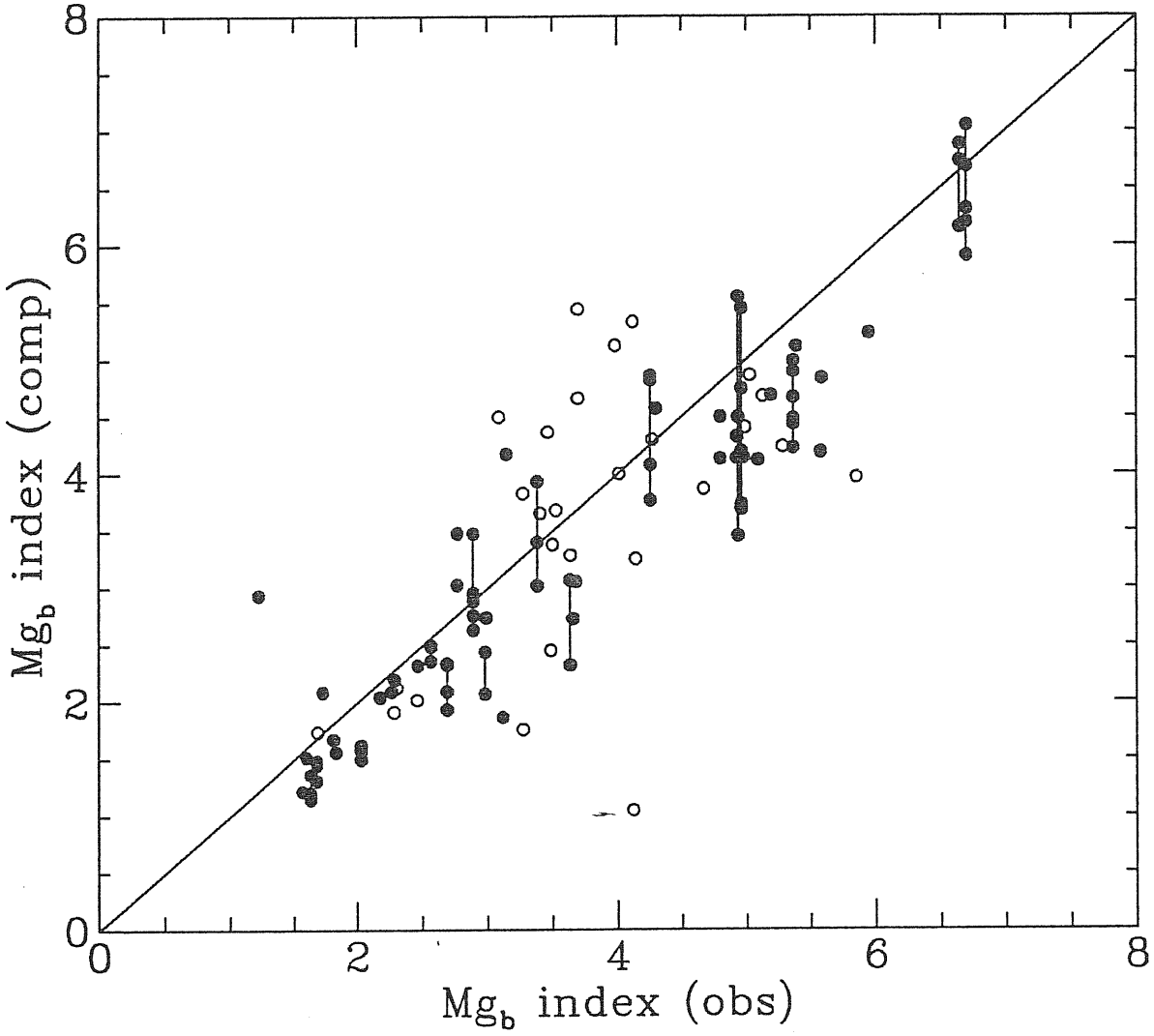

Figure 4.9: Comparison between observed and computed Mg$_b$ indices. Vertical bars connect the points corresponding to different determinations of atmospheric parameters for a given star.

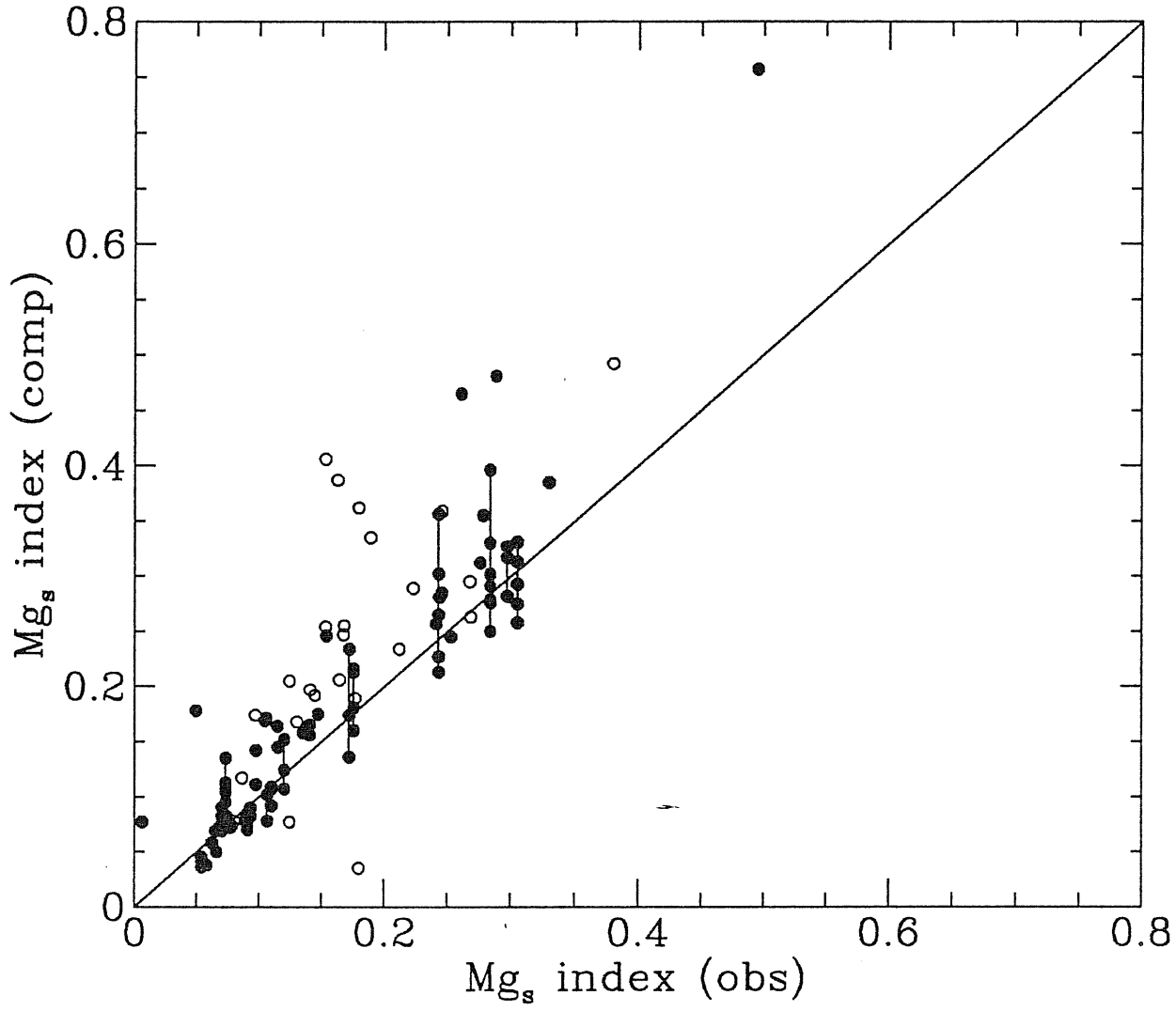

Figure 4.10: Comparison between observed and computed Mg_s indices. Vertical bars connect the points corresponding to different determinations of atmospheric parameters for a given star.

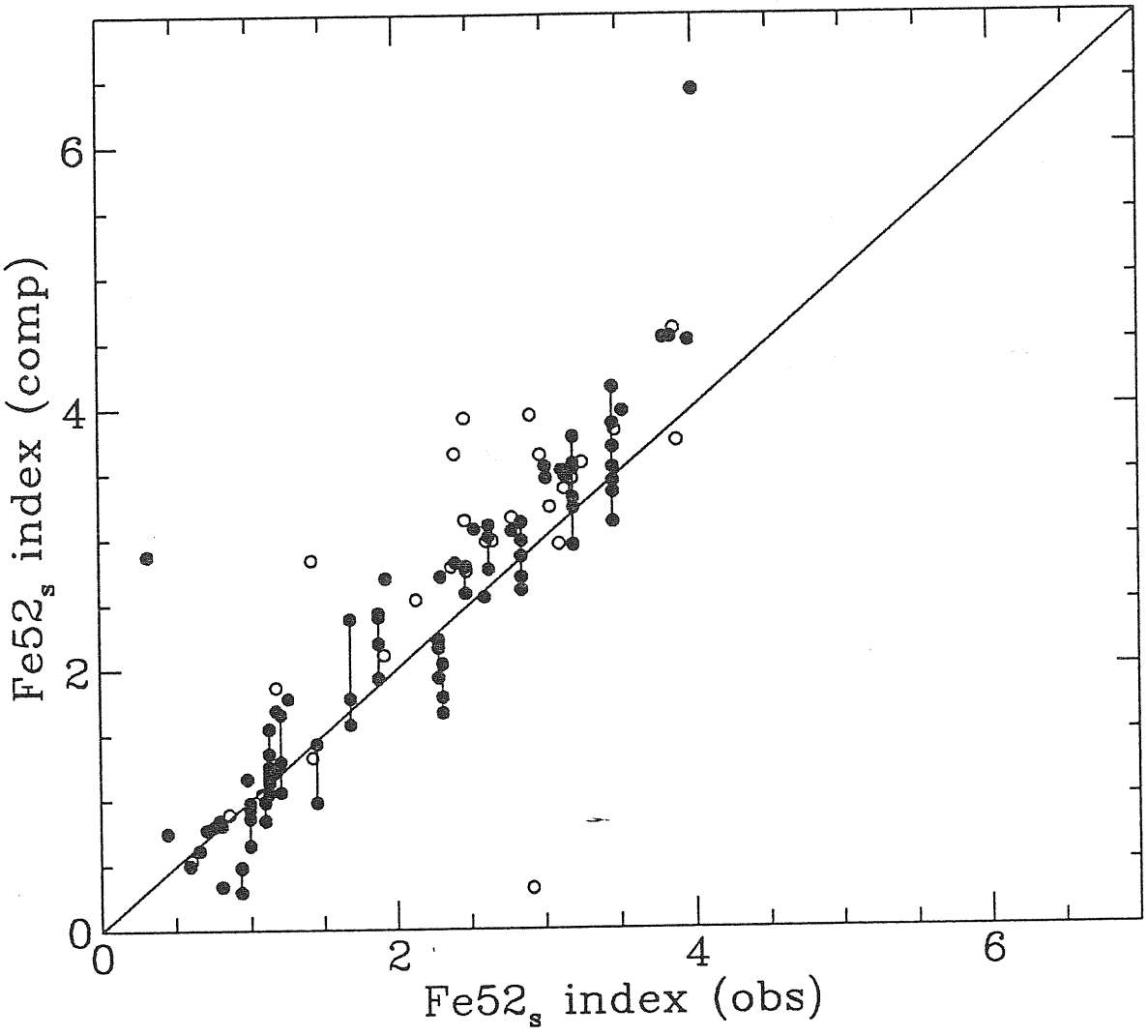

Figure 4.11: Comparison between observed and computed Fe52$_s$ indices. Vertical bars connect the points corresponding to different determinations of atmospheric parameters for a given star.

Table 4.4: Standard deviations from the residual spectra

star	σ	star	σ	star	σ
48682	0.0349	102870	0.0258	140573	0.0463
49161	0.1193	102870	0.0241	140573	0.0468
52973	0.0519	102870	0.0243	140573	0.0616
52973	0.0478	102870	0.0246	140573	0.0457
52973	0.0510	102870	0.0251	140573	0.0488
58207	0.0510	102870	0.0248	142980	0.0615
58207	0.1113	102870	0.0287	144284	0.0286
61064	0.0387	109511	0.1359	145000	0.0604
63700	0.0661	109511	0.0897	145148	0.0350
65714	0.0637	110014	0.0912	145675	0.0386
72184	0.0410	113022	0.1438	145675	0.0365
72324	0.0466	114710	0.0209	145675	0.0385
72324	0.0309	114710	0.0169	145675	0.0351
73665	0.0391	114710	0.0225	145675	0.0363
73710	0.1625	115604	0.0721	147677	0.0365
74739	0.0497	115604	0.0666	148513	0.0959
75732	0.0563	115604	0.0590	150680	0.0403
75732	0.0558	115617	0.0334	150680	0.0609
75732	0.0564	115617	0.0252	153956	0.0677
81873	0.0398	115617	0.0365	159181	0.0473
83951	0.0254	116976	0.0518	159181	0.0474
85503	0.0534	120136	0.0259	159181	0.0477
85503	0.0556	120136	0.0222	159181	0.0493
85503	0.0613	120136	0.0235	159925	0.0434
85503	0.0524	120136	0.0216	160922	0.0559
85503	0.0541	121370	0.0499	161096	0.0629
85503	0.0529	121370	0.0423	161797	0.0345
85503	0.0821	124570	0.0231	161797	0.0352
87822	0.0298	124570	0.0217	161797	0.0398
88230	0.1779	124570	0.0216	161797	0.0404
90277	0.0309	127227	0.1047	162917	0.0187
91125	0.0478	129989	0.0634	163770	0.0791
93257	0.0577	130948	0.0474	163993	0.0487
100563	0.0185	135482	0.0755	166208	0.0579
101013	0.1206	136028	0.1316	166229	0.0629
102328	0.0797	137391	0.0233	167858	0.0198
102634	0.0262	137759	0.0398	169916	0.0984
102634	0.0307	139357	0.0693	171802	0.0619

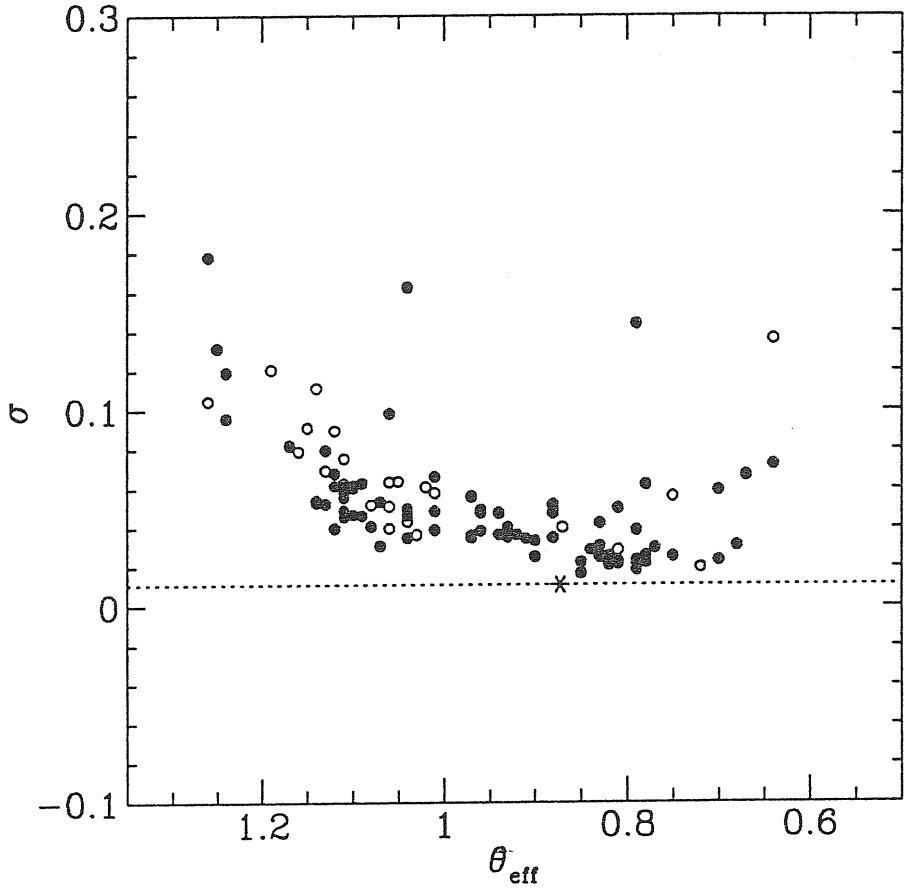

Figure 4.12: Standard deviation of the residual spectra for the 114 determinations as a function of $\theta_{\rm eff}$. The starred symbol and dotted line correspond to the solar value. Primary and secondary data are represented by solid and empty dots respectively. Note that the deviations seem to increase towards low temperatures.

4.4.1 Selecting the set of atmospheric parameters

Based on the results obtained above, we are now in position of labelling stars as SMR. We have selected the stars for which the best match is obtained (i.e. a small σ). The only selection criteria we have imposed is that stars have $\sigma \leq 0.1$. For those stars with several determinations of the atmospheric parameters, we have kept only the set that produces the smallest deviation.

After this selection we have re-plotted the observed spectral indices of the resulting 55 objects as a function of effective temperature as in Figures 4.6–4.8. In the illustration for the magnesium indices (Figs 4.13 and 4.14) note that the separation of the stars in two gravity trends is even neater. For the iron index (Fig. 4.15) we have that the spread of the points has been reduced.

In table 4.5 we list the set of metal-rich stars together with the abundance determination of the best fit. Stars are tabulated in order of increasing abundance.

The apparent trend indicating that the deviations increase at low temperatures should be investigated in further detail in the future: High resolution data are highly desirable to have deeper insight into the differences between models and observations.

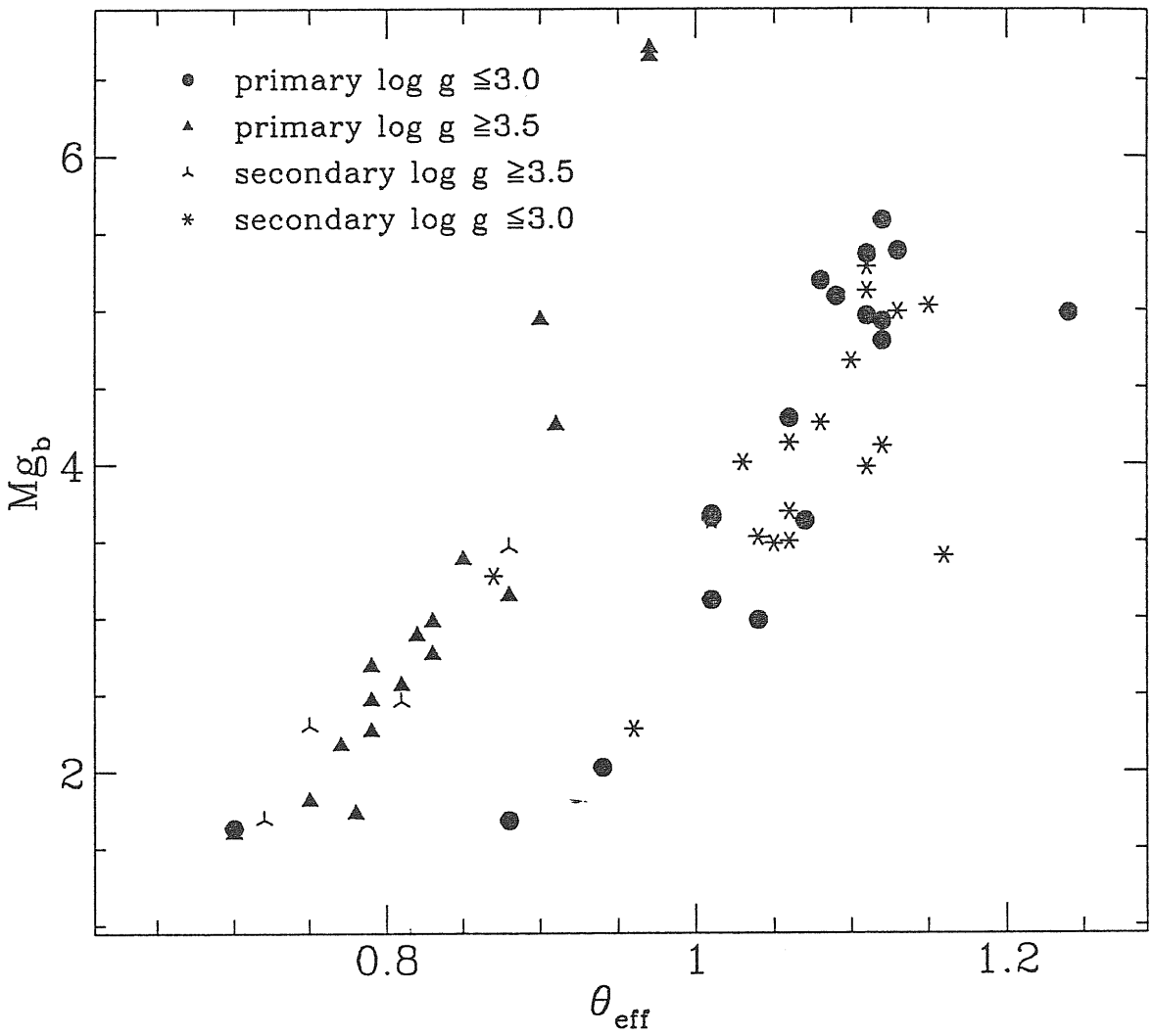

Figure 4.13: Mg_b of selected stars as a function of effective temperature.

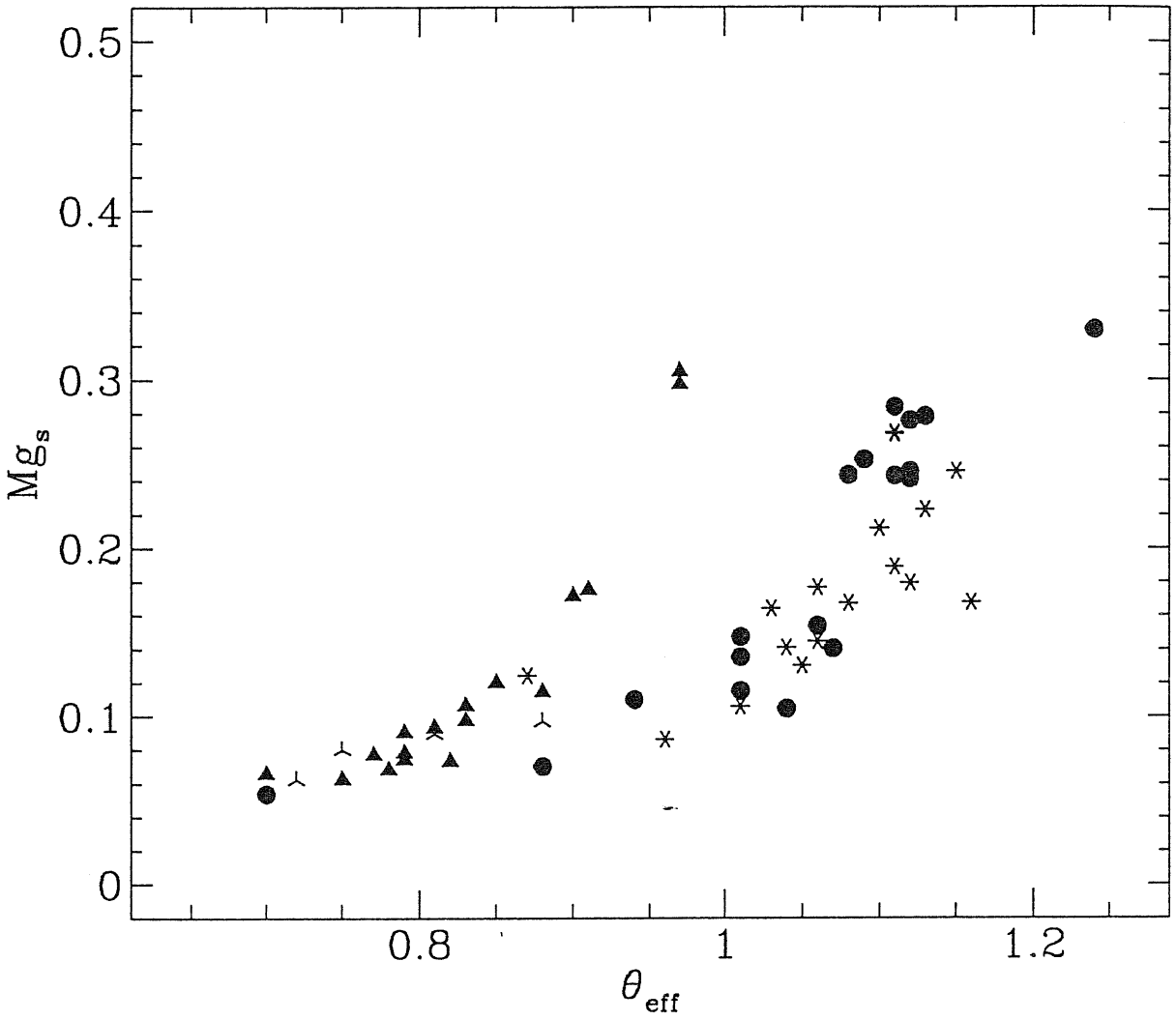

Figure 4.14: Mg_s of selected stars as a function of effective temperature. Symbols are as in figure 4.13.

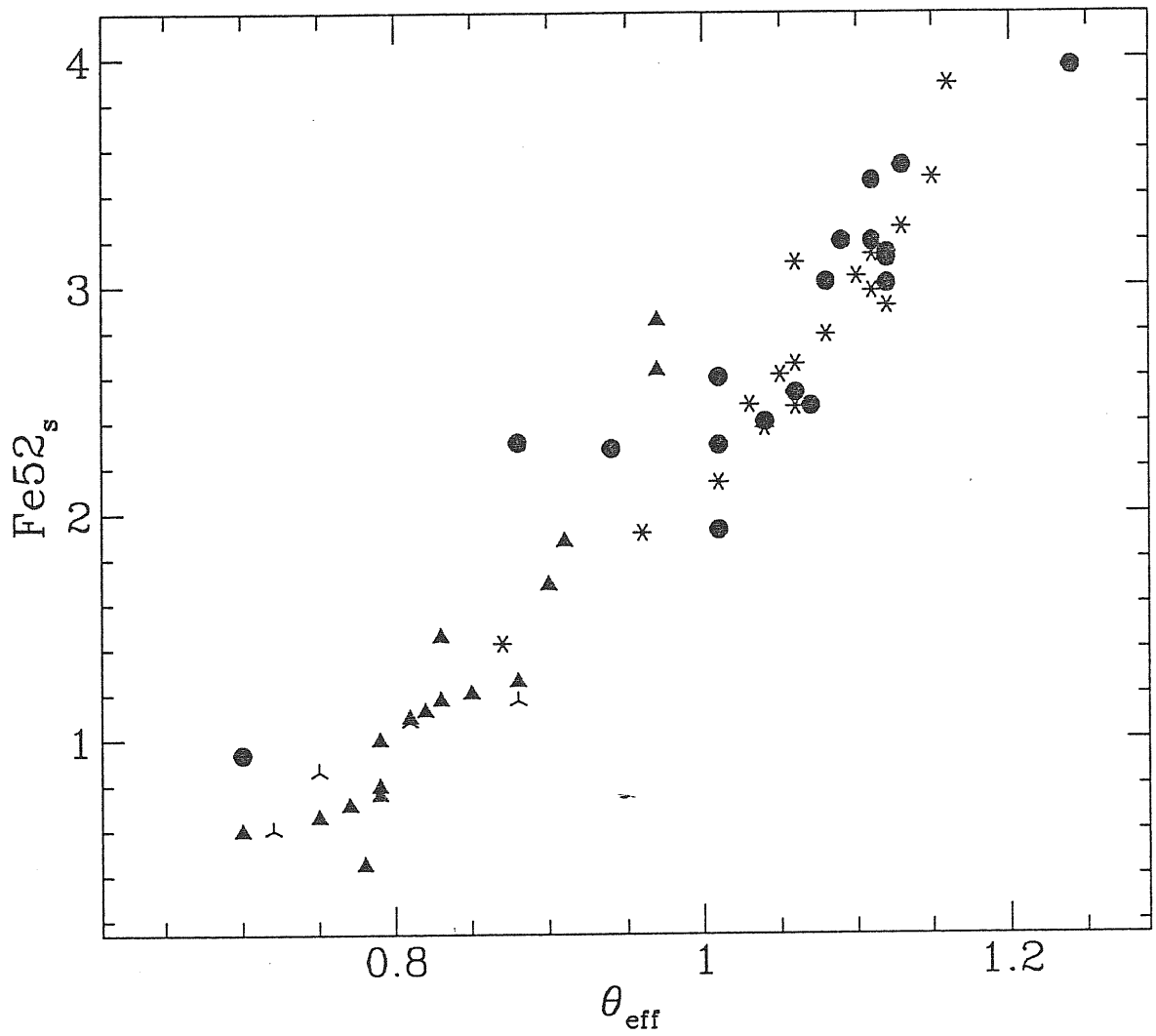

Figure 4.15: $Fe52_s$ of selected stars as a function of effective temperature. Symbols are as in figure 4.13.

Table 4.5: Fiducial set of SMR stars

star	[Fe/H]	star	[Fe/H]
171802	0.10	58207	0.16
145000	0.10	81873	0.16
166208	0.10	167858	0.17
142980	0.10	115604	0.18
162917	0.10	145675	0.18
163770	0.11	87822	0.19
147677	0.11	90277	0.19
93257	0.11	130948	0.20
116976	0.11	74739	0.20
159925	0.11	148513	0.20
169916	0.11	135482	0.21
100563	0.12	144284	0.23
153956	0.12	63700	0.24
137759	0.12	65714	0.24
166229	0.12	75732	0.24
124570	0.13	140573	0.25
139357	0.13	102870	0.26
92125	0.13	163993	0.27
145148	0.13	137391	0.28
129989	0.13	159181	0.29
102634	0.14	72184	0.34
120136	0.14	121370	0.38
83951	0.14	160922	0.40
161096	0.14	102328	0.41
48682	0.15	109511	0.42
110014	0.16	61064	0.44
73665	0.16	52973	0.49
161797	0.16		

Chapter 5

Integrated Spectra of Single Stellar Populations

Numerous reviews have been written regarding population synthesis techniques and their use for understanding the underlying stellar population(s) giving rise to an integrated spectrum with some particular characteristics (Tinsley 1975, O'Connell 1986). On what follows we will concentrate in the analysis of single stellar populations (SSP), that is, single generations of coeval and initially chemically homogeneous stars. In the last section of this chapter we will present the very preliminary results obtained for elliptical galaxies.

A very simplified picture of the Population Synthesis (PS) is illustrated in figure 5.1. The starting point are a set of stellar evolutionary tracks and a stellar flux library. Stars are distributed along the zero age main sequence (ZAMS) as prescribed by the stellar birthrate. Colors and other spectral properties are analyzed at different epochs as the population evolves. Therefore, among the basic requirements in population synthesis are the correct evaluation of the relative number of stars at different evolutionary phases, the inclusion of all relevant stages of stellar evolution and, very important, the continuity in the HR diagram. Nevertheless, the partial fulfillment of these basic requirements represents one of the main problems associated with population synthesis:

- Incomplete knowledge of stellar evolution, exclusion of relevant evolutionary phases, and inhomogeneity of stellar tracks. Most libraries of stellar evolutionary tracks used currently in the context of EPS are heterogeneous or despite being very homogeneous (Maeder & Meynet 1991) cover only the evolution from the main sequence to the red giant branch, thus not considering from the horizontal branch and beyond. There are other data sets which are homogeneous and complete up to the asymptotic giant branch phase (Bertelli et al. 1986), but the input physical data such as opacities are not updated.

- In order to fit the integrated spectra of assemblies of stars it is necessary to have stellar fluxes for the whole range of stellar parameters. Observational data are particularly incomplete for metal-rich (as those present in the Bulge; Rich 1988) and very metal poor stars of low luminosity.

In this chapter we explore some spectral properties of SSPs by using a homogeneous and complete collection of isochrones computed by the Padova group (see Chiosi, Bertelli & Bressan 1988, Bertelli et al. 1990). As stellar templates we will the stellar spectra library described in chapter 3.

5.1 From stellar to integrated properties

In this section we explain in some detail the procedure we have followed to determine integrated spectral properties of a SSP. We have closely followed the procedure of Bressan, Chiosi & Tantalo (1995-hereafter BCT95) to whom the reader is referred for more details. In fact the only difference between their and our approach is the stellar spectroscopic data used.

The integrated monochromatic flux from a SSP of metallicity Z and age t' is given by

$$F_{SSP}(t', Z) = \int_{m_l}^{m_u} \phi(m) f_\lambda(m, t', Z) dm \tag{5.1}$$

Where $f_\lambda(m, t, Z)$ is the monochromatic flux from a star of mass m, age t' and chemical composition Z. The limits m_l and m_u are the mass range of stars born in an event of stars formation. For our calculations we will consider m_l =0.15 and m_u= 120 $M_\odot$.

The initial mass function (IMF),

$$\phi(m)dm = A \times m^{-s} dm \tag{5.2}$$

describes the number of stars born in mass intervals $(m, m + dm)$. A is a normalization constant such that

$$\int_{m*}^{m_u} \phi(m) \times m \times dm = \zeta \tag{5.3}$$

where ζ is the fraction of the total mass in the form of stars stored in the IMF above m_*. The total mass has been normalized to 1 $M_\odot$. The slope of the IMF to be considered here is s = 2.35 (Salpeter 1955), however other possible values can be used (Scalo 1986).

In order to carry out the integral in equation 5.1 we have divided the isochrone into 122 steps corresponding to elemental portions in luminosity and effective temperature or, equivalently, in intervals of mass, surface gravity and number of stars (per initial mass interval) according to the IMF.

The set of isochrones, kindly made available by A. Bressan in computer readable form, cover the age range between 1 to 20 Gyr. Three metallicities, Z=0.02 (solar), Z=0.004 and Z=0.008 because they are covered by our grid of synthetic

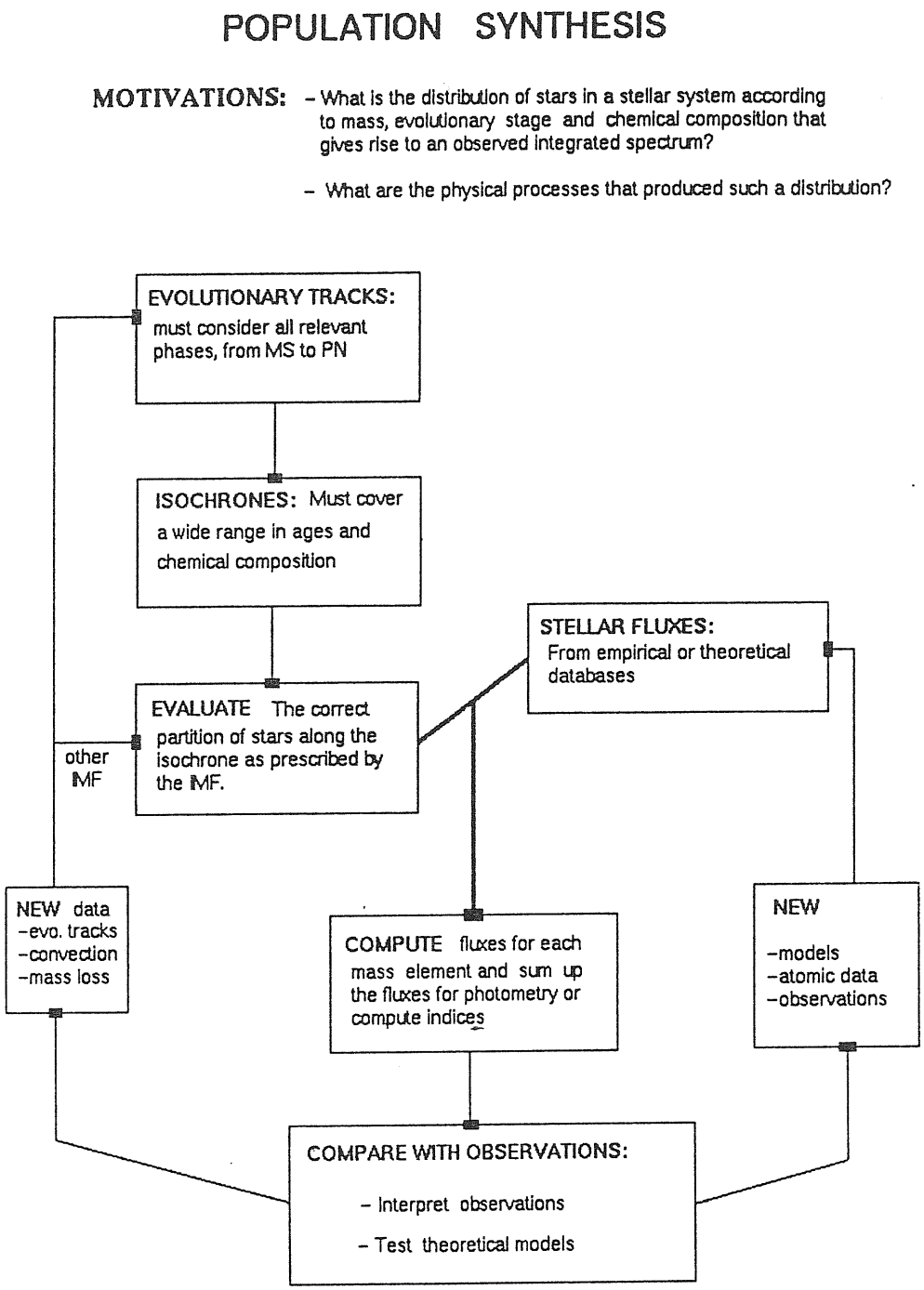

Figure 5.1: Diagram representing the population synthesis technique

spectra. Figure 5.2 shows some of the isochrones used in the calculations. The inner box encloses the parameter space covered by our grid of synthetic spectra. Note that our grid of synthetic spectra does not cover low gravity stars (log g < 1.0) and stars in the cool edge of the main sequence. Below we give an estimation of the contribution of these low gravity stars to the integrated Mg_2 index.

5.2 Spectral indices versus age

Bressan, Chiosi & Fagotto (1994-hereafter BCF94) and BCT95 have computed color indices in the Johnson system $UBVRIJKLMN$ for a vast set of SSPs of different ages and metallicities by using Kurucz's library of spectral energy distributions complemented with empirical data from several sources. In order to derive narrow band indices these authors computed the continuum bandpass flux, $F_{C\lambda}$, from the library of stellar spectra of BCF94, and then they calculated the flux in the central bandpass $F_{I\lambda}$ by means of the fitting functions of WFGB94.

We have computed a grid of fluxes $F_{C\lambda}$ and $F_{I\lambda}$ directly from our library of synthetic spectra. Since the cases computed in the grid not necessarily agree with the intervals in mass and T_{eff} in which the isochrone was divided, we have linearly interpolated within the grid to properly associate a flux to the isochrone element.

F_{SSP} in equation 5.1 represents either the integrated $F_{C\lambda}$ or $F_{I\lambda}$ therefore, the integrated index is derived following the definitions given in chapter 3. In order to account for the low gravity stars not covered by our grid of stellar spectra, we have assigned to them the value of the fluxes of the nearest point of the grid. This may sound a rough approximation, but acceptable within the exploratory nature of the material presented in this chapter.

The index-age relationship for five of the indices in a SSP of Z=0.02 is shown in figure 5.3. We have divided into two panels to separate the indices measured in magnitudes (top panel) from those measured as equivalent widths (bottom panel). For all indices it is evident that at 18 Gyr there is a turnover in the tendency. Note that the two iron indices occupy the nearly same locus for each age considered.

We have mentioned in the introductory chapter that one the main problems and motivations in PS is the univoke determination of the age and metal contents of stellar systems, a task that has probed to be difficult due to the similar effects of both parameters on their spectra.

To get insight of the role played by age and metallicity we present in figure 5.4 the Mg_2 index for three different values of Z and the age interval from 1 to 20 Gyr. Perhaps the most remarkable point in Fig. 5.4 is the fact that index sequences never overlap, indicating that age and metal abundance effects should be separable. The index variation within each sequence is less for lower metallicity systems. In fact, the variation of the index for Z=0.004 goes from 0.127 at 1 Gyr

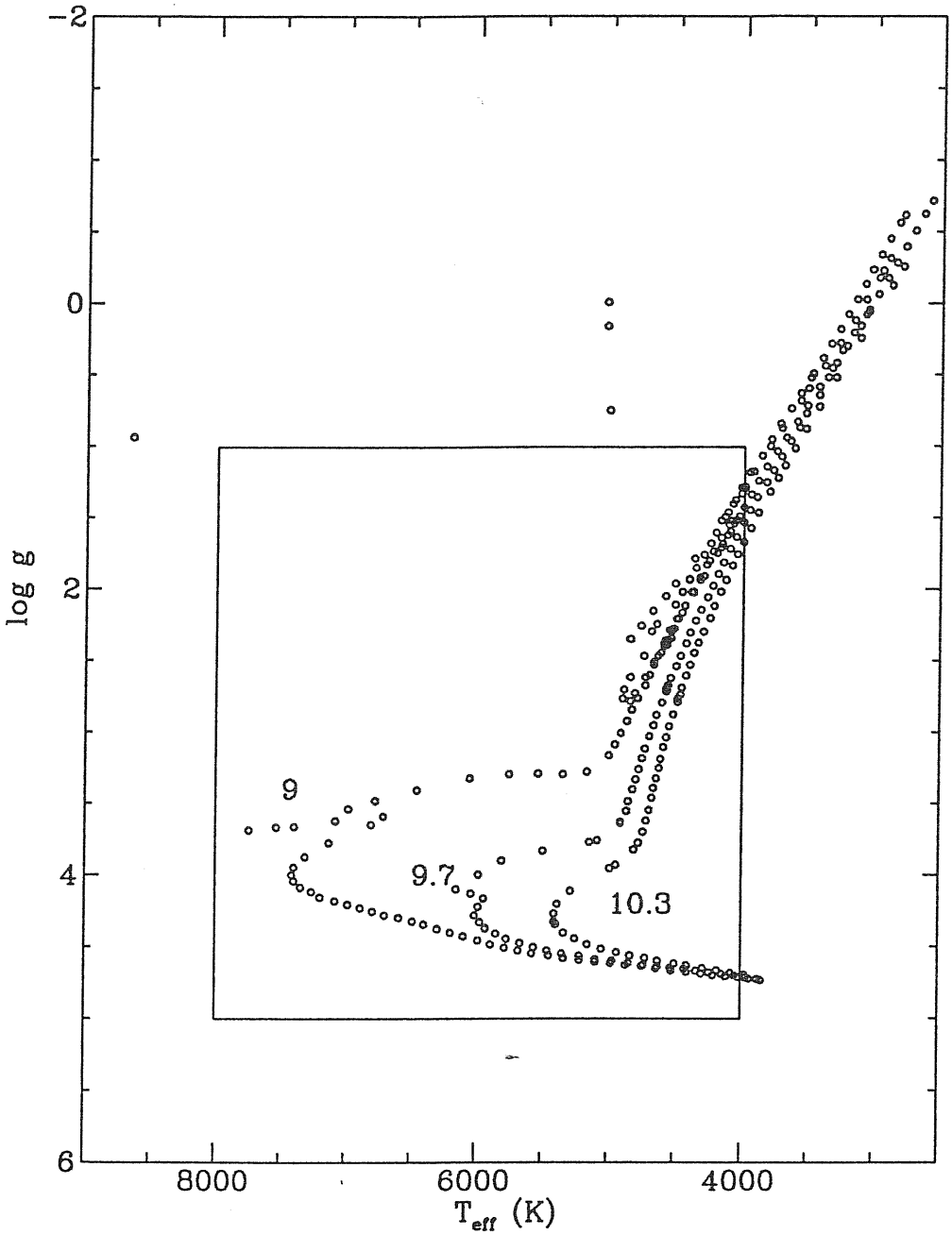

Figure 5.2: Isochrones of different ages for solar metallicity, Z=0.02. The inner box illustrates the parameter space covered by the synthetic stellar fluxes.

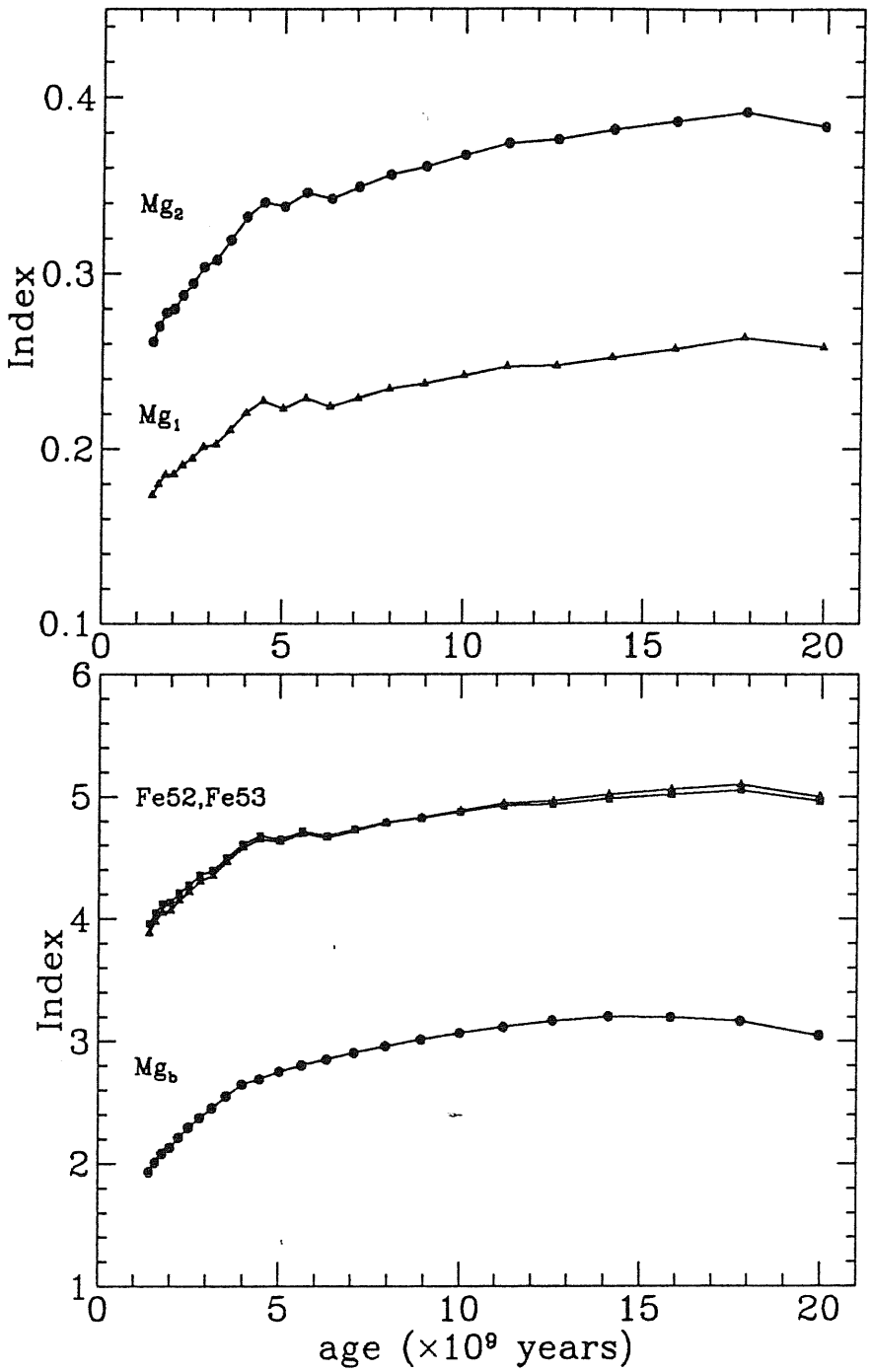

Figure 5.3: Iron and Magnesium indices as a function of age for a SSP of solar metallicity. The upper and lower panels display the indices measured in magnitudes and equivalent widths. For populations older than 18 Gyr the there is a turnover of the trend of the indices.

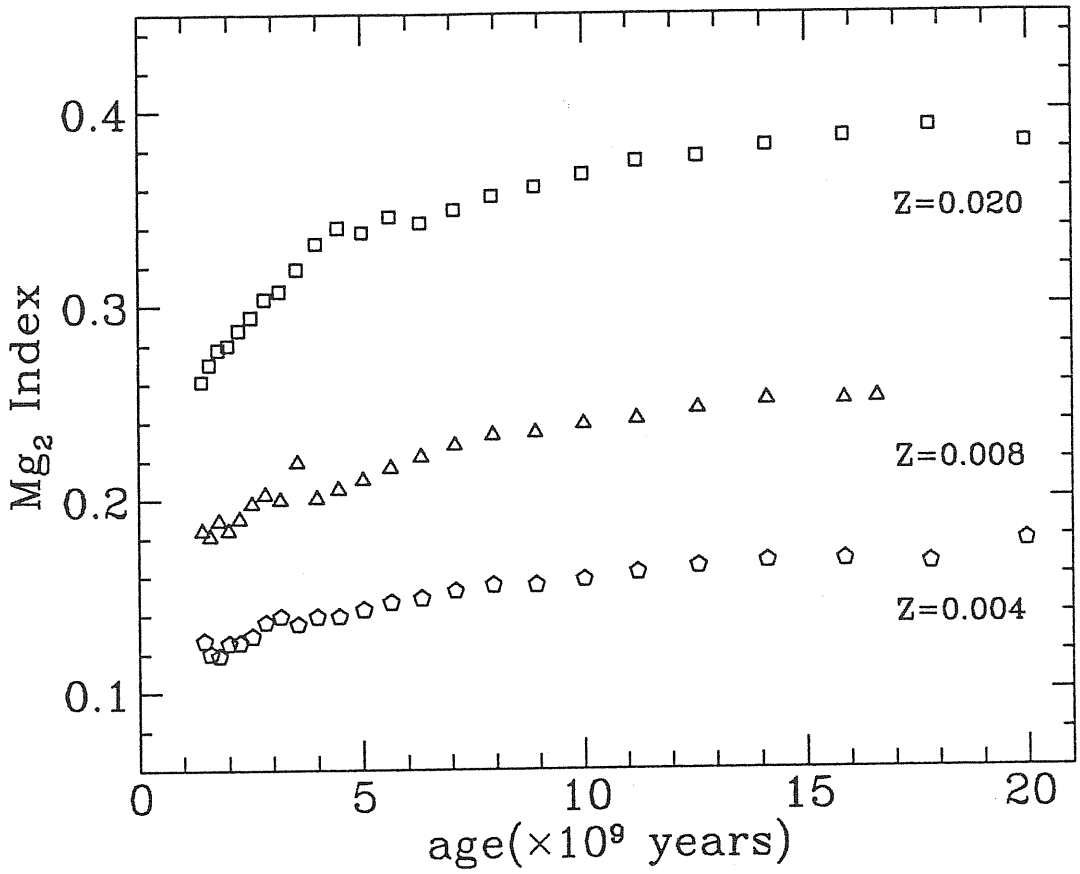

Figure 5.4: Mg_2 index as a function of age for different metallicities. Note that over the whole age range the index values never overlap.

to 0.177 at 20 Gyr, this is only 0.05 mag, while for Z=0.02 the variation reaches about 0.12 mag. The indices for all isochrones considered are tabulated in Table 5.1.

5.2.1 Contributions to the integrated Mg_2 index

In order to explore the relative contribution of stars in different evolutionary stages let us first recall the main stages on the evolution of a star and explain briefly the main changes undergone by the stars (of low and intermediate mass) in each phase and their loci in the HR diagram. For further details we refer the reader to the books specialized on stellar structure and evolution or recent reviews (Iben 1991; Chiosi, Bertelli & Bressan 1992).

- Main Sequence (MS): Convective core hydrogen burning phase. The stars spend about 80% of their lives at this stage. Based on the Voight-Russel theorem the MS is commonly divided upper and lower main sequence the limiting mass being M $\approx$ 1.5 $M_\odot$ (depending on the chemical composition). Energy production in stars of the upper main sequence takes place through

Table 5.1: Integrated spectral indices for SSP of different ages and metallicities

Metallicity	age (Gyr)	Mg_2	Mg_1	Mg_b	Fe5270	Fe5335
Z=0.020	1.413	0.261	0.173	1.934	3.884	3.960
	1.585	0.270	0.179	2.011	3.977	4.049
	1.778	0.277	0.185	2.082	4.051	4.120
	1.995	0.279	0.185	2.132	4.069	4.136
	2.239	0.287	0.190	2.214	4.152	4.213
	2.512	0.294	0.194	2.296	4.219	4.274
	2.818	0.303	0.201	2.375	4.306	4.358
	3.162	0.307	0.202	2.453	4.353	4.395
	3.548	0.319	0.210	2.551	4.465	4.498
	3.981	0.332	0.220	2.648	4.582	4.610
	4.467	0.340	0.227	2.691	4.648	4.677
	5.012	0.337	0.222	2.752	4.629	4.650
	5.623	0.345	0.229	2.804	4.696	4.715
	6.310	0.342	0.224	2.852	4.663	4.677
	7.079	0.349	0.229	2.907	4.723	4.732
	7.943	0.356	0.234	2.960	4.785	4.788
	8.913	0.360	0.237	3.014	4.827	4.824
	10.000	0.367	0.241	3.066	4.884	4.874
	11.220	0.373	0.247	3.116	4.943	4.926
	12.589	0.376	0.247	3.166	4.963	4.937
	14.125	0.381	0.252	3.200	5.014	4.980
	15.849	0.386	0.256	3.194	5.059	5.017
	17.783	0.391	0.263	3.163	5.097	5.052
	19.953	0.383	0.257	3.047	5.000	4.965
Z=0.008	1.413	0.184	0.115	1.383	3.033	2.960
	1.585	0.180	0.111	1.398	3.022	2.941
	1.778	0.189	0.117	1.460	3.127	3.036
	1.995	0.183	0.112	1.474	3.049	2.967
	2.239	0.189	0.116	1.538	3.127	3.037
	2.512	0.197	0.120	1.630	3.235	3.131
	2.818	0.202	0.124	1.657	3.282	3.176
	3.162	0.199	0.119	1.717	3.247	3.140
	3.548	0.219	0.136	1.768	3.477	3.351
	3.981	0.200	0.119	1.758	3.236	3.132
	4.467	0.205	0.122	1.803	3.287	3.179
	5.012	0.210	0.125	1.853	3.339	3.227
	5.623	0.216	0.129	1.903	3.411	3.292
	6.310	0.222	0.133	1.953	3.476	3.349
	7.079	0.227	0.137	2.006	3.540	3.406
	7.943	0.232	0.140	2.056	3.596	3.455
	8.913	0.234	0.140	2.103	3.604	3.459
	10.000	0.238	0.143	2.142	3.651	3.499
	11.220	0.240	0.143	2.203	3.669	3.514
	12.589	0.246	0.147	2.242	3.717	3.556
	14.125	0.250	0.150	2.271	3.757	3.591
	15.849	0.250	0.150	2.290	3.732	3.570
	16.596	0.251	0.151	2.289	3.736	3.574
Z=0.004	1.445	0.127	0.072	1.017	2.329	2.226
	1.585	0.120	0.066	1.003	2.246	2.147
	1.778	0.119	0.065	1.014	2.237	2.136
	1.995	0.125	0.069	1.053	2.326	2.218
	2.239	0.126	0.069	1.078	2.341	2.229
	2.512	0.129	0.071	1.112	2.398	2.278
	2.818	0.136	0.075	1.174	2.513	2.379
	3.162	0.139	0.077	1.196	2.530	2.398
	3.548	0.135	0.073	1.215	2.471	2.344
	3.981	0.139	0.076	1.249	2.520	2.388
	4.467	0.139	0.075	1.277	2.512	2.382
	5.012	0.143	0.077	1.312	2.559	2.424
	5.623	0.146	0.080	1.346	2.606	2.465
	6.310	0.148	0.080	1.381	2.626	2.484
	7.079	0.152	0.083	1.418	2.675	2.527
	7.943	0.155	0.084	1.449	2.716	2.563
	8.913	0.155	0.083	1.485	2.700	2.549
	10.000	0.158	0.085	1.515	2.734	2.578
	11.220	0.161	0.087	1.550	2.776	2.615
	12.589	0.164	0.089	1.589	2.795	2.634
	14.125	0.167	0.090	1.621	2.812	2.651
	15.849	0.167	0.091	1.624	2.801	2.643
	17.783	0.166	0.090	1.634	2.705	2.563
	19.953	0.177	0.098	1.741	2.824	2.668

the CNO cycle and is highly concentrated in the inner most convective core surrounded by a radiative envelope while lower MS stars have a radiative core surrounded by a partially convective envelope and the energy is produced through the PP chain.

- Subgiant Branch (SGB): Stars in this phase are characterized by a hydrogen burning shell surrounding an isothermal He core. The H-burning shell forms just outside the core and moves outward the stars. In the trip from the MS to the base of the Hayashi line the burning in the shell becomes less able to provide energy. In addition this energy is absorbed in the expanding envelope leading to a decrease in the surface temperature. Once the material in the envelope is transparent enough, the envelope stops its expansion and the star its motion towards lower temperatures.

- Red Giant Branch (RGB): When the expansion of the envelope terminates, the star climbs along the RGB (Hayashi line). The energy is still provided by a H-burning shell. The burning in this shell adds helium to the degenerated He core increasing the temperature of the core and hence consequently that of the burning shell. The luminosity of the star is proportional to the energy release in the shell (therefore to the shell temperature) thus we see the movement upward the RGB. This motion terminates when the temperature in the core is enough to induce the onset of the 3α reaction which abruptly removes the degeneracy in the core.

- Horizontal Branch (HB): Stars in the HB form a special group characterized for being a rather stable late phase in their evolution closely resembling the MS. The He-burning phase lasts for about 20-30% of the lifetime in the main sequence. The locus occupied by the HB stars in the HRD is roughly a line (equal brightness) of length (spread in T_{eff}) which depends mainly on the chemical composition and mass of the main sequence precursor. Mass loss during the RGB phase also plays a role in dictating the HB morphology.

- Asymptotic Giant Branch (AGB): After the HB stars exhaust the supply of Helium in their cores their evolution proceeds again to higher luminosities and redder colors along a path almost parallel to the RGB. The AGB phase is divided in two segments; the E-AGB (early AGB) and TP-AGB (thermally pulsing AGB). The E-AGB phase includes stars from the exhaustion of central He until the H-burning shell is reignited. The TP-AGB extends from the this reignition to the loss of the H envelope through stellar wind.

- Post-Asymptotic Giant Branch (P-AGB): Final evolution from the AGB to the white dwarf (WD) stage through the planetary nebulae phase.

The contribution of stars in a particular evolutionary stage to the integrated Mg_2 index of a SSPs depends on several factors. Referred to stars an isochrone element these factors are:

i)- the luminosity

ii)- the number relative to the total population

iii)- the strength of the index of stars in that stage

An illustrative example of these factors is shown for the Mg_2 index in figures 5.5–5.7. We plot, respectively, the contribution to the flux in the pseudocontinuum relative to the total flux of the population, the index in individual stars along the isochrone, and finally the cumulative index as we include older stars, as a function of the initial mass of the stars in the element. In the three diagrams we considered an isochrone of solar metallicity of 15.84 Gyr.

The choice of initial mass permits to follow in a clear manner the changes in the cumulative index and in the flux. The vertical scale on the right of each diagram allows a direct identification of the type of stars producing such changes. In Figure 5.5, for example, we see that stars along the main sequence contribute to about 40% to the flux while the remaining 60% is provided by advanced stellar phases. Luminous AGB stars ($\log g \leq 1.5$) contribute to slightly more than 10%. Regarding the index of individual stars, we see, as already presented in previous chapters, that the highest values correspond to cool dwarf stars and to stars on the RGB and AGB.

In figure 5.7 the combination of number, luminosity and index strength in stars is illustrated. According to this diagram stars on the RGB and AGB contribute very little to the index, which appear dominated by the less luminous, but far more numerous dwarf stars. The index starts with a very high value and it is maintained all the way till the hottest edge of the main sequence at the TO. The index then sharply decreases until the stars at the bottom of the RGB begin to contribute. Their contribution, and that of AGB stars serves mainly to keep the index value nearly constant. In brief, the final value of the index in the SSP, according to our analysis, is regulated by the starting high value of and its subsequent dilution by TO stars. This result is in net contradiction with the results found by other authors (Buzzoni 1995 and references therein) in which AGB and RGB stars are found to be the main contributors to the index.

By inspection of the comparison between indices obtained from WFGB94 fitting functions and from our grid of synthetic spectra (Fig. 3.14) we can speculate on the origin of this discrepancy. If the index of dwarf stars is indeed approximately 0.2 magnitudes lower than that predicted by the synthetic spectra, and assuming that the TO stars contribute in the same way by using fitting functions, then the relative contribution of RGB and AGB stars would be significantly enhanced. Nevertheless, before any conclusion can be drawn at this respect, the detailed analysis of an homogenous sample of cool stars with reliable atmospheric parameters is necessary. We have also to bear in mind the statement cited in the first paragraph of section 3.5.

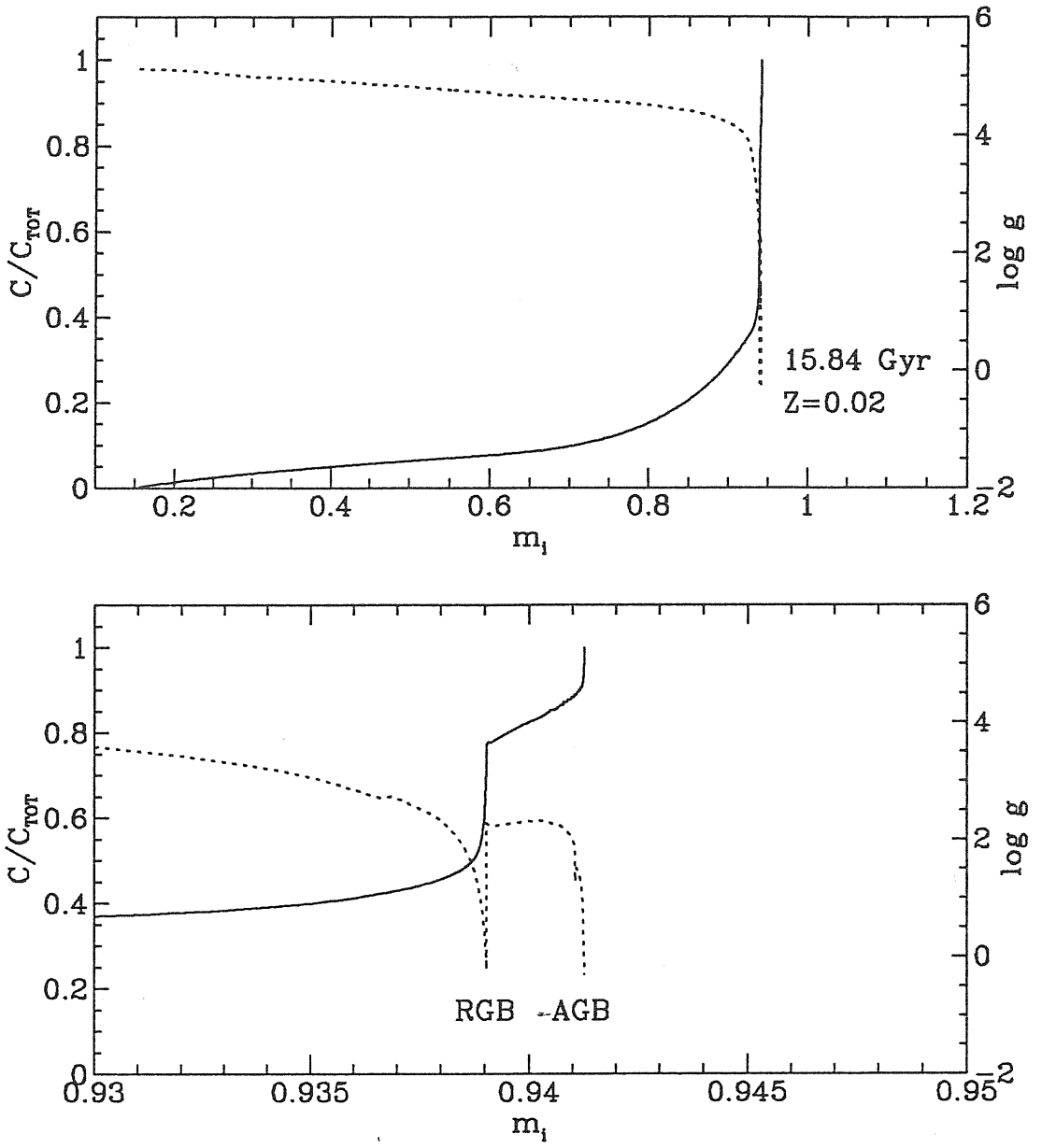

Figure 5.5: a)- Cumulative flux in the pseudocontinuum bandpass in a SSP of 15.84 Gyr and Z=0.02. The contribution of of the different types of stars to the visual luminosity can be estimated if we separate stellar type using the gravity sale on the right. b)- Zoomed region to illustrate the contribution of advance stellar stages.

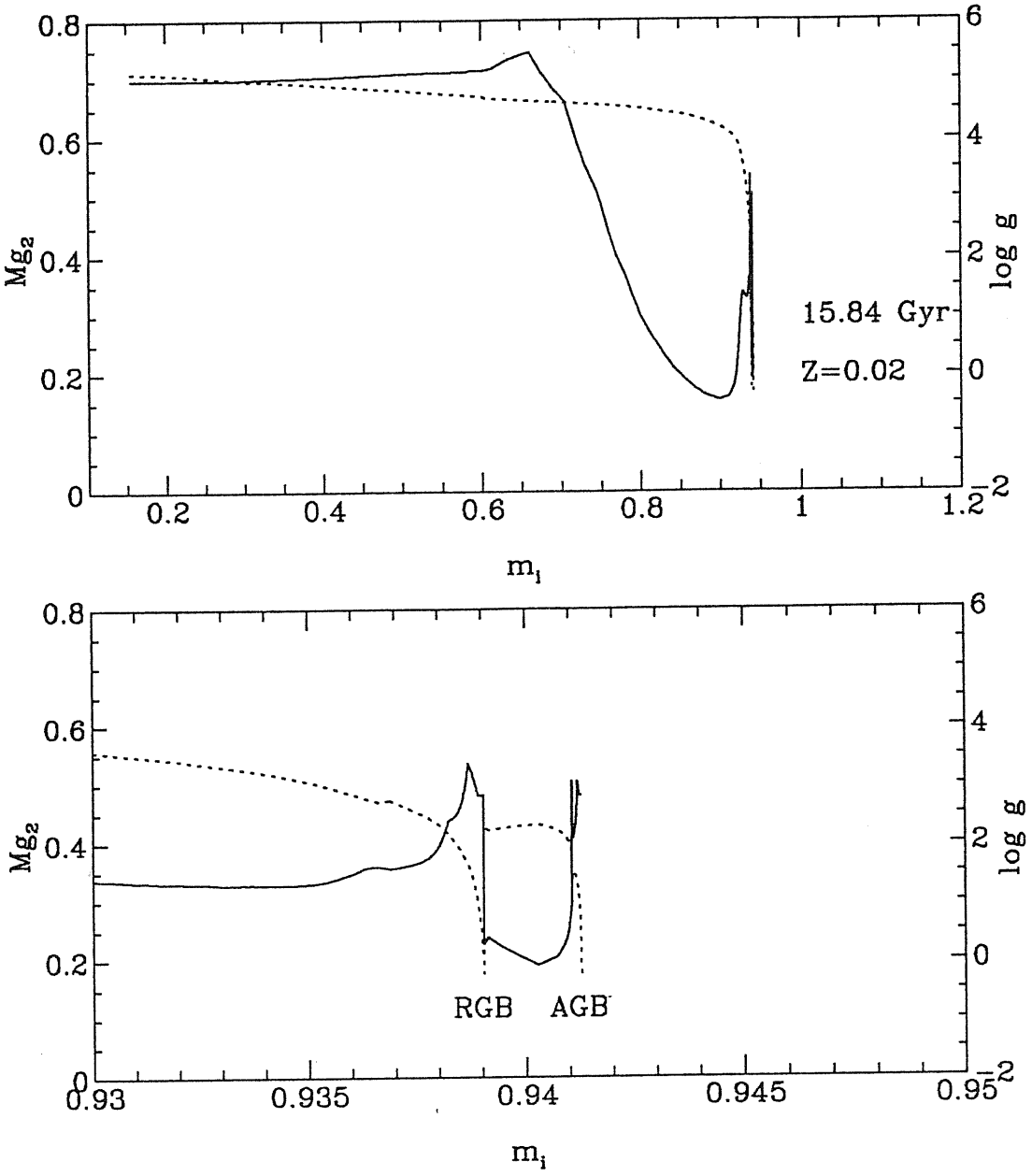

Figure 5.6: a)- Mg_2 index vs initial mass in individual stars along an isochrone of age 15.84 Gyr and solar metallicity. b)- Zoomed region to display the contribution of advanced stellar stages

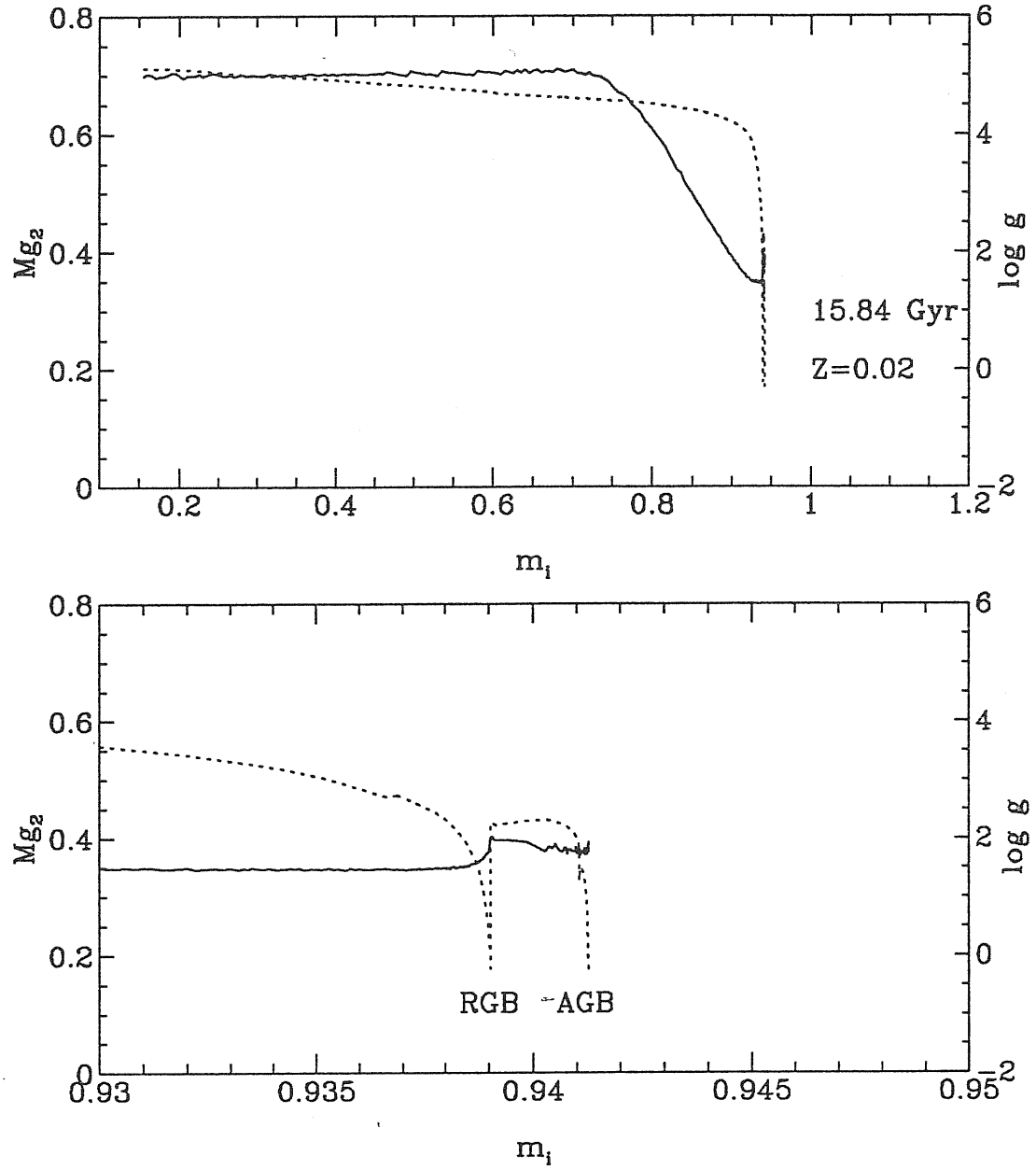

Figure 5.7: a)- Cumulative Mg_2 index vs initial mass in a SSP of 15.84 Gyr and Z=0.02. The integrated Mg_2 index starts with very high values (stars of the lower MS) then stars at the turnoff and stars in the MS near the turnoff cause an abrupt decrease of the index. b)- The index is slightly increased by stars in the RGB and the AGB to reach the final value of 0.387.

5.3 A Step Ahead: Elliptical Galaxies

In section 5.1 we saw how to compute the integrated spectral properties of SSPs. In this section we go a step ahead in computing the integrated spectral properties for a more complex system, an elliptical galaxy. It is worth reminding that the results are in the theoretical framework therefore any direct comparison with empirical data has to be deferred after the definition of transformation relationships between the theoretical and the empirical systems.

It is beyond the aims of this thesis to describe in detail the possible paths that can be followed to compute the integrated spectrophotometric properties of early type galaxies (ETGs) and the analytical procedures followed. We suggest the reader to look at the extensive analyses presented by Buzzoni et al. (1992,1993), BCF94, BCT95 and Buzzoni (1995).

The derivation of the integrated properties of an ETG depends on three main ingredients; the past history of the star formation rate (SFR), the IMF and the chemical composition $Z(t)$. The first two parameters depend on the theory of star formation. The IMF will be as in section 5.1. The third one is a product of the chemical evolution of the system i.e. depends on the chemical evolutionary model used in the computations.

The integrated monochromatic flux emitted by ensembles of stars in a galaxy of age T is given by

$$F_\lambda(T) = \int_0^T \int_{m_l}^{m_u} b(m,t,Z) f_\lambda(m,t',Z) dt dm \tag{5.4}$$

where $b(m,t)$ is the stellar birthrate which gives the number of stars with masses in the interval $(m, m+dm)$ born in the time interval $(t, t+dt)$, and $f_\lambda(m,t',Z)$ has the same meaning as in equation 5.1. Note that $t' = T - t$.

Provided we can separate the birth rate into two functions, the IMF (described above) and the SFR, $\Psi(t,Z)$ which is the mass converted into stars per unit time [$M_\odot$/yr], equation 5.4 can be rewritten as

$$F_\lambda(T) = \int_0^T \Psi(t,Z) F_{SSP}(t',Z) dt \tag{5.5}$$

where $F_{SSP}(t',Z)$ as we have already seen, is the monochromatic flux of a SSP of age t' and metallicity Z. In brief, a galaxy can be modelled by a convolution of SSPs of different ages and metallicities whenever the birth rate can be decomposed into a SFR times the IMF.

The SFR has a functional dependence on the mass of the available gas at time t, $Mg(t)$, such that

$$\Psi(t) = \nu Mg(t)^k \tag{5.6}$$

given in $M_\odot$ yr^{-1}. The constant ν represents the inverse of the SFR time scale. In general the dependence of $\Psi(t)$ is taken to be linear $k = 1$ or quadratic $k = 2$. In the linear case the SFR and the contents of gas decreases exponentially

with time while for the quadratic one the decrease at early times is more rapidly and more slowly at later times. In out our analysis we will consider $k = 1$.

The chemical composition at time t is derived from the theory of galactic chemical evolution. The chemical evolutionary models (Matteucci & Tornambé 1987; Yoshii & Arimoto 1987; BCF94, BCT95; Tantalo et al. 1995) are, in general, based on three important properties of elliptical galaxies, one of which was described in the introductory chapter:
a)- The UVX up-turn in the integrated spectral energy distribution present in all elliptical galaxies and its correlation with metallicity or with the Mg_2 index.
b)- The color-magnitude relation. Photometric indices get redder with decreasing magnitude or equivalently with increasing mass of the galaxy (see Faber 1977).
c)- The color-red shift relation. Johnson colors such as B-R tend to be bluer in high red shift galaxies ($z \geq 1$), implying, probably, that star formation continued for long periods of time (see BCF94 for references).

These important constraints are accounted in the context of two schemes that can be followed, namely the close box approximation and the mass infall model. Finally, some other important input parameters are needed for the model; mass of the luminous and dark matter, the gravitational potential and the age of the galaxy. The complete analytic procedure regarding the chemical evolution is described in BCF94 and BCT95.

Suffice here to say that in order to compute the integrated spectral indices of elliptical galaxies we have: 1)- taken integrated fluxes in the continuum and the central band pass of each index from the computations for the SSPs developed in the previous section; 2)- assumed the SFR as in equation 5.6, and 3)- followed the infall formalism as suggested by BCF94.

The Mg_2 index as a function of age in three galaxies of different mass is illustrated in Fig. 5.8. The masses of the galaxies are the actual masses and are different from the initial mass (part of the mass has been expelled by galactic winds). The interesting points to note in this figure are:

i)- the value of the index highly depends on the mass of the galaxy,

ii)- the trend of the index is very similar for systems older than 5 Gyr, while strong differences in the behavior of the index appear at the early epochs of high mass galaxy evolution ($1 \leq$ age ≤ 5 Gyr) with variations of about 0.11 mag. For the low mass galaxy the index changes about 0.04 mag

iii)- the flat behavior for ages greater than 5 Gyr indicate that even if the mass of the galaxy is known the age cannot be determined from the Mg_2 index alone.

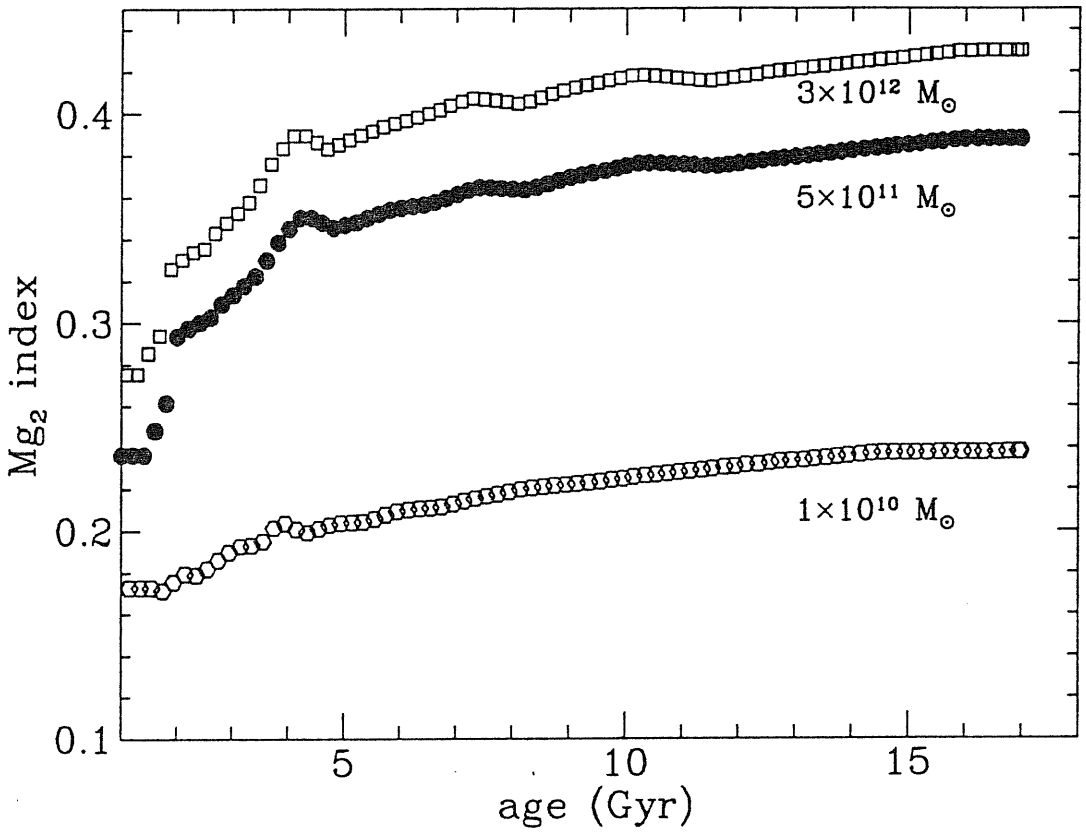

Figure 5.8: The Mg_2 index as a function of age in three galaxies of different mass.

Chapter 6

Discussion and Conclusions

6.1 Summary of the main results of this work

In this dissertation, the dependence of magnesium and iron absorption line spectral indices on stellar atmospheric parameters is investigated in detail. The problem of the absolute metallicity scale in super solar stars is addressed with the aims of providing a fiducial sample of objects leading towards a better understanding of the phenomenon and to complement empirical stellar data bases.

Preliminary work is presented regarding the integrated indices in SSPs and elliptical galaxies.

The main results in this work can be listed as follows:

- Based on a very detailed analysis of the solar spectrum, we have derived an atomic and molecular line list with revised line parameters. This line list was then used to compute an extensive grid of synthetic spectra (nearly 700) at high resolution homogeneously covering the atmospheric parameter space suitable for the analysis of cool star spectra. The computations were done using the most recent version of Kurucz's model atmospheres and computer codes to calculate synthetic spectra. The grid has multiple applications in several astrophysical contexts. Two of these applications were implemented in this work.

- Absorption line indices. Among the major scientific outputs in this dissertation is the detailed analysis of absorption spectral indices computed from the grid of synthetic spectra. The vast set of spectra and the control over the atmospheric parameters allowed by the use of model atmospheres, provide a unique opportunity to get insight into the index strength variations in terms of effective temperature, surface gravity and metallicity. We have illustrated these variations in terms of reference stellar parameters. A multivariate analysis was performed

on the whole set of synthetic Mg_2 values, and the polynomial *fitting function* that best correlates the Mg_2 index with atmospheric parameters was derived. The results indicate that fitting functions introduce non-negligible uncertainties when used to compute indices, even if the parameters space is homogeneously covered as in the case of our index grid, thus pointing out that care should be taken when using fitting functions.

- A subset of the observed SMR stars have been identified as true metal rich by comparing their observed spectra to suitable theoretical ones. For stars with more than one set of atmospheric parameters we have selected the set that best match the theoretical spectra. Observations of the complete selected sample of SMR stars are planned for this and next year. Telescope time has been allocated at the Guillermo Haro Observatory for December 1995 and two observational runs are expected for next year. The completion of this project of important for numerous reasons as explained in chapter 4.

- We have applied the grid of synthetic spectra to study the properties of single stellar populations. The results of our analysis indicate that dwarf and TO stars dominate the strength of the Mg_2 index in a SSP. We have also found that, for the metallicities considered, Mg_2 indices never overlap for different metal contents indicating that metallicity is well separated from age effects. Our analysis also showed that the change of the index with age is very smooth compared with the results of other authors who make use of empirical stellar libraries. In this regard, no conclusive statements can be drawn due to the approximations introduced to account for M giants whose spectra are not covered by our grid. As stressed chapters 3 and 5, in order to cast light on the sources of the discrepancies found, theoretical and observational data should be transformed into the same reference system.

Increasing evidence can be found in the literature that populations in ETGs display an enhancement of α elements with respect to iron. We plan to compute a grid of model atmospheres (not available as for the models of solar partitions) and compute the synthetic spectra for those models. The analysis of spectral features using these models and the synthetic spectra presented in this work would give clues in the understanding of galaxian spectra.

The analysis of the integrated properties of old stellar systems will be continued. The work presented here conforms the basement of a large project that we expect will contribute in the understanding of the chemical evolution of old stellar systems.

Appendix A: Computer programs for spectrum synthesis

The procedure and the codes have been extensively discussed in Kurucz & Avrett (1981). For easy reference we explain here the main computer programs used in the computation of stellar synthetic spectra. They appear below in the same order as when they are used. We have also included a piece of the line list to show how line data is tabulated. This information is also available in the comments provided by Dr. Kurucz at the head of each code.

MOLDECK: This program punches out molecular number densities and partition functions for the selected model atmosphere. The information is appended at the bottom of the model for later use in *SPECTRV.*

XNFPELSYN: This program computes the partition distribution functions of the electrons at every layer in the atmosphere.

SYNBEG: This is the starting program in the SYNTHE series. It reads the input parameters of the desired synthetic spectrum, this is, the spectral interval, the resolving power and microturbulent velocity (rms added to the velocity considered in the model). It can also be specified if the lines are to be treated in LTE or NLTE, in the later case a NLTE starting model is necessary. Another assignment for this program is to initialize the tapes where the atomic and molecular line data are to be stored for later use.

RNLTE: Whenever it is used this program is run immediately after *SYNBEG.* Reads the lines that can be treated in NLTE if the starting model considers NLTE. These lines are treated with exact Voight and Fano Profiles.

RLINE: Reads all LTE lines. When it is used it has to be run after *RNLTE.*

SYNTHE: Line opacity and source function are computed for the group of LTE lines.

SPECTRV: This program is based on the seventh version of the model atmosphere program ATLAS (Kurucz 1970). It processes the NLTE lines. At every wavelength the line opacity and source function are computed and summed to the results from *SYNTHE*. The source function reduces to the Planck function in LTE. For both *SYNTHE* and *SPECTRV* the wavelength, exact upper and lower energy levels, the oscillator strengths and damping constants have to be specified. Then it computes intensity or flux at the surface at each wavelength point.

ROTATE: Permits to rotationally broaden the computed spectrum. If $v_{rot} = 0$ km s^{-1} the output is flux otherwise the output is the specific intensity.

BROADEN: Instrumental broadening and macroturbulent velocity can be accounted with this program.

Appendix B: Stellar Spectral Indices in Tabular Form

In this appendix we present in tabular form the grid of spectral indices computed from the library of synthetic spectra. All indices refer to the wavelength extrema listed by WFGB94. The tables are available in computer readable form upon request from malagnini@univ.trieste.it.

Table B.1. Grid of indices for models of [M/H]=-1.0

T_{eff}	log g	[M/H]	Mg_2	Mg_1	Mg_b	Fe5270	Fe5335
4000	1.000	-1.00	0.267	0.187	1.579	3.922	3.480
4000	1.500	-1.00	0.331	0.251	1.937	4.035	3.613
4000	2.000	-1.00	0.403	0.324	2.270	4.226	3.815
4000	2.500	-1.00	0.478	0.403	2.571	4.504	4.112
4000	3.000	-1.00	0.554	0.481	2.831	4.855	4.490
4000	3.500	-1.00	0.576	0.496	2.930	4.936	4.583
4000	4.000	-1.00	0.564	0.480	2.762	4.748	4.385
4000	4.500	-1.00	0.575	0.488	2.592	4.690	4.328
4000	5.000	-1.00	0.617	0.526	2.416	4.888	4.566
4250	1.000	-1.00	0.133	0.071	0.801	3.248	2.834
4250	1.500	-1.00	0.169	0.092	1.354	3.339	2.944
4250	2.000	-1.00	0.221	0.128	1.990	3.487	3.089
4250	2.500	-1.00	0.286	0.179	2.639	3.708	3.295
4250	3.000	-1.00	0.363	0.244	3.250	4.016	3.590
4250	3.500	-1.00	0.451	0.322	3.782	4.412	3.989
4250	4.000	-1.00	0.516	0.379	4.085	4.703	4.302
4250	4.500	-1.00	0.526	0.388	3.973	4.663	4.289
4250	5.000	-1.00	0.540	0.406	3.683	4.599	4.269
4500	1.000	-1.00	0.082	0.039	0.212	2.571	2.252
4500	1.500	-1.00	0.094	0.041	0.597	2.650	2.354
4500	2.000	-1.00	0.117	0.048	1.149	2.775	2.477
4500	2.500	-1.00	0.153	0.063	1.849	2.955	2.633
4500	3.000	-1.00	0.205	0.092	2.666	3.212	2.854
4500	3.500	-1.00	0.273	0.135	3.519	3.545	3.149
4500	4.000	-1.00	0.355	0.193	4.318	3.947	3.531
4500	4.500	-1.00	0.456	0.274	4.978	4.431	4.030
4500	5.000	-1.00	0.484	0.296	5.038	4.481	4.130
4750	1.000	-1.00	0.058	0.024	-0.023	2.040	1.804
4750	1.500	-1.00	0.064	0.024	0.209	2.083	1.884
4750	2.000	-1.00	0.074	0.024	0.583	2.154	1.971
4750	2.500	-1.00	0.090	0.026	1.102	2.278	2.083
4750	3.000	-1.00	0.116	0.032	1.794	2.480	2.250
4750	3.500	-1.00	0.156	0.045	2.639	2.757	2.475
4750	4.000	-1.00	0.212	0.069	3.600	3.109	2.777
4750	4.500	-1.00	0.285	0.109	4.600	3.530	3.165
4750	5.000	-1.00	0.373	0.165	5.479	3.971	3.618
5000	1.000	-1.00	0.041	0.012	-0.036	1.638	1.456
5000	1.500	-1.00	0.044	0.013	0.103	1.647	1.515
5000	2.000	-1.00	0.050	0.013	0.334	1.674	1.570
5000	2.500	-1.00	0.060	0.013	0.688	1.750	1.649
5000	3.000	-1.00	0.074	0.013	1.186	1.885	1.764
5000	3.500	-1.00	0.096	0.015	1.843	2.094	1.929
5000	4.000	-1.00	0.128	0.021	2.667	2.376	2.158
5000	4.500	-1.00	0.175	0.034	3.654	2.734	2.463
5000	5.000	-1.00	0.235	0.056	4.722	3.131	2.830
5250	1.000	-1.00	0.029	0.005	-0.020	1.338	1.194
5250	1.500	-1.00	0.031	0.005	0.062	1.325	1.233
5250	2.000	-1.00	0.035	0.006	0.211	1.333	1.274
5250	2.500	-1.00	0.041	0.006	0.449	1.370	1.324
5250	3.000	-1.00	0.051	0.006	0.802	1.450	1.396
5250	3.500	-1.00	0.065	0.005	1.283	1.583	1.503
5250	4.000	-1.00	0.085	0.006	1.919	1.785	1.663
5250	4.500	-1.00	0.113	0.008	2.717	2.055	1.886
5250	5.000	-1.00	0.152	0.014	3.700	2.396	2.183

Table B.1 (Continued)

T_{eff}	log g	[M/H]	Mg_2	Mg_1	Mg_b	Fe5270	Fe5335
5500	1.000	-1.00	0.024	0.002	0.025	1.135	1.026
5500	1.500	-1.00	0.025	0.002	0.076	1.108	1.047
5500	2.000	-1.00	0.027	0.002	0.167	1.097	1.069
5500	2.500	-1.00	0.031	0.002	0.321	1.103	1.094
5500	3.000	-1.00	0.037	0.002	0.558	1.139	1.131
5500	3.500	-1.00	0.046	0.001	0.907	1.217	1.193
5500	4.000	-1.00	0.059	0.001	1.374	1.340	1.289
5500	4.500	-1.00	0.077	0.000	1.982	1.524	1.436
5500	5.000	-1.00	0.102	0.000	2.752	1.767	1.642
5750	1.000	-1.00	0.021	0.000	0.086	0.958	0.880
5750	1.500	-1.00	0.022	0.000	0.121	0.935	0.897
5750	2.000	-1.00	0.023	0.000	0.179	0.917	0.910
5750	2.500	-1.00	0.025	0.000	0.273	0.912	0.923
5750	3.000	-1.00	0.028	0.000	0.426	0.925	0.940
5750	3.500	-1.00	0.034	-0.000	0.665	0.963	0.971
5750	4.000	-1.00	0.043	-0.000	1.009	1.035	1.025
5750	4.500	-1.00	0.055	-0.001	1.470	1.149	1.114
5750	5.000	-1.00	0.074	-0.003	2.103	1.330	1.263
6000	1.000	-1.00	0.022	0.001	0.112	0.920	0.827
6000	1.500	-1.00	0.020	-0.000	0.182	0.788	0.767
6000	2.000	-1.00	0.020	-0.000	0.218	0.773	0.778
6000	2.500	-1.00	0.021	-0.001	0.274	0.764	0.785
6000	3.000	-1.00	0.023	-0.001	0.365	0.766	0.791
6000	3.500	-1.00	0.026	-0.001	0.519	0.782	0.805
6000	4.000	-1.00	0.032	-0.001	0.758	0.822	0.832
6000	4.500	-1.00	0.041	-0.002	1.104	0.892	0.883
6000	5.000	-1.00	0.053	-0.004	1.567	0.997	0.965
7000	1.000	-1.00	0.018	-0.001	0.372	0.405	0.397
7000	1.500	-1.00	0.018	-0.002	0.377	0.421	0.420
7000	2.000	-1.00	0.017	-0.003	0.383	0.424	0.435
7000	2.500	-1.00	0.016	-0.004	0.388	0.427	0.435
7000	3.000	-1.00	0.015	-0.004	0.397	0.428	0.439
7000	3.500	-1.00	0.014	-0.005	0.412	0.373	0.390
7000	4.000	-1.00	0.014	-0.005	0.441	0.386	0.395
7000	4.500	-1.00	0.016	-0.005	0.507	0.402	0.400
7000	5.000	-1.00	0.019	-0.005	0.631	0.425	0.410
8000	1.000	-1.00	0.013	0.002	0.307	0.021	0.095
8000	1.500	-1.00	0.015	0.002	0.368	0.050	0.126
8000	2.000	-1.00	0.015	0.001	0.394	0.077	0.149
8000	2.500	-1.00	0.014	-0.001	0.406	0.102	0.165
8000	3.000	-1.00	0.012	-0.004	0.410	0.128	0.180
8000	3.500	-1.00	0.009	-0.008	0.412	0.152	0.191
8000	4.000	-1.00	0.007	-0.010	0.414	0.176	0.202
8000	4.500	-1.00	0.006	-0.012	0.422	0.197	0.208
8000	5.000	-1.00	0.005	-0.012	0.421	0.179	0.184

Table B.2. Grid of indices for models of [M/H]=-0.5

T_{eff}	log g	[M/H]	Mg_2	Mg_1	Mg_b	Fe5270	Fe5335
4000	1.000	-0.50	0.373	0.280	2.103	4.821	4.532
4000	1.500	-0.50	0.430	0.344	2.292	4.857	4.633
4000	2.000	-0.50	0.492	0.414	2.457	4.995	4.823
4000	2.500	-0.50	0.554	0.482	2.632	5.233	5.106
4000	3.000	-0.50	0.619	0.550	2.833	5.588	5.505
4000	3.500	-0.50	0.673	0.603	2.975	5.951	5.880
4000	4.000	-0.50	0.657	0.583	2.792	5.874	5.721
4000	4.500	-0.50	0.637	0.560	2.541	5.665	5.404
4000	5.000	-0.50	0.670	0.591	2.421	5.806	5.447
4250	1.000	-0.50	0.216	0.132	1.528	4.272	3.796
4250	1.500	-0.50	0.257	0.160	2.038	4.295	3.904
4250	2.000	-0.50	0.313	0.204	2.586	4.389	4.056
4250	2.500	-0.50	0.381	0.261	3.124	4.576	4.282
4250	3.000	-0.50	0.457	0.328	3.616	4.868	4.612
4250	3.500	-0.50	0.539	0.404	4.030	5.272	5.057
4250	4.000	-0.50	0.624	0.484	4.298	5.759	5.571
4250	4.500	-0.50	0.646	0.508	4.151	5.909	5.688
4250	5.000	-0.50	0.630	0.501	3.717	5.763	5.497
4500	1.000	-0.50	0.141	0.087	0.661	3.610	3.088
4500	1.500	-0.50	0.155	0.085	1.114	3.639	3.202
4500	2.000	-0.50	0.183	0.094	1.755	3.725	3.344
4500	2.500	-0.50	0.228	0.115	2.532	3.875	3.528
4500	3.000	-0.50	0.289	0.153	3.375	4.113	3.785
4500	3.500	-0.50	0.365	0.204	4.191	4.451	4.140
4500	4.000	-0.50	0.454	0.272	4.904	4.895	4.610
4500	4.500	-0.50	0.552	0.355	5.408	5.448	5.184
4500	5.000	-0.50	0.611	0.413	5.418	5.787	5.519
4750	1.000	-0.50	0.104	0.065	0.197	2.957	2.479
4750	1.500	-0.50	0.109	0.062	0.492	2.990	2.594
4750	2.000	-0.50	0.120	0.058	0.957	3.061	2.717
4750	2.500	-0.50	0.142	0.059	1.610	3.188	2.873
4750	3.000	-0.50	0.177	0.067	2.457	3.386	3.080
4750	3.500	-0.50	0.229	0.086	3.451	3.672	3.361
4750	4.000	-0.50	0.299	0.121	4.504	4.055	3.739
4750	4.500	-0.50	0.384	0.172	5.486	4.529	4.220
4750	5.000	-0.50	0.484	0.243	6.261	5.108	4.808
5000	1.000	-0.50	0.075	0.040	-0.033	2.429	2.009
5000	1.500	-0.50	0.080	0.041	0.162	2.451	2.118
5000	2.000	-0.50	0.087	0.040	0.485	2.482	2.216
5000	2.500	-0.50	0.099	0.038	0.975	2.566	2.337
5000	3.000	-0.50	0.118	0.037	1.642	2.711	2.494
5000	3.500	-0.50	0.148	0.039	2.509	2.947	2.716
5000	4.000	-0.50	0.192	0.048	3.548	3.269	3.011
5000	4.500	-0.50	0.254	0.069	4.717	3.688	3.405
5000	5.000	-0.50	0.334	0.104	5.891	4.190	3.899
5250	1.000	-0.50	0.052	0.021	-0.065	2.034	1.661
5250	1.500	-0.50	0.055	0.022	0.046	2.015	1.737
5250	2.000	-0.50	0.061	0.023	0.261	2.025	1.817
5250	2.500	-0.50	0.070	0.023	0.609	2.066	1.906
5250	3.000	-0.50	0.084	0.022	1.109	2.160	2.023
5250	3.500	-0.50	0.103	0.021	1.781	2.326	2.184
5250	4.000	-0.50	0.131	0.022	2.646	2.581	2.412
5250	4.500	-0.50	0.172	0.026	3.697	2.927	2.721
5250	5.000	-0.50	0.227	0.037	4.908	3.360	3.119

Table B.2 (Continued)

T_{eff}	log g	[M/H]	Mg_2	Mg_1	Mg_b	Fe5270	Fe5335
5500	1.000	-0.50	0.038	0.011	-0.091	1.718	1.387
5500	1.500	-0.50	0.040	0.012	-0.017	1.700	1.452
5500	2.000	-0.50	0.044	0.012	0.127	1.685	1.510
5500	2.500	-0.50	0.050	0.012	0.375	1.696	1.576
5500	3.000	-0.50	0.060	0.012	0.747	1.743	1.658
5500	3.500	-0.50	0.074	0.011	1.265	1.848	1.770
5500	4.000	-0.50	0.094	0.011	1.950	2.029	1.934
5500	4.500	-0.50	0.122	0.010	2.823	2.295	2.168
5500	5.000	-0.50	0.159	0.012	3.866	2.642	2.475
5750	1.000	-0.50	0.031	0.007	-0.079	1.490	1.191
5750	1.500	-0.50	0.032	0.006	-0.032	1.461	1.238
5750	2.000	-0.50	0.034	0.006	0.065	1.438	1.284
5750	2.500	-0.50	0.037	0.006	0.234	1.423	1.327
5750	3.000	-0.50	0.044	0.006	0.504	1.436	1.380
5750	3.500	-0.50	0.054	0.005	0.899	1.495	1.456
5750	4.000	-0.50	0.069	0.005	1.437	1.612	1.569
5750	4.500	-0.50	0.089	0.004	2.135	1.800	1.734
5750	5.000	-0.50	0.117	0.003	3.019	2.070	1.972
6000	1.000	-0.50	0.030	0.006	-0.080	1.438	1.120
6000	1.500	-0.50	0.027	0.004	-0.010	1.268	1.069
6000	2.000	-0.50	0.028	0.003	0.055	1.240	1.104
6000	2.500	-0.50	0.030	0.003	0.171	1.217	1.135
6000	3.000	-0.50	0.034	0.003	0.356	1.210	1.169
6000	3.500	-0.50	0.041	0.002	0.644	1.234	1.216
6000	4.000	-0.50	0.051	0.001	1.056	1.302	1.288
6000	4.500	-0.50	0.066	0.000	1.606	1.423	1.398
6000	5.000	-0.50	0.087	-0.000	2.320	1.614	1.566
7000	1.000	-0.50	0.022	0.001	0.195	0.776	0.585
7000	1.500	-0.50	0.022	0.000	0.199	0.792	0.629
7000	2.000	-0.50	0.021	-0.001	0.220	0.785	0.658
7000	2.500	-0.50	0.020	-0.001	0.248	0.771	0.682
7000	3.000	-0.50	0.020	-0.002	0.292	0.753	0.696
7000	3.500	-0.50	0.019	-0.003	0.364	0.657	0.636
7000	4.000	-0.50	0.021	-0.004	0.449	0.660	0.650
7000	4.500	-0.50	0.024	-0.004	0.600	0.676	0.669
7000	5.000	-0.50	0.031	-0.004	0.853	0.712	0.700
8000	1.000	-0.50	0.015	0.001	0.366	0.141	0.136
8000	1.500	-0.50	0.017	0.001	0.404	0.206	0.201
8000	2.000	-0.50	0.017	0.000	0.418	0.252	0.246
8000	2.500	-0.50	0.016	-0.002	0.422	0.290	0.281
8000	3.000	-0.50	0.014	-0.005	0.424	0.322	0.309
8000	3.500	-0.50	0.012	-0.009	0.427	0.348	0.333
8000	4.000	-0.50	0.010	-0.011	0.437	0.371	0.353
8000	4.500	-0.50	0.010	-0.013	0.464	0.389	0.370
8000	5.000	-0.50	0.009	-0.013	0.496	0.359	0.342

B.3. Grid of indices for models of [M/H]=+0.0

T_{eff}	log g	[M/H]	Mg_2	Mg_1	Mg_b	Fe5270	Fe5335
4000	1.000	0.00	0.481	0.370	2.746	5.706	5.767
4000	1.500	0.00	0.525	0.428	2.701	5.661	5.819
4000	2.000	0.00	0.570	0.485	2.716	5.727	5.948
4000	2.500	0.00	0.614	0.536	2.802	5.909	6.176
4000	3.000	0.00	0.660	0.584	2.954	6.212	6.506
4000	3.500	0.00	0.710	0.634	3.105	6.645	6.920
4000	4.000	0.00	0.745	0.670	3.047	6.998	7.184
4000	4.500	0.00	0.727	0.655	2.692	6.911	6.892
4000	5.000	0.00	0.700	0.627	2.422	6.733	6.501
4250	1.000	0.00	0.324	0.215	2.501	5.297	5.011
4250	1.500	0.00	0.366	0.248	2.870	5.239	5.105
4250	2.000	0.00	0.420	0.295	3.255	5.275	5.241
4250	2.500	0.00	0.483	0.351	3.639	5.425	5.462
4250	3.000	0.00	0.550	0.412	3.990	5.694	5.794
4250	3.500	0.00	0.620	0.476	4.288	6.095	6.241
4250	4.000	0.00	0.692	0.547	4.477	6.628	6.788
4250	4.500	0.00	0.747	0.607	4.370	7.098	7.204
4250	5.000	0.00	0.745	0.616	3.883	7.138	7.095
4500	1.000	0.00	0.224	0.157	1.439	4.727	4.165
4500	1.500	0.00	0.241	0.154	1.919	4.697	4.307
4500	2.000	0.00	0.274	0.163	2.573	4.721	4.457
4500	2.500	0.00	0.325	0.190	3.346	4.833	4.659
4500	3.000	0.00	0.392	0.232	4.131	5.044	4.943
4500	3.500	0.00	0.470	0.287	4.843	5.376	5.341
4500	4.000	0.00	0.555	0.353	5.409	5.846	5.865
4500	4.500	0.00	0.645	0.433	5.752	6.456	6.497
4500	5.000	0.00	0.723	0.515	5.678	7.050	7.061
4750	1.000	0.00	0.173	0.134	0.668	4.067	3.379
4750	1.500	0.00	0.178	0.124	1.005	4.075	3.547
4750	2.000	0.00	0.190	0.115	1.545	4.108	3.705
4750	2.500	0.00	0.216	0.113	2.321	4.201	3.890
4750	3.000	0.00	0.259	0.122	3.295	4.373	4.135
4750	3.500	0.00	0.322	0.147	4.372	4.648	4.469
4750	4.000	0.00	0.400	0.188	5.408	5.035	4.915
4750	4.500	0.00	0.492	0.246	6.278	5.567	5.490
4750	5.000	0.00	0.592	0.323	6.844	6.234	6.177
5000	1.000	0.00	0.134	0.099	0.295	3.458	2.742
5000	1.500	0.00	0.137	0.097	0.484	3.467	2.901
5000	2.000	0.00	0.144	0.092	0.854	3.497	3.048
5000	2.500	0.00	0.157	0.085	1.451	3.576	3.216
5000	3.000	0.00	0.180	0.079	2.276	3.717	3.420
5000	3.500	0.00	0.219	0.081	3.337	3.947	3.698
5000	4.000	0.00	0.276	0.093	4.565	4.281	4.070
5000	4.500	0.00	0.352	0.121	5.832	4.730	4.559
5000	5.000	0.00	0.443	0.166	6.958	5.311	5.169
5250	1.000	0.00	0.096	0.059	0.107	2.940	2.238
5250	1.500	0.00	0.101	0.063	0.220	2.950	2.388
5250	2.000	0.00	0.107	0.063	0.470	2.960	2.515
5250	2.500	0.00	0.117	0.062	0.900	3.006	2.651
5250	3.000	0.00	0.133	0.058	1.531	3.103	2.815
5250	3.500	0.00	0.158	0.054	2.402	3.286	3.042
5250	4.000	0.00	0.195	0.053	3.510	3.567	3.348
5250	4.500	0.00	0.249	0.058	4.813	3.953	3.751
5250	5.000	0.00	0.320	0.075	6.204	4.450	4.266

Table B.3 (Continued)

T_{eff}	log g	[M/H]	Mg_2	Mg_1	Mg_b	Fe5270	Fe5335
5500	1.000	0.00	0.067	0.031	-0.031	2.497	1.841
5500	1.500	0.00	0.071	0.035	0.031	2.499	1.971
5500	2.000	0.00	0.076	0.037	0.207	2.498	2.081
5500	2.500	0.00	0.085	0.038	0.534	2.523	2.201
5500	3.000	0.00	0.098	0.038	1.027	2.584	2.334
5500	3.500	0.00	0.117	0.036	1.722	2.713	2.510
5500	4.000	0.00	0.144	0.034	2.635	2.930	2.753
5500	4.500	0.00	0.182	0.032	3.766	3.244	3.072
5500	5.000	0.00	0.234	0.034	5.112	3.666	3.496
5750	1.000	0.00	0.051	0.017	-0.096	2.170	1.564
5750	1.500	0.00	0.052	0.018	-0.067	2.151	1.659
5750	2.000	0.00	0.055	0.020	0.049	2.139	1.750
5750	2.500	0.00	0.062	0.021	0.287	2.142	1.847
5750	3.000	0.00	0.071	0.022	0.667	2.167	1.950
5750	3.500	0.00	0.086	0.021	1.224	2.249	2.088
5750	4.000	0.00	0.107	0.020	1.969	2.401	2.272
5750	4.500	0.00	0.136	0.019	2.923	2.647	2.527
5750	5.000	0.00	0.176	0.017	4.092	2.993	2.866
6000	1.000	0.00	0.046	0.013	-0.120	2.078	1.455
6000	1.500	0.00	0.041	0.011	-0.111	1.888	1.432
6000	2.000	0.00	0.042	0.011	-0.035	1.863	1.500
6000	2.500	0.00	0.046	0.012	0.130	1.840	1.566
6000	3.000	0.00	0.053	0.012	0.417	1.842	1.647
6000	3.500	0.00	0.064	0.012	0.852	1.879	1.746
6000	4.000	0.00	0.080	0.011	1.454	1.979	1.885
6000	4.500	0.00	0.103	0.010	2.243	2.157	2.080
6000	5.000	0.00	0.133	0.008	3.227	2.422	2.342
7000	1.000	0.00	0.028	0.005	-0.042	1.215	0.826
7000	1.500	0.00	0.028	0.004	-0.049	1.252	0.887
7000	2.000	0.00	0.026	0.002	-0.026	1.254	0.932
7000	2.500	0.00	0.026	0.001	0.028	1.233	0.967
7000	3.000	0.00	0.026	-0.000	0.121	1.204	1.000
7000	3.500	0.00	0.026	-0.001	0.258	1.065	0.946
7000	4.000	0.00	0.030	-0.002	0.449	1.057	0.983
7000	4.500	0.00	0.036	-0.002	0.748	1.074	1.034
7000	5.000	0.00	0.048	-0.003	1.196	1.136	1.115
8000	1.000	0.00	0.017	0.001	0.330	0.340	0.186
8000	1.500	0.00	0.020	0.002	0.321	0.462	0.293
8000	2.000	0.00	0.020	0.000	0.314	0.542	0.371
8000	2.500	0.00	0.019	-0.001	0.311	0.599	0.435
8000	3.000	0.00	0.017	-0.004	0.316	0.639	0.488
8000	3.500	0.00	0.015	-0.008	0.334	0.664	0.533
8000	4.000	0.00	0.014	-0.011	0.375	0.679	0.569
8000	4.500	0.00	0.015	-0.013	0.455	0.687	0.602
8000	5.000	0.00	0.015	-0.014	0.562	0.636	0.579

Table B.4. Grid of indices for models of [M/H]=+0.1

T_{eff}	log g	[M/H]	Mg_2	Mg_1	Mg_b	Fe5270	Fe5335
4000	1.000	0.10	0.501	0.384	2.823	5.907	6.041
4000	1.500	0.10	0.541	0.441	2.743	5.834	6.073
4000	2.000	0.10	0.581	0.493	2.761	5.878	6.181
4000	2.500	0.10	0.623	0.541	2.843	6.042	6.390
4000	3.000	0.10	0.666	0.586	2.996	6.335	6.702
4000	3.500	0.10	0.713	0.633	3.152	6.761	7.105
4000	4.000	0.10	0.754	0.676	3.126	7.178	7.432
4000	4.500	0.10	0.746	0.672	2.785	7.189	7.238
4000	5.000	0.10	0.716	0.643	2.475	6.995	6.802
4250	1.000	0.10	0.347	0.231	2.676	5.514	5.293
4250	1.500	0.10	0.388	0.265	3.012	5.432	5.375
4250	2.000	0.10	0.440	0.310	3.371	5.450	5.497
4250	2.500	0.10	0.501	0.366	3.732	5.588	5.710
4250	3.000	0.10	0.566	0.425	4.066	5.849	6.034
4250	3.500	0.10	0.632	0.486	4.353	6.250	6.476
4250	4.000	0.10	0.702	0.553	4.538	6.782	7.017
4250	4.500	0.10	0.760	0.616	4.446	7.304	7.483
4250	5.000	0.10	0.763	0.632	3.957	7.409	7.431
4500	1.000	0.10	0.242	0.171	1.597	4.964	4.436
4500	1.500	0.10	0.260	0.168	2.087	4.910	4.573
4500	2.000	0.10	0.293	0.178	2.738	4.917	4.714
4500	2.500	0.10	0.345	0.205	3.504	5.014	4.910
4500	3.000	0.10	0.412	0.247	4.273	5.220	5.194
4500	3.500	0.10	0.489	0.302	4.963	5.552	5.595
4500	4.000	0.10	0.573	0.367	5.508	6.031	6.122
4500	4.500	0.10	0.661	0.444	5.831	6.645	6.756
4500	5.000	0.10	0.740	0.527	5.750	7.274	7.357
4750	1.000	0.10	0.189	0.150	0.787	4.304	3.607
4750	1.500	0.10	0.193	0.138	1.130	4.297	3.778
4750	2.000	0.10	0.206	0.128	1.686	4.320	3.940
4750	2.500	0.10	0.232	0.126	2.478	4.402	4.126
4750	3.000	0.10	0.277	0.135	3.471	4.571	4.376
4750	3.500	0.10	0.342	0.161	4.555	4.844	4.719
4750	4.000	0.10	0.421	0.203	5.579	5.235	5.175
4750	4.500	0.10	0.512	0.261	6.418	5.773	5.760
4750	5.000	0.10	0.611	0.336	6.947	6.448	6.454
5000	1.000	0.10	0.148	0.114	0.371	3.687	2.930
5000	1.500	0.10	0.151	0.112	0.563	3.693	3.101
5000	2.000	0.10	0.158	0.105	0.944	3.725	3.263
5000	2.500	0.10	0.171	0.097	1.546	3.797	3.433
5000	3.000	0.10	0.196	0.091	2.407	3.938	3.649
5000	3.500	0.10	0.236	0.091	3.506	4.164	3.935
5000	4.000	0.10	0.295	0.104	4.765	4.496	4.318
5000	4.500	0.10	0.373	0.132	6.037	4.946	4.820
5000	5.000	0.10	0.465	0.178	7.141	5.535	5.446
5250	1.000	0.10	0.110	0.071	0.116	3.183	2.408
5250	1.500	0.10	0.115	0.075	0.223	3.192	2.574
5250	2.000	0.10	0.121	0.076	0.492	3.202	2.716
5250	2.500	0.10	0.131	0.073	0.943	3.239	2.856
5250	3.000	0.10	0.147	0.068	1.613	3.337	3.031
5250	3.500	0.10	0.172	0.063	2.527	3.511	3.260
5250	4.000	0.10	0.212	0.061	3.688	3.794	3.580
5250	4.500	0.10	0.268	0.067	5.042	4.180	3.998
5250	5.000	0.10	0.342	0.085	6.450	4.684	4.531

Table B.4 (Continued)

T_{eff}	log g	[M/H]	Mg_2	Mg_1	Mg_b	Fe5270	Fe5335
5500	1.000	0.10	0.078	0.038	0.019	2.714	1.975
5500	1.500	0.10	0.082	0.043	0.073	2.720	2.126
5500	2.000	0.10	0.088	0.046	0.250	2.731	2.258
5500	2.500	0.10	0.096	0.047	0.580	2.752	2.384
5500	3.000	0.10	0.110	0.046	1.102	2.814	2.528
5500	3.500	0.10	0.129	0.044	1.825	2.938	2.710
5500	4.000	0.10	0.158	0.041	2.788	3.158	2.965
5500	4.500	0.10	0.198	0.039	3.977	3.474	3.300
5500	5.000	0.10	0.253	0.041	5.383	3.907	3.747
5750	1.000	0.10	0.057	0.020	-0.057	2.354	1.669
5750	1.500	0.10	0.059	0.023	-0.031	2.352	1.789
5750	2.000	0.10	0.063	0.025	0.087	2.341	1.901
5750	2.500	0.10	0.070	0.027	0.331	2.347	2.007
5750	3.000	0.10	0.081	0.027	0.732	2.372	2.123
5750	3.500	0.10	0.096	0.027	1.316	2.463	2.266
5750	4.000	0.10	0.119	0.026	2.109	2.622	2.468
5750	4.500	0.10	0.149	0.024	3.108	2.868	2.731
5750	5.000	0.10	0.191	0.022	4.338	3.222	3.090
6000	1.000	0.10	0.051	0.015	-0.088	2.243	1.543
6000	1.500	0.10	0.046	0.013	-0.088	2.061	1.539
6000	2.000	0.10	0.048	0.014	-0.009	2.050	1.627
6000	2.500	0.10	0.053	0.015	0.164	2.036	1.708
6000	3.000	0.10	0.060	0.015	0.467	2.041	1.798
6000	3.500	0.10	0.072	0.015	0.932	2.082	1.909
6000	4.000	0.10	0.089	0.014	1.567	2.173	2.051
6000	4.500	0.10	0.113	0.013	2.409	2.361	2.263
6000	5.000	0.10	0.145	0.011	3.443	2.630	2.538
7000	1.000	0.10	0.030	0.006	-0.082	1.302	0.877
7000	1.500	0.10	0.029	0.005	-0.093	1.352	0.946
7000	2.000	0.10	0.028	0.003	-0.069	1.361	0.996
7000	2.500	0.10	0.028	0.001	-0.008	1.346	1.037
7000	3.000	0.10	0.028	0.000	0.098	1.322	1.075
7000	3.500	0.10	0.028	-0.001	0.253	1.180	1.029
7000	4.000	0.10	0.032	-0.001	0.472	1.170	1.072
7000	4.500	0.10	0.040	-0.002	0.808	1.189	1.132
7000	5.000	0.10	0.053	-0.003	1.299	1.255	1.225
8000	1.000	0.10	0.017	0.002	0.308	0.386	0.200
8000	1.500	0.10	0.020	0.002	0.288	0.521	0.316
8000	2.000	0.10	0.021	0.001	0.275	0.609	0.401
8000	2.500	0.10	0.020	-0.001	0.270	0.671	0.470
8000	3.000	0.10	0.018	-0.004	0.276	0.713	0.530
8000	3.500	0.10	0.016	-0.008	0.298	0.738	0.579
8000	4.000	0.10	0.015	-0.011	0.349	0.752	0.621
8000	4.500	0.10	0.016	-0.013	0.447	0.760	0.658
8000	5.000	0.10	0.017	-0.014	0.577	0.707	0.639

Table B.5. Grid of indices for models of [M/H]=+0.2

T_{eff}	log g	[M/H]	Mg_2	Mg_1	Mg_b	Fe5270	Fe5335
4000	1.000	0.20	0.522	0.399	2.976	6.107	6.313
4000	1.500	0.20	0.557	0.453	2.849	6.009	6.328
4000	2.000	0.20	0.594	0.502	2.839	6.036	6.420
4000	2.500	0.20	0.632	0.547	2.903	6.183	6.610
4000	3.000	0.20	0.671	0.588	3.046	6.464	6.903
4000	3.500	0.20	0.715	0.631	3.193	6.876	7.288
4000	4.000	0.20	0.758	0.676	3.192	7.324	7.650
4000	4.500	0.20	0.762	0.685	2.875	7.442	7.561
4000	5.000	0.20	0.730	0.657	2.525	7.243	7.098
4250	1.000	0.20	0.372	0.250	2.912	5.727	5.569
4250	1.500	0.20	0.411	0.283	3.201	5.627	5.644
4250	2.000	0.20	0.462	0.329	3.523	5.635	5.763
4250	2.500	0.20	0.520	0.383	3.845	5.760	5.969
4250	3.000	0.20	0.582	0.439	4.152	6.013	6.285
4250	3.500	0.20	0.646	0.497	4.419	6.412	6.719
4250	4.000	0.20	0.711	0.560	4.591	6.939	7.252
4250	4.500	0.20	0.769	0.623	4.498	7.485	7.741
4250	5.000	0.20	0.778	0.645	4.008	7.658	7.754
4500	1.000	0.20	0.262	0.188	1.816	5.193	4.699
4500	1.500	0.20	0.280	0.184	2.295	5.122	4.835
4500	2.000	0.20	0.315	0.195	2.939	5.117	4.979
4500	2.500	0.20	0.367	0.222	3.684	5.203	5.171
4500	3.000	0.20	0.434	0.265	4.432	5.405	5.457
4500	3.500	0.20	0.510	0.319	5.096	5.737	5.862
4500	4.000	0.20	0.592	0.382	5.611	6.222	6.394
4500	4.500	0.20	0.677	0.457	5.901	6.841	7.031
4500	5.000	0.20	0.754	0.539	5.797	7.484	7.645
4750	1.000	0.20	0.205	0.167	0.938	4.540	3.840
4750	1.500	0.20	0.209	0.154	1.279	4.518	4.014
4750	2.000	0.20	0.223	0.143	1.847	4.533	4.183
4750	2.500	0.20	0.250	0.140	2.654	4.606	4.374
4750	3.000	0.20	0.297	0.150	3.665	4.769	4.629
4750	3.500	0.20	0.363	0.176	4.750	5.038	4.977
4750	4.000	0.20	0.443	0.218	5.758	5.435	5.445
4750	4.500	0.20	0.535	0.277	6.568	5.984	6.045
4750	5.000	0.20	0.631	0.352	7.049	6.671	6.750
5000	1.000	0.20	0.163	0.131	0.471	3.912	3.119
5000	1.500	0.20	0.166	0.127	0.658	3.912	3.302
5000	2.000	0.20	0.172	0.120	1.049	3.938	3.474
5000	2.500	0.20	0.186	0.110	1.674	4.009	3.653
5000	3.000	0.20	0.212	0.103	2.564	4.147	3.878
5000	3.500	0.20	0.254	0.103	3.696	4.369	4.173
5000	4.000	0.20	0.315	0.116	4.986	4.705	4.574
5000	4.500	0.20	0.395	0.146	6.259	5.161	5.092
5000	5.000	0.20	0.488	0.193	7.335	5.764	5.737
5250	1.000	0.20	0.124	0.085	0.215	3.392	2.561
5250	1.500	0.20	0.127	0.088	0.296	3.402	2.739
5250	2.000	0.20	0.134	0.089	0.578	3.417	2.898
5250	2.500	0.20	0.144	0.085	1.034	3.452	3.051
5250	3.000	0.20	0.160	0.080	1.723	3.547	3.236
5250	3.500	0.20	0.187	0.074	2.673	3.730	3.479
5250	4.000	0.20	0.228	0.071	3.883	4.011	3.811
5250	4.500	0.20	0.287	0.077	5.282	4.403	4.250
5250	5.000	0.20	0.363	0.095	6.709	4.919	4.804

Table B.5 (Continued)

T_{eff}	log g	[M/H]	Mg_2	Mg_1	Mg_b	Fe5270	Fe5335
5500	1.000	0.20	0.088	0.046	0.070	2.913	2.100
5500	1.500	0.20	0.092	0.052	0.119	2.921	2.258
5500	2.000	0.20	0.099	0.055	0.296	2.946	2.421
5500	2.500	0.20	0.108	0.057	0.634	2.964	2.554
5500	3.000	0.20	0.121	0.056	1.174	3.029	2.711
5500	3.500	0.20	0.142	0.053	1.933	3.153	2.903
5500	4.000	0.20	0.171	0.049	2.941	3.375	3.170
5500	4.500	0.20	0.213	0.046	4.189	3.696	3.521
5500	5.000	0.20	0.271	0.049	5.648	4.138	3.994
5750	1.000	0.20	0.065	0.025	-0.017	2.538	1.770
5750	1.500	0.20	0.067	0.028	-0.003	2.531	1.907
5750	2.000	0.20	0.072	0.031	0.115	2.507	2.018
5750	2.500	0.20	0.078	0.033	0.365	2.538	2.138
5750	3.000	0.20	0.089	0.034	0.780	2.572	2.265
5750	3.500	0.20	0.106	0.033	1.393	2.657	2.425
5750	4.000	0.20	0.129	0.032	2.227	2.820	2.641
5750	4.500	0.20	0.162	0.029	3.285	3.080	2.930
5750	5.000	0.20	0.206	0.027	4.576	3.443	3.308
6000	1.000	0.20	0.057	0.017	-0.059	2.396	1.617
6000	1.500	0.20	0.051	0.016	-0.084	2.227	1.629
6000	2.000	0.20	0.053	0.017	-0.001	2.205	1.723
6000	2.500	0.20	0.058	0.018	0.179	2.202	1.820
6000	3.000	0.20	0.066	0.019	0.499	2.207	1.918
6000	3.500	0.20	0.079	0.019	0.989	2.255	2.043
6000	4.000	0.20	0.097	0.018	1.663	2.357	2.203
6000	4.500	0.20	0.124	0.017	2.558	2.559	2.439
6000	5.000	0.20	0.158	0.015	3.656	2.839	2.734
7000	1.000	0.20	0.032	0.007	-0.118	1.388	0.928
7000	1.500	0.20	0.031	0.006	-0.132	1.449	1.004
7000	2.000	0.20	0.030	0.004	-0.108	1.469	1.062
7000	2.500	0.20	0.029	0.002	-0.044	1.461	1.108
7000	3.000	0.20	0.030	0.000	0.073	1.441	1.154
7000	3.500	0.20	0.030	-0.000	0.240	1.294	1.108
7000	4.000	0.20	0.035	-0.001	0.485	1.282	1.156
7000	4.500	0.20	0.044	-0.002	0.861	1.304	1.230
7000	5.000	0.20	0.057	-0.003	1.392	1.372	1.333
8000	1.000	0.20	0.018	0.002	0.282	0.433	0.216
8000	1.500	0.20	0.021	0.003	0.249	0.582	0.341
8000	2.000	0.20	0.022	0.001	0.229	0.678	0.433
8000	2.500	0.20	0.021	-0.000	0.223	0.744	0.508
8000	3.000	0.20	0.019	-0.003	0.229	0.790	0.574
8000	3.500	0.20	0.017	-0.008	0.257	0.817	0.628
8000	4.000	0.20	0.016	-0.011	0.319	0.830	0.675
8000	4.500	0.20	0.017	-0.014	0.436	0.836	0.716
8000	5.000	0.20	0.019	-0.014	0.591	0.784	0.705

Table B.6. Grid of indices for models of [M/H]=+0.3

T_{eff}	log g	[M/H]	Mg_2	Mg_1	Mg_b	Fe5270	Fe5335
4000	1.000	0.30	0.542	0.413	3.144	6.315	6.588
4000	1.500	0.30	0.573	0.463	2.970	6.194	6.585
4000	2.000	0.30	0.606	0.510	2.928	6.200	6.661
4000	2.500	0.30	0.640	0.551	2.972	6.330	6.833
4000	3.000	0.30	0.676	0.589	3.098	6.595	7.105
4000	3.500	0.30	0.716	0.629	3.240	6.989	7.469
4000	4.000	0.30	0.760	0.673	3.249	7.457	7.849
4000	4.500	0.30	0.774	0.694	2.970	7.676	7.867
4000	5.000	0.30	0.741	0.666	2.568	7.481	7.400
4250	1.000	0.30	0.397	0.268	3.165	5.946	5.851
4250	1.500	0.30	0.435	0.301	3.403	5.828	5.920
4250	2.000	0.30	0.484	0.346	3.680	5.822	6.034
4250	2.500	0.30	0.539	0.398	3.963	5.935	6.232
4250	3.000	0.30	0.598	0.452	4.243	6.182	6.540
4250	3.500	0.30	0.658	0.507	4.489	6.575	6.962
4250	4.000	0.30	0.719	0.565	4.647	7.094	7.486
4250	4.500	0.30	0.775	0.626	4.548	7.650	7.983
4250	5.000	0.30	0.793	0.658	4.076	7.913	8.083
4500	1.000	0.30	0.283	0.205	2.050	5.422	4.966
4500	1.500	0.30	0.302	0.202	2.521	5.335	5.105
4500	2.000	0.30	0.337	0.212	3.150	5.317	5.249
4500	2.500	0.30	0.390	0.240	3.875	5.395	5.441
4500	3.000	0.30	0.456	0.283	4.597	5.593	5.728
4500	3.500	0.30	0.531	0.336	5.231	5.926	6.137
4500	4.000	0.30	0.611	0.398	5.718	6.416	6.669
4500	4.500	0.30	0.693	0.470	5.974	7.036	7.307
4500	5.000	0.30	0.767	0.549	5.843	7.687	7.929
4750	1.000	0.30	0.222	0.184	1.098	4.771	4.078
4750	1.500	0.30	0.226	0.170	1.443	4.741	4.261
4750	2.000	0.30	0.241	0.159	2.022	4.746	4.437
4750	2.500	0.30	0.270	0.155	2.845	4.811	4.633
4750	3.000	0.30	0.318	0.165	3.867	4.970	4.893
4750	3.500	0.30	0.385	0.192	4.950	5.237	5.248
4750	4.000	0.30	0.466	0.235	5.940	5.640	5.727
4750	4.500	0.30	0.557	0.293	6.713	6.196	6.335
4750	5.000	0.30	0.651	0.367	7.146	6.892	7.050
5000	1.000	0.30	0.179	0.148	0.582	4.133	3.316
5000	1.500	0.30	0.181	0.144	0.768	4.135	3.518
5000	2.000	0.30	0.187	0.135	1.164	4.154	3.698
5000	2.500	0.30	0.202	0.125	1.818	4.223	3.889
5000	3.000	0.30	0.228	0.116	2.741	4.355	4.121
5000	3.500	0.30	0.272	0.116	3.905	4.578	4.427
5000	4.000	0.30	0.336	0.130	5.216	4.915	4.841
5000	4.500	0.30	0.418	0.159	6.483	5.381	5.376
5000	5.000	0.30	0.512	0.207	7.523	5.992	6.033
5250	1.000	0.30	0.137	0.099	0.313	3.591	2.715
5250	1.500	0.30	0.141	0.103	0.394	3.614	2.919
5250	2.000	0.30	0.147	0.103	0.670	3.624	3.084
5250	2.500	0.30	0.158	0.099	1.153	3.665	3.251
5250	3.000	0.30	0.175	0.092	1.872	3.758	3.453
5250	3.500	0.30	0.202	0.085	2.831	3.950	3.709
5250	4.000	0.30	0.245	0.081	4.090	4.233	4.055
5250	4.500	0.30	0.307	0.087	5.528	4.625	4.509
5250	5.000	0.30	0.386	0.107	6.973	5.155	5.088

Table B.6 (Continued)

T_{eff}	log g	[M/H]	Mg_2	Mg_1	Mg_b	Fe5270	Fe5335
5500	1.000	0.30	0.100	0.056	0.131	3.122	2.235
5500	1.500	0.30	0.104	0.063	0.184	3.139	2.418
5500	2.000	0.30	0.110	0.066	0.357	3.147	2.576
5500	2.500	0.30	0.119	0.068	0.703	3.173	2.727
5500	3.000	0.30	0.133	0.066	1.251	3.232	2.887
5500	3.500	0.30	0.155	0.063	2.046	3.375	3.107
5500	4.000	0.30	0.186	0.058	3.099	3.595	3.385
5500	4.500	0.30	0.229	0.055	4.407	3.920	3.753
5500	5.000	0.30	0.291	0.057	5.917	4.373	4.250
5750	1.000	0.30	0.073	0.030	0.030	2.722	1.865
5750	1.500	0.30	0.075	0.034	0.038	2.724	2.021
5750	2.000	0.30	0.080	0.038	0.152	2.726	2.158
5750	2.500	0.30	0.087	0.040	0.408	2.741	2.291
5750	3.000	0.30	0.099	0.041	0.838	2.776	2.428
5750	3.500	0.30	0.116	0.041	1.479	2.867	2.601
5750	4.000	0.30	0.141	0.039	2.350	3.033	2.828
5750	4.500	0.30	0.175	0.036	3.463	3.296	3.133
5750	5.000	0.30	0.222	0.034	4.816	3.669	3.535
6000	1.000	0.30	0.063	0.020	-0.020	2.555	1.693
6000	1.500	0.30	0.057	0.019	-0.061	2.390	1.722
6000	2.000	0.30	0.059	0.021	0.017	2.379	1.835
6000	2.500	0.30	0.065	0.023	0.202	2.382	1.946
6000	3.000	0.30	0.074	0.024	0.540	2.396	2.058
6000	3.500	0.30	0.087	0.024	1.052	2.448	2.195
6000	4.000	0.30	0.107	0.023	1.771	2.559	2.372
6000	4.500	0.30	0.134	0.022	2.706	2.759	2.616
6000	5.000	0.30	0.171	0.019	3.869	3.054	2.937
7000	1.000	0.30	0.034	0.008	-0.147	1.472	0.976
7000	1.500	0.30	0.033	0.007	-0.166	1.547	1.060
7000	2.000	0.30	0.032	0.005	-0.142	1.581	1.129
7000	2.500	0.30	0.032	0.003	-0.074	1.583	1.185
7000	3.000	0.30	0.033	0.001	0.051	1.566	1.236
7000	3.500	0.30	0.033	-0.000	0.227	1.417	1.193
7000	4.000	0.30	0.038	-0.001	0.497	1.398	1.244
7000	4.500	0.30	0.048	-0.001	0.911	1.425	1.328
7000	5.000	0.30	0.063	-0.002	1.494	1.503	1.450
8000	1.000	0.30	0.019	0.003	0.252	0.481	0.233
8000	1.500	0.30	0.022	0.003	0.205	0.644	0.368
8000	2.000	0.30	0.022	0.002	0.179	0.748	0.467
8000	2.500	0.30	0.022	0.000	0.169	0.820	0.549
8000	3.000	0.30	0.020	-0.003	0.177	0.869	0.619
8000	3.500	0.30	0.018	-0.008	0.211	0.898	0.680
8000	4.000	0.30	0.017	-0.011	0.286	0.912	0.731
8000	4.500	0.30	0.018	-0.014	0.424	0.918	0.779
8000	5.000	0.30	0.020	-0.015	0.594	0.846	0.757

Table B.7. Grid of indices for models of [M/H]=+0.5

T_{eff}	log g	[M/H]	Mg_2	Mg_1	Mg_b	Fe5270	Fe5335
4000	1.000	0.50	0.581	0.436	3.524	6.767	7.141
4000	1.500	0.50	0.602	0.481	3.242	6.592	7.103
4000	2.000	0.50	0.627	0.521	3.127	6.549	7.143
4000	2.500	0.50	0.654	0.556	3.123	6.637	7.276
4000	3.000	0.50	0.685	0.589	3.232	6.841	7.508
4000	3.500	0.50	0.719	0.622	3.385	7.212	7.834
4000	4.000	0.50	0.758	0.661	3.374	7.690	8.203
4000	4.500	0.50	0.789	0.699	3.187	8.027	8.403
4000	5.000	0.50	0.779	0.700	2.760	8.069	8.117
4250	1.000	0.50	0.449	0.304	3.722	6.406	6.424
4250	1.500	0.50	0.483	0.337	3.849	6.250	6.481
4250	2.000	0.50	0.526	0.380	4.022	6.213	6.584
4250	2.500	0.50	0.576	0.428	4.223	6.302	6.766
4250	3.000	0.50	0.628	0.476	4.440	6.533	7.052
4250	3.500	0.50	0.681	0.523	4.645	6.907	7.451
4250	4.000	0.50	0.734	0.573	4.770	7.403	7.948
4250	4.500	0.50	0.784	0.627	4.664	7.954	8.444
4250	5.000	0.50	0.809	0.666	4.200	8.327	8.658
4500	1.000	0.50	0.327	0.240	2.589	5.888	5.518
4500	1.500	0.50	0.348	0.237	3.033	5.771	5.661
4500	2.000	0.50	0.384	0.249	3.614	5.729	5.806
4500	2.500	0.50	0.436	0.277	4.280	5.792	6.002
4500	3.000	0.50	0.501	0.319	4.938	5.980	6.291
4500	3.500	0.50	0.574	0.369	5.507	6.321	6.699
4500	4.000	0.50	0.648	0.427	5.936	6.811	7.229
4500	4.500	0.50	0.722	0.492	6.126	7.429	7.862
4500	5.000	0.50	0.788	0.563	5.937	8.077	8.484
4750	1.000	0.50	0.258	0.220	1.487	5.240	4.584
4750	1.500	0.50	0.263	0.205	1.842	5.193	4.787
4750	2.000	0.50	0.278	0.191	2.421	5.171	4.967
4750	2.500	0.50	0.310	0.188	3.265	5.225	5.176
4750	3.000	0.50	0.362	0.198	4.295	5.374	5.444
4750	3.500	0.50	0.431	0.226	5.369	5.643	5.814
4750	4.000	0.50	0.513	0.269	6.315	6.061	6.313
4750	4.500	0.50	0.602	0.325	7.015	6.633	6.938
4750	5.000	0.50	0.691	0.397	7.340	7.343	7.666
5000	1.000	0.50	0.211	0.186	0.853	4.580	3.750
5000	1.500	0.50	0.213	0.179	1.038	4.569	3.974
5000	2.000	0.50	0.219	0.168	1.445	4.582	4.176
5000	2.500	0.50	0.234	0.155	2.121	4.639	4.382
5000	3.000	0.50	0.264	0.145	3.114	4.767	4.630
5000	3.500	0.50	0.312	0.144	4.365	4.984	4.960
5000	4.000	0.50	0.380	0.158	5.685	5.337	5.398
5000	4.500	0.50	0.465	0.190	6.939	5.826	5.968
5000	5.000	0.50	0.560	0.238	7.895	6.461	6.656
5250	1.000	0.50	0.168	0.133	0.533	4.020	3.076
5250	1.500	0.50	0.171	0.136	0.619	4.030	3.304
5250	2.000	0.50	0.177	0.135	0.914	4.045	3.502
5250	2.500	0.50	0.187	0.129	1.382	4.091	3.694
5250	3.000	0.50	0.205	0.120	2.141	4.187	3.910
5250	3.500	0.50	0.235	0.110	3.171	4.384	4.197
5250	4.000	0.50	0.283	0.105	4.531	4.667	4.569
5250	4.500	0.50	0.349	0.111	6.041	5.074	5.062
5250	5.000	0.50	0.433	0.132	7.491	5.626	5.682

Table B.7 (Continued)

T_{eff}	log g	[M/H]	Mg_2	Mg_1	Mg_b	Fe5270	Fe5335
5500	1.000	0.50	0.128	0.081	0.282	3.547	2.532
5500	1.500	0.50	0.131	0.088	0.322	3.558	2.745
5500	2.000	0.50	0.137	0.093	0.497	3.577	2.939
5500	2.500	0.50	0.146	0.094	0.849	3.605	3.115
5500	3.000	0.50	0.161	0.091	1.425	3.693	3.320
5500	3.500	0.50	0.183	0.086	2.295	3.813	3.541
5500	4.000	0.50	0.217	0.079	3.440	4.049	3.857
5500	4.500	0.50	0.265	0.074	4.875	4.381	4.262
5500	5.000	0.50	0.332	0.076	6.478	4.854	4.802
5750	1.000	0.50	0.102	0.049	0.232	3.259	2.188
5750	1.500	0.50	0.095	0.050	0.152	3.112	2.280
5750	2.000	0.50	0.101	0.056	0.261	3.137	2.461
5750	2.500	0.50	0.109	0.059	0.518	3.157	2.620
5750	3.000	0.50	0.121	0.061	0.973	3.202	2.786
5750	3.500	0.50	0.140	0.060	1.665	3.300	2.985
5750	4.000	0.50	0.168	0.057	2.619	3.479	3.245
5750	4.500	0.50	0.205	0.053	3.846	3.754	3.584
5750	5.000	0.50	0.257	0.049	5.328	4.142	4.031
6000	1.000	0.50	0.078	0.028	0.086	2.883	1.857
6000	1.500	0.50	0.079	0.032	0.070	2.922	2.046
6000	2.000	0.50	0.074	0.031	0.074	2.747	2.081
6000	2.500	0.50	0.080	0.034	0.272	2.765	2.222
6000	3.000	0.50	0.091	0.036	0.633	2.796	2.365
6000	3.500	0.50	0.106	0.037	1.192	2.862	2.535
6000	4.000	0.50	0.128	0.036	1.983	2.982	2.733
6000	4.500	0.50	0.159	0.035	3.024	3.199	3.017
6000	5.000	0.50	0.201	0.032	4.319	3.518	3.388
7000	1.000	0.50	0.038	0.010	-0.185	1.640	1.060
7000	1.500	0.50	0.038	0.008	-0.208	1.752	1.173
7000	2.000	0.50	0.037	0.006	-0.187	1.818	1.271
7000	2.500	0.50	0.037	0.004	-0.125	1.834	1.342
7000	3.000	0.50	0.039	0.002	0.018	1.838	1.415
7000	3.500	0.50	0.043	0.001	0.266	1.825	1.481
7000	4.000	0.50	0.045	0.000	0.533	1.667	1.442
7000	4.500	0.50	0.058	-0.000	1.034	1.732	1.580
7000	5.000	0.50	0.074	-0.001	1.706	1.795	1.703
8000	1.000	0.50	0.021	0.004	0.181	0.576	0.279
8000	1.500	0.50	0.024	0.005	0.105	0.765	0.432
8000	2.000	0.50	0.024	0.004	0.066	0.885	0.543
8000	2.500	0.50	0.023	0.001	0.052	0.971	0.636
8000	3.000	0.50	0.022	-0.002	0.063	1.031	0.719
8000	3.500	0.50	0.019	-0.007	0.109	1.069	0.793
8000	4.000	0.50	0.019	-0.011	0.214	1.087	0.855
8000	4.500	0.50	0.021	-0.014	0.397	1.093	0.913
8000	5.000	0.50	0.027	-0.016	0.703	1.109	0.980

Bibliography

[1] Aller, L., 1963, The Atmospheres of the Sun and Stars, 2nd edition ed. New York:Ronald Press

[2] Anders, E., Grevesse, N. 1989, Geochimica et Cosmochimica Acta, 53, 197

[3] Baade, W. : 1944, ApJ,100, 147

[4] Barbaro, G. & Olivi, F. M., 1989, ApJ, 337, 125

[5] Barbuy, B. 1989, ASSci, 157, 111

[6] Barbuy, B. 1994, ApJ, 430, 218

[7] Barbuy, B., Erdelyi–Mendes, M., & Milone, A. 1992, A&AS,93,235

[8] Bell, R., & Gustaffson, B., 1989, MNRAS, 236, 653

[9] Bertelli, G., Betto, R., Bressan, A., Chiosi, C., Nasi, E., & Vallenari, A., 1990, A&AS, 85, 845

[10] Bertelli, G., Bressan, A., Chiosi, C., & Angerer, K., 1986, A&AS, 66, 191

[11] Bertola, F., Capaccioli, M. & Oke, J. B., 1982, ApJ, 254, 494

[12] Bica, E., in proceedings in IAU Symposium 149-Stellar Populations, ed. B. Barbuy & A. Renzini, 215

[13] Bonifacio, P., 1991, Master Science thesis, SISSA

[14] Bressan, A., Chiosi, C., & Fagotto, F., 1994, ApJS, 94, 63 (BCF94)

[15] Bressan, A., Chiosi C., & Tantalo, R., , 1995, A&A, in press (BCT95)

[16] Brocatto, E., Matteucci, F., Mazzitelli, I., & Tornambé, A., 1990, ApJ, 459, 348

[17] Brown, J. A., Sneden, C., Lambert, D. L., & Dutchover, E., 1989, ApJS, 71, 293

[18] Burstein, D., Bertola, F., Buson, L. M., Faber S. M., & Lauer, T. R., 1988, ApJ , 328, 440

[19] Burstein, D., Faber, S. M., Gaskell, C. M., & Krumm, N., 1984, ApJ, 287, 586

[20] Buzzoni, A., 1989, ApJS, 71, 817

[21] Buzzoni, A., 1995, ApJS, 98, 69

[22] Buzzoni, A., Gariboldi, G., & Mantegazza, L., 1992, AJ,103,1814

[23] Buzzoni, A., Mantegazza, L., & Gariboldi, G., 1994, AJ, 107, 513

[24] Campbell, B., 1986, ApJ, 307, 750

[25] Cayrel de Strobel G., Hauck, B., François, P., Thévenin, F., Friel, E., Mermilliod, M., Borde, S. 1992, A&AS, 95, 273 (C91)

[26] Chavez, M., Malagnini, M. L., & Morossi C., 1995, ApJ, 440, 210

[27] Chavez, M., Stalio, R., & Holberg, J. B., 1995, ApJ, 449, 280

[28] Chiosi, C., Bertelli, G., & Bressan A., 1988, A&A, 196, 84

[29] Chiosi, C., Bertelli, G., & Bressan, A., 1992, ARAA, 30, 235

[30] Clariá, J. J., Piatti, A. E., & Lapasset, E., 1994, PASP, 106, 436

[31] Code, A. D., 1969, PASP, 81, 475

[32] Code, A. D. & Welsh, G. A., 1979, ApJ, 228, 95

[33] Desikachary, K., & Gray, D. F., 1978, ApJ, 226, 907

[34] Deutsch, A. J., 1955, In *Principles Fundamentaux de Classification Stellaire*, Vol.25, Paris, CNRS

[35] Dorman, B., O'Connell, W. R., & Rood, R. T., 1995, ApJ, 442, 105

[36] Faber, S. M., 1977, in The Evolution of Galaxies and Stellar Populations, ed. B. M. Tinsley & R. B. Larson, (New Haven:Yale Univ. Obs.), 157

[37] Faber, S. M., 1983, *Highlights in Astronomy*, Vol. 6, 165

[38] Faber, S. M., Burstein, D., & Dressler, A., 1977, AJ, 82, 941.

[39] Faber, S. M., Friel, E. D., Burstein, D., Gaskell, C. M., 1985, ApJS, 57, 711

[40] Faber, S. M., Trager, S. S., Gonzalez, J. J., & Worthey, G., 1995, in proceedings in IAU Symposium 164-Stellar Populations, ed. P. C. Van der Kruit & G. Gilmore, 249

[41] Ferguson, H. C., et al. 1991, ApJL, 381, L69

[42] Ferguson, H. C., & Davidsen, A. F., 1993, ApJ, 408, 92

[43] Gorgas J., Faber, S. M., Burstein, D., Gonzales J. J., Courteau S., & Prosser C. 1993, ApJS, 86, 157

[44] Gratton, R. G., & Sneden, C., 1990, A&A, 234, 366

[45] Greggio, L., & Renzini, A., 1990, ApJ, 364, 35

[46] Gulati, R. K., 1991, PhD thesis, SISSA

[47] Gulati, R. K., Malagnini, M. L., & Morossi, C. 1991, A&A, 247, 447

[48] Gulati, R. K., Malagnini, M. L., & Morossi, C. 1993, ApJ, 413, 166 (GMM93)

[49] Gutierrez-Moreno, A., Moreno, H., Cortés, G., & Wenderoth, E., 1988, PASP, 100, 973

[50] Gustaffson, B., Bell, R. A., Erikson, K., & Nordlund, A., 1975, A&A, 42, 407

[51] Gustaffson, B., & Jorgensen U. G., 1994, A&A Rev., 6, 19

[52] Hills, J.G., 1971, A&A, 12, 1

[53] Iben, I Jr, 1991, ApJS, 76, 55

[54] Johnson, H. L. & Sandage, A., 1955, ApJ, 121, 616

[55] Jones, L. A., & Worthey, G., 1995a, ApJL, in press

[56] Jones, L. A., & Worthey, G., 1995b, ApJ, submitted

[57] Keenan, P. C., & Keller, G., 1953, Apj, 117, 241

[58] Kiehling, R., 1987, A&AS, 69, 465

[59] Kinman, T. D., 1959, MNRAS, 119, 599

[60] Kurucz, R. : 1970, Smithsonian. Astrophys. Obs. Spec. Rep. No. 309

[61] Kurucz, R. L., 1979, ApJS, 40, 1

[62] Kurucz, R. L. & Avrett, E., 1981, Smithsonian Astrophys. Obs, Spec, Rep., No. 391

[63] Kurucz, R. L., 1991, RMexAA, 23, 187

[64] Kurucz, R. L. 1992, in The stellar populations of galaxies, eds. Barbuy and Renzini, Kluwer Academic Publishers, 225 (K92)

[65] Kurucz, R. L. 1993, CD–Rom 13 and CD–Rom 18 (K93)

[66] Kurucz, R. L., 1995, CfA preprint No. 4080

[67] Laird, J.B., 1985, ApJ, 289, 556

[68] Larson, R. B., 1974, MNRAS, 166, 585

[69] Maeder, A., & Meynet, G., 1991, A&AS, 89, 451

[70] Malagnini, M. L., Chavez, M., & Morossi, C., 1995, in From Stars to Galaxies–The Impact of Stellar Physics on Galaxy Evolution, in preparation

[71] Malagnini, M. L., & Morossi, C., 1983, in Statistical Methods in Astronomy, ESA-SP, 201, 27

[72] Malagnini, M.L., Morossi, C., Buser, R., & Parthasaraty, ., 1992, A&A, 261, 558

[73] Malagnini, M. L., Morossi, C., Buzzoni, A., & Mantegazza, L., 1994, in Stellar Populations-2nd Teramo Workshop, Mem.S.A.It., 65, 803

[74] Maltby, P., et al. 1986. ApJ, 306, 284

[75] Matteucci, F., & Tornambé, A. 1987, A&A, 185, 51

[76] Mayall, N. U., 1946, ApJ, 104, 290

[77] McQuitty, R. J., Jaffe, T. R., Friel, E. D., Dalle Ore, C. M. 1994, AJ, 107, 359

[78] McWilliam, A., 1990, ApJS, 74, 1075

[79] Mihalas, D., 1978, Stellar Atmospheres, W.H. Freeman & Co., San Francisco., 2nd. Edition

[80] Morgan, W. W., 1956, PASP, 68, 509

[81] Morgan, W. W., 1959, AJ, 64, 432

[82] Morossi, C., Franchini, M., Malagnini, M. L., Kurucz, R. L., & Buser, R., 1993, A&A, 277, 173

[83] Mould, J. 1978, ApJ, 220, 434

[84] O'Connell, D. J. K., 1958, *Specola Astronomica Vaticana*, Vol. 5, Vatican City.

[85] O'Connell, R. W., 1986, in Spectral Evolution of Galaxies, ed. C.Chiosi and A. Renzini (Dordrecht:Reidel) , 321.

[86] Peterson, R., 1976, ApJS, 30, 61

[87] Peterson, R., Dalle Ore C. M., & Kurucz, R. L., 1993, ApJ, 404, 333

[88] Renzini, A, & Buzzoni, A., 1986, in Spectral Evolution of Galaxies, , ed C. Chiosi & A. Renzini, (Dordecht:Reidel), 195

[89] Rich, M. R., 1988, AJ, 95, 828

[90] Rountree, J., & Sonnenborn, G., 1991, ApJ, 369, 515

[91] Salpeter, E. E., 1955, ApJ, 121, 161

[92] Scalo, J. M., 1986, Fund. Cosmic Phys., 11, 1

[93] Schmidt-Kaler, Th., 1982, Landolt-Börntein Catalogue, VI/2b

[94] Spinrad, H., Greenstein, J. L., Taylor, B. J., & King, I. R., 1970, ApJ, 162, 891

[95] Spinrad, H., Taylor, B.J., 1969, ApJ. 157, 1279

[96] Spinrad, H., Taylor, B.J., 1971, ApJS, 22, 445

[97] Strom, S. E., Strom, K. M., & Carbon, D. F., 1971, A&A, 12, 177

[98] Tantalo, R., Chiosi, C., Bressan, A., & Fagotto, F., 1995, A&A, in press

[99] Taylor, B., 1991, ApJS, 76, 715

[100] Thévenin, F., 1989, A&AS, 77, 137

[101] Thévenin, F., & Foy, R., 1983, A&A, 122, 261

[102] Tinsley, B.M. : 1975, Mem.S.A.It., 46, 3

[103] Tinsley, B.M., 1980, Fund. Cosmic Phys., 5, 287

[104] Worthey, G., 1992, PhD thesis, University of California, Santa Cruz

[105] Worthey, G., Faber, S. M., Gonzalez, J. J., & Burstein, D., 1994, ApJS, 94, 687 (WFGB94)

[106] Worthey, G., Trager, S. S., & Faber, S. M., 1995, in Fresh Views on Elliptical Galaxies, ed. A. Buzzoni, A. Renzini & A. Serrano, in press.

[107] Yoshii, Y., & Arimoto, N., 1987, A&A, 188, 13

THE ASTROPHYSICAL JOURNAL, 440:210–215, 1995 February 10

NEW SYNTHETIC Mg_2 INDICES

M. CHAVEZ
International School for Advanced Studies (SISSA/ISAS), Strada Costiera 11, I-34014 Trieste, Italy; and
Instituto Nacional de Astrofisica, Optica y Electronica (INAOE), Mexico
M. L. MALAGNINI
Dipartimento di Astronomia, Università degli Studi di Trieste, Via Tiepolo 11, I-34131 Trieste, Italy
AND
C. MOROSSI
Osservatorio Astronomico di Trieste, Via Tiepolo 11, I-34131 Trieste, Italy
Received 1994 May 4; accepted 1994 August 26

ABSTRACT

Using the most recent grid of Kurucz model atmospheres and his improved set of numerical codes to compute synthetic stellar spectra, we have calculated the strength of the magnesium absorption feature at 5175 Å (Mg_2 index) from a set of 141 computed synthetic spectra. The index values refer to the effective temperature range 4000–6000 K, surface gravity from 1.5 to 4.5 dex, and metallicity from −0.5 to 1.0 dex. The computed index for the solar model matches very well the value obtained from observational data. Above 5000 K, the new Mg_2 values and previous calculations agree to within 0.02 mag, but discrepancies can reach almost 0.58 mag for cool, metal-rich, low-gravity stars, so that large values of Mg_2 previously obtained for low temperature dwarfs are now obtained for giants as well.

A comparison with observational data is also presented.

Subject headings: galaxies: photometry — galaxies: stellar content — stars: atmospheres

1. INTRODUCTION

In order to analyze the integrated light of stellar systems and its link to the basic parameters of a stellar population, it is fundamental to understand and to calibrate the behavior of the photometric and spectroscopic properties of the components (stars) in terms of the atmospheric stellar quantities, namely, temperature, gravity, and metallicity. These calibrations are coupled, in the context of the evolutionary synthesis, with a convenient set of evolutionary tracks to give insight into the overall changes of the radiation emitted by ensembles of stars with different characteristics. Once we know the dependence of the characteristics of the integrated radiation on all the free parameters involved, we should be able to determine the history and chemical evolution of stellar populations.

Empirical calibrations of several spectral indices (Faber et al. 1985; Buzzoni, Gariboldi, & Mantegazza 1992; Gorgas et al. 1993; Worthey et al. 1994, hereafter GW94) had led to a deeper understanding of their dependence on stellar atmospheric parameters.

Theoretical work initiated by Mould (1978) and continued by Gulati, Malagnini, & Morossi (1991, 1993, hereafter GMM93), Barbuy, Erdelyi-Mendes, & Milone (1992), McQuitty et al. (1994), and Barbuy (1994) has concentrated on a strong feature of magnesium at 5175 Å. In the following, we will refer to the Mg_2 index defined by Faber et al. (1985) mainly because of its potential in the analysis of integrated light of galaxies and because of the extensive set of observational data available (Gorgas et al. 1993; GW94).

The purpose of this paper is to present new synthetic Mg_2 indices, computed using the new set of Kurucz models (Kurucz 1993a) and codes to produce synthetic spectra (Kurucz 1993b, hereafter, with Kurucz 1993a, K93), and to compare them with already published indices (GMM93), based on previous Kurucz atmosphere models (1992, hereafter K92).

In § 2 we briefly describe the main differences between K92 and K93 grids of model atmospheres, atomic data, and codes. Section 3 is devoted to illustrating the relationships of the new set of Mg_2 indices to the atmospheric parameters, and the differences from the indices obtained by GMM93. In § 4, theoretical predictions are compared with empirical data, and conclusions are presented.

2. THE SYNTHETIC Mg_2 INDEX

GMM93 presented a grid of synthetic spectral indices based on a subset of the K92 grid of model atmospheres. This set of models included improvements with respect to previous versions and with respect to grids developed by other authors. These improvements were mainly the extension to a larger effective temperature range (from 50,000 K down to 3500 K), an increased set of atomic data in the opacity distribution functions, and, very important, the inclusion of opacity of diatomic molecules. GMM93 results showed that, for the case of the Mg_2 index, agreement within the observational errors is obtained when comparing synthetic indices with Gorgas et al. (1993) empirical calibrations, and with solar data.

The newest grid of Kurucz models (K93) contains a number of improvements and changes with respect to K92 models. Let us enumerate some of the principal changes (Kurucz 1994):

1. The new models contain 72 depth points starting at Rosseland optical depth 10^{-7} instead of 64 starting at 10^{-6}. This improvement removes the abrupt temperature drop at the surface that appeared in the earlier models, reduces the molecular abundances near the surface, and decreases the central depth of strong lines.

2. A bug in the Fe I continuous opacity at low temperatures was present in both the model atmosphere and spectrum synthesis programs. In K93 the bug was corrected.

3. A new SYNTHE series of programs to compute synthetic spectra includes a detailed treatment of scattering in the source function by default; in previous versions the default was a fast approximation based on the assumption of a small scattering fraction that led to trouble if applied where scattering is large.

The iron bug would produce an error that correlates both with temperature and with abundances. For instance, the temperature drop at the surface in the 64-depth model of the low-temperature giant star Arcturus affected the molecular number densities, and some of the molecular lines became weaker in the 72-depth model because the number densities decreased. This effect and the scattering change must be important in some cases.

We have used K93 models and codes to compute 141 synthetic stellar spectra. They refer to nine values of effective temperature in the range 4000–6000 K, surface gravities 1.5, 3.0, and 4.5 dex for metallicities −0.50, 0.5, and 1.0 dex, and log g from 1.5 to 4.5, with a step of 0.5 dex, for [M/H] = 0.0.

The solar metal abundances are from Anders & Grevesse (1989), and helium abundance is fixed at 10% by number. For nonsolar metallicities, the abundance of any element is scaled by the same ratio as [M/H]. The ratio of mixing length to scale height $l/h = 1.25$ is used for the treatment of convection (for more details, see K92).

The main computational characteristics of the synthetic spectra are the following:

1. microturbulence velocity $\xi = 2\ \mathrm{km\ s^{-1}}$;
2. resolving power $(\lambda/\Delta\lambda) = 250{,}000$;
3. rotational velocity of $0\ \mathrm{km\ s^{-1}}$.

In computing the synthetic Mg_2 indices, we adopted the definition of Faber et al. (1985; see Table 1 of GMM93) and used different values of the Gaussian broadening function (FWHM) to convolve the synthetic spectra. In what follows, we refer only to FWHM = 9 Å, in order to compare our results with those of GMM93 (Table 4) and with empirical data collected in the GW94 catalog.

3. RESULTS AND COMPARISON WITH GMM93

Table 1, and Figures 1 and 2, report the results obtained so far. The reliability of the new indices for temperatures in the range 5000–6000 K is confirmed by the result reported in Table 1 for the Sun. The synthetic Mg_2 value, computed starting from the solar model given in CD-Rom 18 (K93), matches very well that obtained from the solar observational data. The solar empirical index is derived from the high-resolution Fourier transform spectrometer (FTS) solar spectrum observed at the Kitt Peak Observatory (Kurucz et al. 1984), provided by Kurucz in computer-readable form. The index is computed by using the same procedure applied to any synthetic spectrum, according to the definition by Faber et al. (1985). Because of the high resolution of the spectrum (resolving power $\lambda/\Delta\lambda = 522{,}000$) and high signal-to-noise ratio (2000–9000), negligible photometric error, if any, is expected (errors lower than 1% in the residual flux are reported).

TABLE 1

Mg_2 INDEX FOR THE SUN (in magnitudes)

	SYNTHETIC	
OBSERVED	GMM93	This Work
0.135.....	0.145	0.135

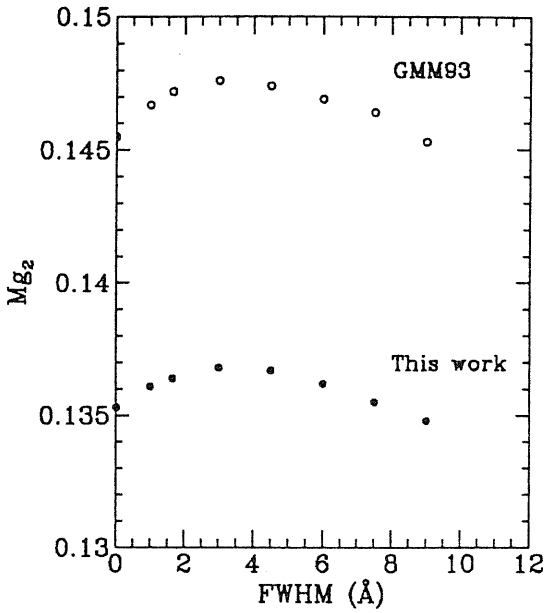

FIG. 1.—Dependence of the index on the FWHM of the Gaussian profile used in the convolution of the solar synthetic spectrum. Empty and filled symbols represent values from GMM93 and those obtained in this work, respectively.

Uncertainties in the computed solar index are estimated on the order of 0.005 mag when using different solar models in computing synthetic spectra. These uncertainties, as well as the difference between the synthetic GMM93 index and the empirical solar value, are on the same order as the expected errors for stellar observations.

The dependence of the index on instrumental resolution is displayed in Figure 1, with reference to the solar indices (empty circles correspond to the values given by GMM93, and filled ones to our results). Note that the trend is the same for both sets of data, with the new values located ~0.01 mag below, and that variations with FWHM of the broadening function are within a few thousandths of a magnitude.

Figure 2 contains three panels, where we plot new Mg_2 values versus the effective temperature parameter $\theta_{\rm eff}$ ($\equiv 5040/T_{\rm eff}$). Each panel refers to one surface gravity value (1.5, 3.0, and 4.5 dex, respectively) and to four different metallicities; filled circles represent the indices computed for nine $T_{\rm eff}$ values, from 4000 K to 6000 K, at a step of 250 K.

The trend of the index with $\theta_{\rm eff}$, at fixed gravity, is quite similar when varying metallicity, while a clear difference is present at low temperature between giant and dwarf models. Indeed, for dwarfs a plateau is reached, while it is not for giants. In the panel referring to log $g = 4.5$ dex, the value computed for the solar model (5777/4.43770/0.00) is also plotted (*starred symbol*).

Figure 3 shows the comparison of GMM93 results with the present ones in 12 panels; each panel refers to one gravity and one metallicity (the difference for the Sun is marked as in Fig. 2).

The general trend of the differences between the two sets of data, illustrated in this figure, is the following: (1) new Mg_2 indices tend to be higher than in GMM93 at low temperatures

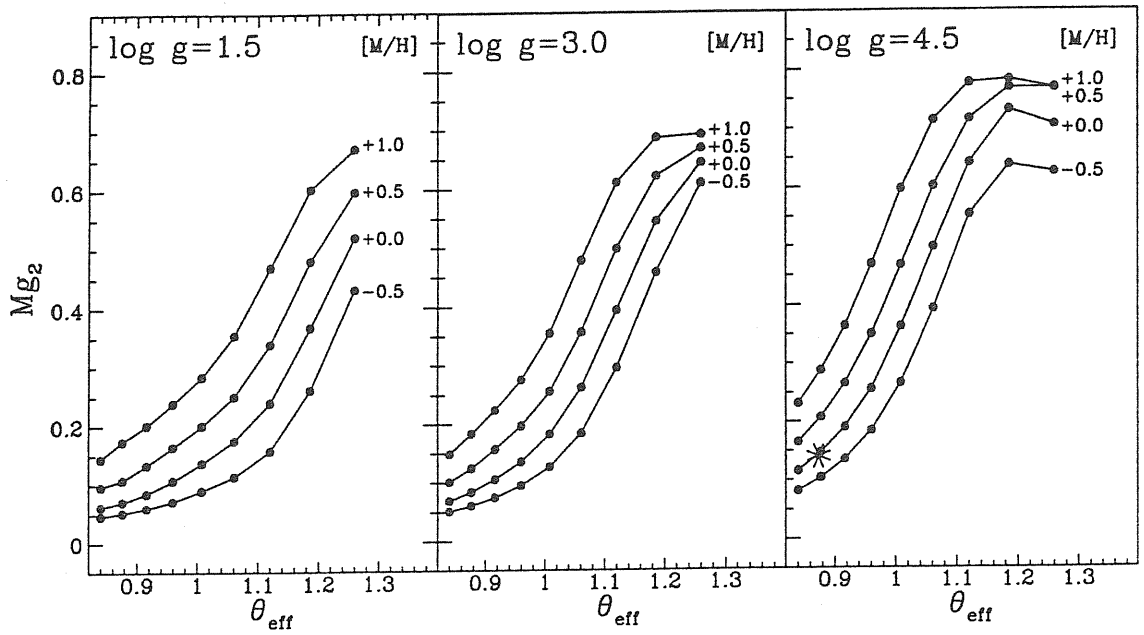

FIG. 2.—New synthetic indices for different metallicities and gravities as functions of θ_{eff}. The solar value is represented by a starred symbol.

and gravities, and at high metallicities; (2) the temperature above which old and new results do not differ significantly, irrespective of gravity, depends on metallicity. It goes from $T_{eff} = 4500$ K, for [M/H] = −0.5, up to 5250 K, for [M/H] = +1.0 dex.

In order to illustrate the effect of these differences in the interpretation of stellar data, we chose the case (4000/1.5), for which the differences are the highest The use of the new SYNTHE code starting from the same model as in GMM93 produced $Mg_2 = 0.5196$, to be compared with the new value ($Mg_2 = 0.5211$), and with the old one ($Mg_2 = 0.260$). We find that the differences in the models do not produce significant differences in the indices.

By comparing the new values for $T_{eff} = 4000$ K, log $g = 1.5$ dex, and different metallicities to the old ones, we find that new Mg_2 values are close to GMM93 ones reported for gravities higher than 1.5 dex: the difference in gravity goes from 0.75 dex for [M/H] = −0.5 up to 3.0 dex for [M/H] = 1.0. The net result is that Mg_2 values previously attributed to low-temperature dwarfs are now obtained for giants.

From these results and other tests, we conclude that the major differences in the indices are due to the different treatments of scattering in the codes, while only minor effects are due to differences in the models.

4. COMPARISON WITH OBSERVATIONAL DATA

To compare with observational data, we chose the most homogeneous collection of measured Mg_2 indices, presented by the Lick group (GW94) and kindly made available to us in a computer-readable form by the authors.

To establish the link between theoretical predictions and empirical data, the knowledge of atmospheric parameters, which naturally label the synthetic values, is required for the stars. We chose the most complete collection of (θ_{eff}, log g, [Fe/H]), with [Fe/H] derived from high-resolution analysis, i.e., A Catalogue of [Fe/H] Determinations: 1991 Edition (Cayrel de Strobel et al. 1992, hereafter C91). In the models, all metals are scaled by the same factor, thus the observed [Fe/H] values correspond to the theoretical [M/H] values.

The cross-check of the stars present in GW94 and of the determinations given in C91 produced a list of 501 entries. Out of this set, we extracted the determinations falling in the parameter ranges of our grid, leading to a final list of 141 determinations, referring to 67 stars.

The C91 atmospheric parameters were used to obtain synthetic Mg_2 indices from our grid by interpolating linearly in the three-dimensional space (θ_{eff}, log g, [M/H]). Table 2 contains, for the 67 stars present in C91 and GW94 in order of HD number, the atmospheric parameter determinations from C91, the observed indices from GW94, and the computed ones. The table is available in computer-readable form from M. L. M. (malagnini@univ.trieste.it).

The comparison between observed and synthetic indices is illustrated in Figure 4, where synthetic values from different determinations for the same star are connected by vertical bars.

In general, the points cluster around the 45° line, but it is clear that a large spread is present. The amplitude of the spread is much larger not only than the observational errors but also than the uncertainties expected in the synthetic values. By looking at different determinations for the same star, we can attribute most of the spread to uncertainties in the atmospheric parameters. This effect strongly affects the reliability of any empirical Mg_2 calibration based on heterogeneous and/or non–statistically unbiased data sets.

From Table 2 it results that the mean of the calculated indices is 0.03 mag (or 0.02 mag, if the two cool dwarfs with Mg_2[obs] > 0.4 mag—namely, HD 88230 and HD 219134—are excluded) larger than the mean of the observed values. This result is due to some extent to the use of linear interpolation for computing the synthetic values, while detailed investigation on individual stars with Mg_2(obs) > 0.4 mag is required to

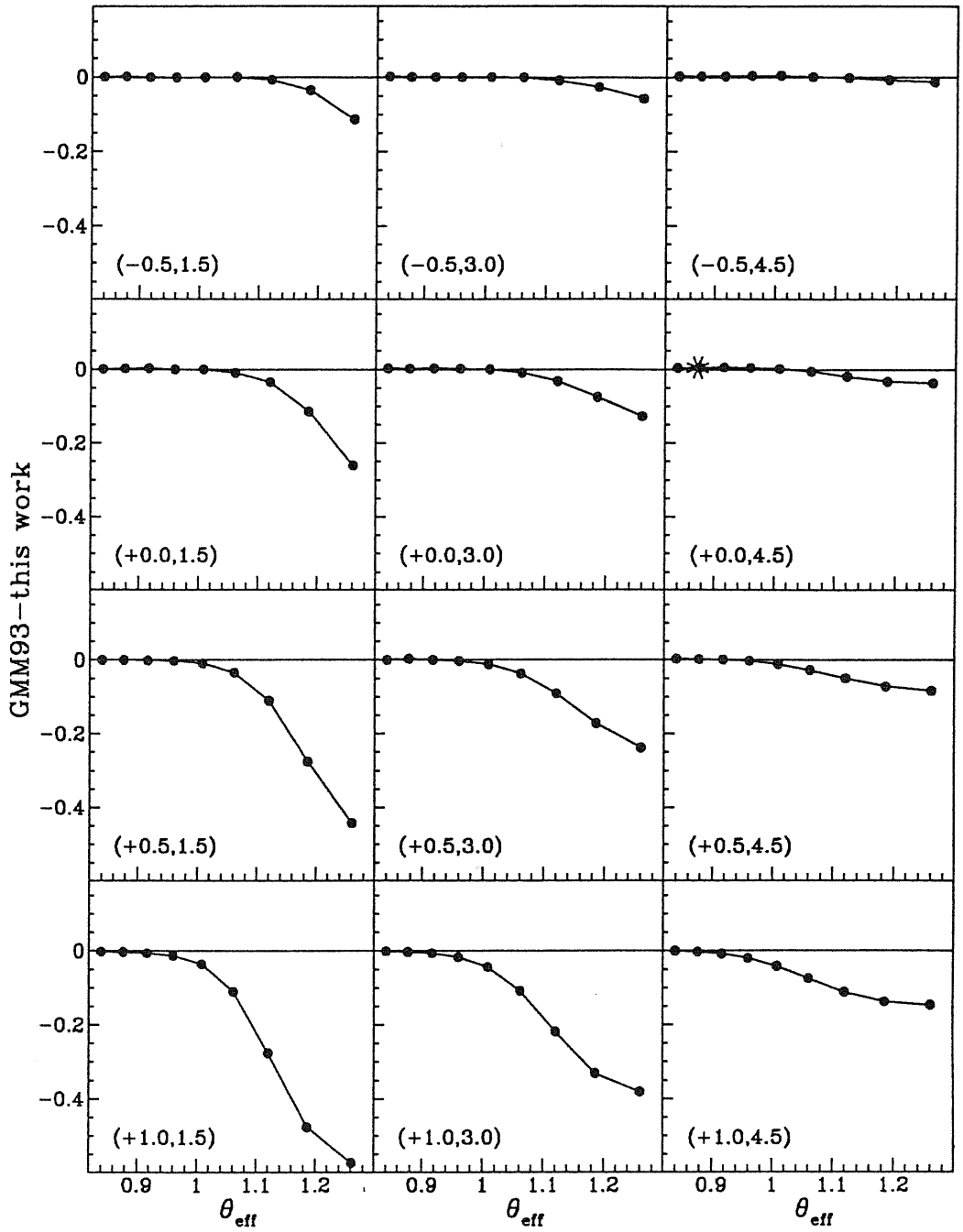

FIG. 3.—Differences between GMM93 and new synthetic indices for different metallicities and gravities as functions of θ_{eff}. The values of [M/H] and log g are given in parentheses in each panel. The solar case is represented by a starred symbol.

confirm the trend shown in Figure 4 by HD 88230 and HD 219134.

The absence in the observational database of cool dwarfs with atmospheric parameters from high resolution, prevents us from reaching any conclusive statement on the presence and level of any saturation in the index values (see discussion in Buzzoni et al. 1992).

In conclusion, the K93 release is expected to provide the best basis for stellar population studies, as its predictions are very closely confirmed by solar observations in different spectral regions, but comparisons with empirical spectral indices still present open problems, mainly because of insufficient accuracy in the determinations of stellar atmospheric parameters.

In the future we plan to produce extensive grids of Mg_2 and other spectral indices, covering the complete K93 metallicity range.

TABLE 2

ATMOSPHERIC PARAMETERS AND Mg_2 INDICES

HD	θ_{eff}	log g	[Fe/H]	Mg_2(obs)	Mg_2(comp)	HD	θ_{eff}	log g	[Fe/H]	Mg_2(obs)	Mg_2(comp)	HD	θ_{eff}	log g	[Fe/H]	Mg_2(obs)	Mg_2(comp)
3651	0.98	4.40	-0.17	0.277	0.262	85503	1.14	2.30	-0.11	0.327	0.333	142373	0.85	4.30	-0.40	0.078	0.090
4307	0.89	3.93	-0.36	0.088	0.106		1.11	2.35	0.48		0.405		0.86	4.00	-0.45		0.085
4614	0.89	4.37	-0.17	0.078	0.140		1.07	2.82	0.11		0.285	143761	0.87	3.98	-0.17	0.116	0.108
	0.88	4.40	-0.20		0.130		1.11	2.30	0.35		0.370	145675	0.97	4.50	0.22	0.298	0.321
10307	0.87	4.38	-0.03	0.127	0.134		1.17	2.20	0.31		0.474		0.97	4.40	0.18		0.303
10380	1.26	1.50	-0.35	0.315	0.458	86728	0.88	4.12	-0.08	0.144	0.128		0.93	4.50	0.31		0.261
	1.26	1.50	-0.30		0.467		0.87	4.40	0.03		0.141	153210	1.10	2.30	0.07	0.263	0.286
10476	0.97	4.50	-0.20	0.271	0.248		0.89	4.33	-0.11		0.143		1.10	2.30	-0.06		0.262
10700	0.95	4.33	-0.49	0.210	0.165	88230	1.26	4.50	0.28	0.518	0.741	161797	0.91	3.91	0.16	0.165	0.166
12929	1.12	2.40	-0.21	0.229	0.283	88284	0.99	3.12	0.09	0.195	0.187		0.93	4.10	0.30		0.228
	1.14	2.50	-0.08		0.360	89010	0.90	4.00	-0.03	0.118	0.139		0.93	4.10	0.32		0.231
	1.07	2.51	-0.25		0.203	95272	1.05	3.01	0.10	0.203	0.263	165908	0.84	4.20	-0.39	0.064	0.082
13974	0.90	4.50	-0.30	0.132	0.143	102870	0.84	4.30	0.29	0.090	0.136		0.85	4.17	-0.42		0.086
14802	0.85	4.40	0.00	0.097	0.120	113226	1.02	2.70	0.01	0.140	0.182	166620	1.04	4.50	-0.20	0.343	0.402
19476	1.02	3.30	0.08	0.188	0.242		1.02	2.70	-0.03		0.178		1.04	4.40	-0.30		0.368
	1.02	3.30	0.08		0.242		1.02	2.70	0.02		0.184	182572	0.89	4.26	0.50	0.184	0.213
	1.01	2.68	0.19		0,198		1.01	2.85	0.04		0.182		0.88	4.13	0.44		0.185
20630	0.89	4.45	0.08	0.135	0.170		1.01	3.00	-0.10		0.173		0.89	4.00	0.21		0.161
	0.89	4.40	-0.01		0.156		1.02	2.70	-0.06		0.175	184406	1.06	2.85	-0.05	0.346	0.238
	0.90	4.50	0.04		0.178		1.01	2.60	0.00		0.163		1.07	2.10	0.00		0.205
22484	0.85	3.87	-0.16	0.090	0.091		1.01	2.75	-0.02		0.169	185144	0.98	4.40	-0.25	0.213	0.250
	0.84	3.96	-0.12		0.088		1.01	3.00	0.17		0.210	186408	0.85	4.30	0.00	0.133	0.116
23249	1.03	3.36	-0.27	0.253	0.218		1.00	2.70	-0.05		0.155	186427	0.86	4.50	0.08	0.136	0.142
	1.02	3.83	-0.07		0.279		0.95	3.22	0.21		0.172		0.87	4.40	0.00		0.137
	1.02	3.80	-0.20		0.259		1.01	2.70	-0.08		0.161	188512	0.99	3.15	0.29	0.179	0.221
	0.95	3.95	0.05		0.206		1.01	2.70	0.10		0.184		0.96	3.79	-0.15		0.182
26965	0.99	4.31	-0.34	0.307	0.245	114710	0.85	4.47	0.27	0.105	0.152	190360	0.90	4.07	0.26	0.199	0.181
34334	1.22	2.10	-0.39	0.340	0.433		0.85	4.40	0.02		0.122	192310	1.01	4.50	-0.04	0.302	0.357
	1.20	2.30	-0.25		0.439	115617	0.90	4.00	-0.03	0.162	0.139		1.03	4.50	-0.11		0.395
34411	0.86	4.11	0.35	0.117	0.153		0.90	4.50	-0.02		0.171		1.01	4.50	-0.08		0.349
	0.86	4.30	0.06		0.131	117176	0.92	3.75	-0.11	0.137	0.135		1.01	4.50	-0.09		0.347
	0.86	4.10	0.30		0.148	124897	1.18	1.73	-0.43	0.273	0.294	196755	0.89	4.40	-0.05	0.114	0.152
35620	1.20	1.50	-0.09	0.361	0.376		1.20	2.00	-0.32		0.390	198149	1.00	2.95	-0.12	0.198	0.159
37160	1.13	2.40	-0.31	0.174	0.291		1.19	1.70	-0.49		0.298		1.00	3.15	0.23		0.223
39587	0.84	4.44	-0.12	0.122	0.106		1.16	1.50	-0.38		0.243		1.06	3.00	-0.50		0.183
	0.85	4.50	-0.05		0.121		1.15	1.97	-0.42		0.269	203344	1.11	2.00	-0.20	0.221	0.231
41636	1.06	1.70	-0.30	0.227	0.144	132345	1.15	2.30	-0.02	0.317	0.371	215648	0.84	4.10	-0.28	0.058	0.085
47205	1.02	3.08	0.07	0.279	0.218		1.15	2.30	0.03		0.380	217476	0.92	1.50	0.10	0.129	0.097
55575	0.87	3.98	-0.44	0.088	0.090	135722	1.05	2.70	-0.50	0.147	0.160	217877	0.84	4.50	-0.10	0.087	0.109
69267	1.17	1.87	-0.21	0.343	0.333	136202	0.84	3.90	0.00	0.072	0.091	219134	1.07	4.50	0.10	0.452	0.538
72324	1.07	2.25	-0.20	0.149	0.193	140573	1.11	2.50	0.23	0.272	0.361		1.08	4.50	0.00		0.543
75732	0.97	4.50	0.24	0.305	0.325		1.09	2.39	-0.07		0.251		1.08	4.40	-0.21		0.485
	0.97	4.40	0.11		0.289		1.10	2.90	0.37		0.415		1.07	4.50	0.00		0.518
	0.97	4.50	0,30		0.336		1.10	2.00	0.17		0.281		1.07	4.50	-0.01		0.516
82328	0.87	3.50	0.01	0.066	0.102	142373	0.87	3.93	-0.29	0.078	0.099		1.07	4.50	0.20		0.559
85503	1.13	2.40	-0.01	0.327	0.337		0.85	4.30	-0.45		0.087	221148	1.07	2.60	0.07	0.370	0.256
	1.14	2.30	0.03		0.357		0.85	4.30	-0.43		0.088	222368	0.85	4.00	-0.18	0.063	0.094

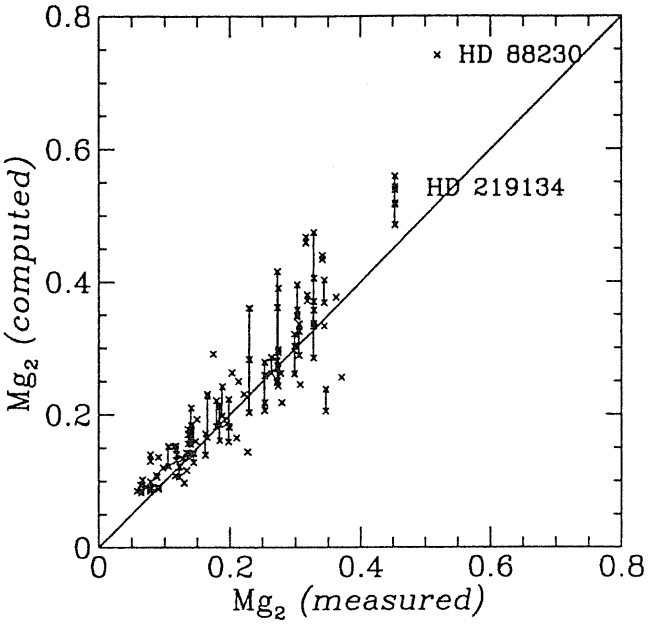

FIG. 4.—Plot of synthetic indices vs. the empirical values. Vertical bars connect the points referring to different determinations of atmospheric parameters given in C91 for the same star.

Further high-resolution analysis of cool stars, mainly late-type dwarfs and super–metal rich stars, is required to compare up-to-date theoretical predictions with empirical calibrations.

We thank G. Worthey for providing us with GW94 catalogue in computer-readable form and R. L. Kurucz and the referee for useful comments and suggestions. This work was partially supported by the Ministero dell'Università e della Ricerca Scientifica e Tecnologica (40% and 60% grants) and by the Consiglio Nazionale delle Ricerche (CNR-GNA and bilateral grants).

REFERENCES

Anders, E., & Grevesse, N. 1989, Geochim. Cosmochim. Acta, 53, 197
Barbuy, B. 1994, ApJ, 430, 218
Barbuy, B., Erdelyi-Mendes, M., & Milone, A. 1992, A&AS, 93, 235
Buzzoni, A., Gariboldi, G., & Mantegazza, L. 1992, AJ, 103, 1814
Cayrel de Strobel, G., Hauck, B., François, P., Thévenin, F., Friel, E., Mermilliod, M., & Borde, S. 1992, A&AS, 95, 273 (C91)
Faber, S. M., Friel, E. D., Burstein, D., & Gaskell, C. M. 1985, ApJS, 57, 711
Gorgas, J., Faber, S. M., Burstein, D., Gonzales, J. J., Courteau, S., & Prosser, C. 1993, ApJS, 86, 157
Gulati, R. K., Malagnini, M. L., & Morossi, C. 1991, A&A, 247, 447
———. 1993, ApJ, 413, 166 (GMM93)
Kurucz, R. L. 1992, in The Stellar Populations of Galaxies, ed. B. Barbuy & A. Renzini (Dordrecht: Kluwer), 225 (K92)
Kurucz, R. L. 1993a, CD-ROM 13, ATLAS9 Stellar Atmosphere Programs and 2 km/s Grid (Cambridge: Smithsonian Astrophys. Obs.)
———. 1993b, CD-ROM 18, SYNTHE Spectrum Synthesis Programs and Line Data (Cambridge: Smithsonian Astrophys. Obs.)
———. 1994, private communication
Kurucz, R. L., Furenlid, I., Brault, J., & Testerman, L. 1984, Solar Flux Atlas from 296 to 1300 nm (Sunspot: Nat. Solar Obs.)
McQuitty, R. J., Jaffe, T. R., Friel, E. D., & Dalle Ore, C. M. 1994, AJ, 107, 359
Mould, J. 1978, ApJ, 220, 434
Worthey, G., Faber, S. M., Gonzalez, J. J., & Burstein, D. 1994, ApJS, 94, 687 (GW94)

An Atlas of synthetic spectra for metallicity calibration of SMR stars

By M. L. MALAGNINI[1] , M. CHAVEZ[2] AND C. MOROSSI[3]

[1]Dipartimento di Astronomia, Università degli Studi di Trieste, Via Tiepolo, 11, I-34131 Trieste, Italy

[2]International School for Advanced Studies, Strada Costiera 11, I-34014 Trieste, Italy and Instituto Nacional de Astrofisica, Optica y Electronica, Apdos. Postales 51 y 216, CP 72000, Puebla Pue. Mexico

[3]Osservatorio Astronomico di Trieste, Via Tiepolo, 11, I-34131 Trieste, Italy

---

We present the Atlas of synthetic spectra, covering the wavelength range 4850–5400 Å , computed starting from the 1993 release of atmosphere models and codes by Kurucz (CD-Rom 13 and CD-Rom 18). In cool stars, the selected wavelength region is characterized mostly by magnesium and iron absorptions. The spectra were synthesized for nine values of effective temperature in the range 4000–6000 K, surface gravities 1.5, 3.0, and 4.5 dex, at metallicities -0.50, 0.5, and 1.0 dex. Solar metal abundance spectra are available in the same temperature range for seven gravity values, from 1.5 to 4.5 with a step of 0.5 dex.

The high resolution used in the computations (resolving power $\lambda/\Delta\lambda = 250{,}000$) makes the Atlas suitable for chemical abundance analyses and for metallicity calibration of SMR stars for which high quality high and low resolution spectroscopic data are now available.

In Figures 1 and 2 we give some examples of synthetic spectra, computed for the atmospheric parameters typical of G dwarfs and giants, zoomed in the regions dominated by iron (Fe I) absorptions.

In each plot, the high resolution spectrum from the Atlas is given, together with two examples of the same spectrum degraded to the resolution of observations now available for abundance analyses of SMR stars (McWilliam and Rich, 1994; McQuitty *et al.*, 1994).

By deriving suitable spectral indices from the synthetic spectra, the role of magnesium and iron spectral features in modelling the chemical evolution of galactic globular clusters can be investigated (Chavez *et al.* 1995).

REFERENCES

Chavez, M., Malagnini, M.L., Morossi, C. 1995, *ApJ*, in press

Kurucz, R. L. 1993, CD-Rom 13 and 18 (K93)

McQuitty, R. J., Jaffe, T. R., Friel, E. D., Dalle Ore, C. M. 1994, *AJ*, **107**, 359

McWilliam, A., Rich, R.M. 1994, *ApJS*, **91**, 749

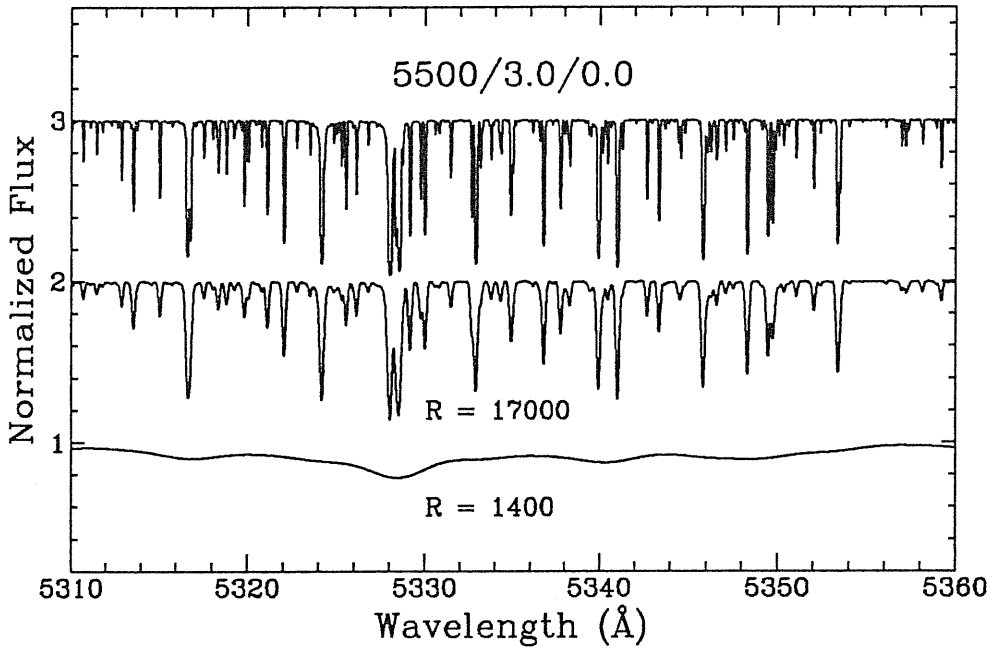

FIGURE 1. Synthetic spectrum computed for T_{eff} = 5500 K, log g = 3.0 dex, and [M/H] = 0.0 dex in the Iron region (the spectra computed at $\lambda/\Delta\lambda$ = 250,000 and 17,000 are vertically shifted by 2.0 and 1.0, respectively)

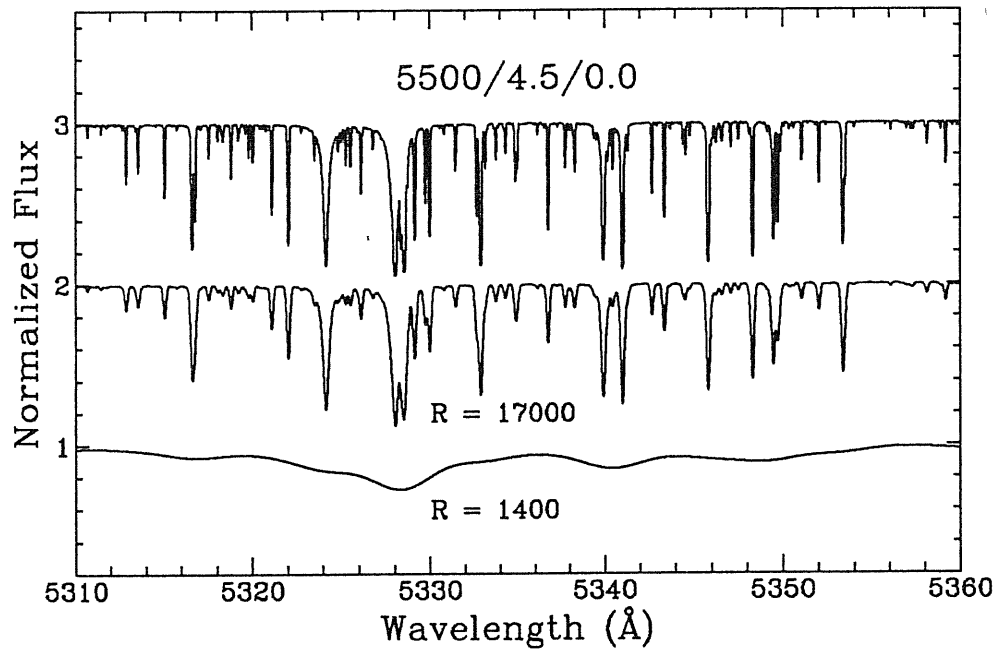

FIGURE 2. Synthetic spectrum computed for T_{eff} = 5500 K, log g = 4.5 dex, and [M/H] = 0.0 dex in the Iron region (the spectra computed at $\lambda/\Delta\lambda$ = 250,000 and 17,000 are vertically shifted by 2.0 and 1.0, respectively)

STELLAR POPULATIONS

PROCEEDINGS OF THE 164TH SYMPOSIUM OF THE
INTERNATIONAL ASTRONOMICAL UNION,
HELD IN THE HAGUE, THE NETHERLANDS,
AUGUST 15–19, 1994

NEW MG_2 INDICES FROM NEW MODEL ATMOSPHERES

M. CHAVEZ
SISSA/ISAS, Trieste, Italy and INAOE, Mexico
email: 38028::CHAVEZ

M.L. MALAGNINI
Dipartimento di Astronomia, University of Trieste, Italy
email: MALAGNINI@UNIV.TRIESTE.IT

AND

C. MOROSSI
Osservatorio Astronomico di Trieste, Italy,
email: 38439::MOROSSI

A new set of spectral indices computed for the Mg feature at 5175 Å is presented. The spectral indices were computed using the most recent grid of model atmospheres and programs to produce synthetic spectra (Kurucz 1993; CD-Rom 18) for the temperature range 4000-6000 K, and gravity interval log g = 1.5-4.5. The indices reported here refer to solar chemical abundance.

We have compared our results with previous empirical (Worthey et al. 1993) and theoretical indices (Gulati et al. 1993) for the same atmospheric parameters. The results indicate that our Mg_2 indices are higher than those calculated previously, with the differences more pronounced at the lowest gravities and temperatures.

The dependence of the strength of this feature on effective temperature is similar for all gravities. When compared to empirical calibrations, the new indices are generally higher than the observed ones at low temperatures and gravities, while for $T_{\rm eff} \geq 5000$ K there is a good match of our results with both previous theoretical calibrations and empirical ones.